Draft version 22 July 2026
Typeset using LaTeX **twocolumn** style in AASTeX631

GWTC-4.0: Tests of General Relativity. II. Parameterized Tests

The LIGO Scientific Collaboration, the Virgo Collaboration, and the KAGRA Collaboration

(Compiled: 22 July 2026)

ABSTRACT

In this second of three papers on tests of general relativity (GR) applied to the compact binary coalescence signals in the fourth Gravitational-Wave Transient Catalog (GWTC-4.0), we present the results of the parameterized tests of GR and constraints on line-of-sight acceleration. We include events up to and including the first part of the fourth observing run (O4a) of the LIGO–Virgo–KAGRA detectors. As in the other two papers in this series, we restrict our analysis to the 42 confident signals, measured by at least two detectors, that have false alarm rates $\leq 10^{-3}\,\mathrm{yr}^{-1}$ from O4a, in addition to the 49 such events from previous observing runs. This paper focuses on the eight tests that constrain parameterized deviations from the expected GR (or unaccelerated) values. These include modifications of post-Newtonian (PN) parameters, spin-induced quadrupole moments different from those of a binary black hole, and possible dispersive or birefringent propagation effects. Overall, we find no evidence for physics beyond GR, for spin-induced quadrupole moments different from those of a Kerr black hole in GR, or for line of sight acceleration, with more than 90% of the events including the null result (no deviation) within their 90% credible intervals. We discuss possible systematics affecting the other events and tests, even though they are statistically not surprising, given noise. The increased number of events analyzed allow us to improve the constraints on deviations from GR. For instance, for the PN coefficients, we improve the constraints by factors of 1.2–5.5, though some of this improvement is due to allowing the PN coefficient deviations to affect more of the waveform. We also provide illustrative translations to some modified theories. Additionally, we update the bound on the mass of the graviton, at 90% credibility, to $m_g \leq 1.92 \times 10^{-23}\,\mathrm{eV}/c^2$. Many of the bounds on possible deviations derived from our events are the best to date.

1. OVERVIEW

This paper is the second of three papers examining the nature of gravity through tests of general relativity (GR)—and more generally of physics beyond the usual assumption of quasi-circular, isolated binaries composed of black holes (BHs) and/or neutron stars (NSs)—performed on the gravitational wave (GW) signals as reported by the LIGO–Virgo–KAGRA Collaboration (LVK) in the fourth Gravitational-Wave Transient Catalog (GWTC-4.0; Abac et al. 2025a, 2026a). Paper I (Abac et al. 2026b) gives an introduction and overview of our suite of events, tests, and shared methods, and also presents the results of the consistency tests. Paper III (Abac et al. 2026c) focuses on tests of the remnants, considering the ringdown and possible echoes. This paper describes the various parameterized tests performed to place quantitative bounds on possible deformations of the GWs observed from compact binary coalescence (CBC) sources, relative to those calculated in GR. Specifically, we apply these tests to binary BH (BBH), NS–BH binary (NSBH), and binary NS (BNS) systems. Where applicable, we describe the improved bounds relative to previous GW catalogs and to existing bounds in the literature.

Specifically, we first examine deviations in post-Newtonian (PN) coefficients. The PN approximation (e.g., Einstein et al. 1938; Chandrasekhar 1965; Maggiore 2007; Poisson & Will 2014) is the standard framework for computing and testing corrections to Newtonian gravity. Tests of gravity in the PN framework have commonly been carried out in the weak field (e.g., Solar System tests; Will 2014, 2018). However, for CBCs, the PN approximation has been iterated to an impressively high order in perturbation theory (Blanchet 2024), so one can even use it to test highly relativistic effects during the end of inspiral (e.g., Blanchet & Sathyaprakash 1994, 1995; Arun et al. 2006a,b). For a binary system, the PN approximation describes corrections to the binary's dynamics as a series in powers of v/c, where v is the binary's orbital velocity. The coefficients we test appear in the GW phase, and thus describe a combination of the binary's conservative and dissipative dynamics.

The lowest few PN parameters can be constrained with binary-pulsar observations (e.g., Taylor & Weisberg 1982, 1989; Kramer et al. 2021), while higher PN orders can only be constrained meaningfully with GW observations, since these allow one to probe the strong-field, dynamical portion of the binary's evolution close to merger. We use two frameworks

The full author list is given at the end.
For correspondence: LSC P&P Committee, for LVK Publications, via lvc.publications@ligo.org

Table 1. Event selection table for the analyses in this paper, from first part of the fourth observing run (O4a) and the previous observing runs O1–O3

						Parameterized			SIM			PRP	
Run	Event Name	SNR	$(1+z)\mathcal{M}/M_\odot$	$\chi_{\rm eff}$	q	TIGER	FTI	PCA	Phenom	EOB	LOSA	MDR	SSB
O1	GW150914	$26.0^{+0.1}_{-0.2}$	$30.7^{+1.8}_{-1.6}$	$-0.04^{+0.12}_{-0.14}$	$0.88^{+0.11}_{-0.22}$	✓	++	⋯	⋯	⋯	⋯	✓	+
	GW151012*	$9.3^{+0.3}_{-0.5}$	$18.8^{+3.4}_{-1.5}$	$0.13^{+0.30}_{-0.22}$	$0.57^{+0.36}_{-0.34}$	++	⋯	⋯	⋯	⋯	⋯	++	+
	GW151226	$12.7^{+0.3}_{-0.3}$	$9.71^{+0.08}_{-0.06}$	$0.20^{+0.23}_{-0.08}$	$0.53^{+0.41}_{-0.34}$	✓$_{\rm I}$	++	⋯	✓	⋯	⋯	✓	+
O2	GW170104	$13.8^{+0.2}_{-0.3}$	$25.7^{+1.7}_{-1.7}$	$-0.04^{+0.15}_{-0.19}$	$0.73^{+0.24}_{-0.26}$	✓	++	⋯	⋯	⋯	⋯	✓	+
	GW170608	$15.3^{+0.2}_{-0.3}$	$8.50^{+0.05}_{-0.05}$	$0.05^{+0.13}_{-0.05}$	$0.74^{+0.23}_{-0.33}$	✓$_{\rm I}$	++	⋯	⋯	⋯	⋯	✓	+
	GW170729*	$10.7^{+0.4}_{-0.5}$	$52.5^{+9.2}_{-12.0}$	$0.33^{+0.23}_{-0.32}$	$0.58^{+0.35}_{-0.23}$	++	⋯	⋯	⋯	⋯	⋯	++	+
	GW170809	$12.8^{+0.2}_{-0.3}$	$29.9^{+2.4}_{-2.0}$	$0.07^{+0.17}_{-0.17}$	$0.71^{+0.25}_{-0.25}$	✓$_{\rm PI}$	⋯	⋯	⋯	⋯	⋯	✓	+
	GW170814	$17.7^{+0.2}_{-0.3}$	$27.0^{+1.5}_{-1.3}$	$0.08^{+0.13}_{-0.13}$	$0.81^{+0.16}_{-0.23}$	✓	++	⋯	⋯	⋯	⋯	✓	+
	GW170817	$32.7^{+0.1}_{-0.1}$	$1.1976^{+0.0004}_{-0.0002}$	$0.02^{+0.06}_{-0.02}$	$0.72^{+0.24}_{-0.21}$	++	++	+	⋯	⋯	✓	++	⋯
	GW170818	$12.0^{+0.3}_{-0.4}$	$32.7^{+2.8}_{-2.5}$	$-0.05^{+0.19}_{-0.22}$	$0.80^{+0.18}_{-0.24}$	✓$_{\rm PI}$	⋯	⋯	⋯	⋯	⋯	✓	+
	GW170823	$12.2^{+0.2}_{-0.3}$	$39.1^{+5.4}_{-4.7}$	$0.07^{+0.21}_{-0.22}$	$0.78^{+0.20}_{-0.30}$	✓$_{\rm PI}$	⋯	⋯	⋯	⋯	⋯	✓	+
O3a	GW190408_181802	$14.6^{+0.2}_{-0.3}$	$23.8^{+1.2}_{-1.5}$	$-0.03^{+0.13}_{-0.17}$	$0.75^{+0.21}_{-0.26}$	✓	++	⋯	⋯	⋯	⋯	✓	+
	GW190412	$19.8^{+0.2}_{-0.3}$	$15.24^{+0.37}_{-0.23}$	$0.21^{+0.12}_{-0.13}$	$0.325^{+0.172}_{-0.097}$	✓	++	✓	✓	⋯	⋯	✓	+
	GW190421_213856	$10.7^{+0.2}_{-0.4}$	$45.9^{+5.7}_{-6.3}$	$-0.10^{+0.21}_{-0.27}$	$0.78^{+0.20}_{-0.32}$	✓$_{\rm PI}$	⋯	⋯	⋯	⋯	⋯	✓	+
	GW190425	$12.4^{+0.3}_{-0.4}$	$1.4873^{+0.0008}_{-0.0006}$	$0.06^{+0.11}_{-0.05}$	$0.67^{+0.29}_{-0.25}$	⋯	⋯	⋯	⋯	⋯	✓	⋯	⋯
	GW190503_185404	$12.1^{+0.2}_{-0.4}$	$37.8^{+6.1}_{-6.7}$	$-0.05^{+0.23}_{-0.30}$	$0.69^{+0.27}_{-0.29}$	✓$_{\rm PI}$	⋯	⋯	⋯	⋯	⋯	✓	+
	GW190512_180714	$12.7^{+0.3}_{-0.4}$	$18.58^{+0.69}_{-0.66}$	$0.02^{+0.13}_{-0.14}$	$0.54^{+0.36}_{-0.18}$	✓	++	⋯	⋯	⋯	⋯	✓	+
	GW190513_205428	$12.5^{+0.3}_{-0.4}$	$30.7^{+6.1}_{-3.4}$	$0.18^{+0.29}_{-0.22}$	$0.52^{+0.41}_{-0.20}$	✓$_{\rm PI}$	⋯	⋯	⋯	⋯	⋯	✓	+
	GW190517_055101	$10.8^{+0.5}_{-0.6}$	$36.2^{+4.2}_{-4.9}$	$0.52^{+0.20}_{-0.26}$	$0.64^{+0.30}_{-0.30}$	✓$_{\rm PI}$	⋯	⋯	⋯	⋯	⋯	✓	+
	GW190519_153544	$15.9^{+0.2}_{-0.3}$	$65.1^{+8.7}_{-10.9}$	$0.33^{+0.20}_{-0.24}$	$0.63^{+0.26}_{-0.22}$	✓$_{\rm PI}$	⋯	⋯	⋯	⋯	⋯	✓	+
	GW190521	$14.3^{+0.4}_{-0.3}$	101^{+29}_{-34}	$-0.14^{+0.50}_{-0.45}$	$0.59^{+0.33}_{-0.38}$	✓$_{\rm PI}$	⋯	⋯	⋯	⋯	⋯	⋯	⋯
	GW190521_074359	$25.9^{+0.1}_{-0.2}$	$39.8^{+3.2}_{-2.7}$	$0.10^{+0.13}_{-0.13}$	$0.77^{+0.19}_{-0.21}$	✓	++	⋯	⋯	⋯	⋯	✓	+
	GW190602_175927	$13.2^{+0.2}_{-0.3}$	73^{+12}_{-18}	$0.12^{+0.25}_{-0.28}$	$0.63^{+0.32}_{-0.34}$	✓$_{\rm PI}$	⋯	⋯	⋯	⋯	⋯	✓	+
	GW190630_185205	$16.4^{+0.2}_{-0.3}$	$29.5^{+2.1}_{-1.7}$	$0.10^{+0.14}_{-0.13}$	$0.68^{+0.28}_{-0.22}$	✓	++	⋯	⋯	⋯	⋯	✓	+
	GW190706_222641	$13.4^{+0.2}_{-0.4}$	77^{+12}_{-18}	$0.32^{+0.24}_{-0.30}$	$0.56^{+0.34}_{-0.25}$	✓$_{\rm PI}$	⋯	⋯	⋯	⋯	⋯	✓	+
	GW190707_093326	$13.1^{+0.2}_{-0.4}$	$9.90^{+0.11}_{-0.10}$	$-0.04^{+0.10}_{-0.09}$	$0.66^{+0.28}_{-0.20}$	✓$_{\rm I}$	++	⋯	⋯	⋯	⋯	✓	+
	GW190708_232457	$13.4^{+0.2}_{-0.3}$	$15.48^{+0.25}_{-0.24}$	$0.05^{+0.11}_{-0.10}$	$0.58^{+0.36}_{-0.18}$	✓	++	⋯	⋯	⋯	⋯	✓	+
	GW190720_000836	$10.9^{+0.3}_{-0.8}$	$10.37^{+0.11}_{-0.11}$	$0.19^{+0.14}_{-0.11}$	$0.53^{+0.35}_{-0.24}$	✓$_{\rm I}$	++	⋯	✓	⋯	⋯	✓	+
	GW190727_060333	$11.7^{+0.2}_{-0.5}$	$45.2^{+5.8}_{-5.5}$	$0.11^{+0.26}_{-0.26}$	$0.79^{+0.18}_{-0.29}$	✓$_{\rm PI}$	⋯	⋯	⋯	⋯	⋯	✓	+
	GW190728_064510	$13.1^{+0.3}_{-0.4}$	$10.14^{+0.11}_{-0.08}$	$0.13^{+0.20}_{-0.07}$	$0.64^{+0.30}_{-0.36}$	✓$_{\rm I}$	++	⋯	✓	⋯	⋯	✓	+
	GW190814	$25.3^{+0.1}_{-0.2}$	$6.42^{+0.02}_{-0.02}$	$0.00^{+0.07}_{-0.07}$	$0.111^{+0.012}_{-0.011}$	✓	++	✓	⋯	⋯	⋯	✓	+
	GW190828_063405	$16.5^{+0.2}_{-0.3}$	$34.6^{+3.5}_{-2.9}$	$0.19^{+0.16}_{-0.17}$	$0.82^{+0.15}_{-0.26}$	✓	++	⋯	✓	⋯	⋯	✓	+
	GW190828_065509	$10.2^{+0.4}_{-0.5}$	$17.33^{+0.61}_{-0.71}$	$0.05^{+0.16}_{-0.17}$	$0.44^{+0.38}_{-0.16}$	✓$_{\rm I}$	++	⋯	⋯	⋯	⋯	✓	+
	GW190910_112807	$14.5^{+0.2}_{-0.3}$	$43.6^{+4.4}_{-4.0}$	$0.00^{+0.17}_{-0.19}$	$0.80^{+0.18}_{-0.23}$	✓$_{\rm PI}$	⋯	⋯	⋯	⋯	⋯	✓	+
	GW190915_235702	$13.1^{+0.2}_{-0.3}$	$32.5^{+3.1}_{-3.1}$	$-0.02^{+0.19}_{-0.23}$	$0.76^{+0.21}_{-0.29}$	✓$_{\rm PI}$	⋯	⋯	⋯	⋯	⋯	✓	+

Table 1 *continued*

Table 1 *(continued)*

Run	Event Name	SNR	$(1+z)\mathcal{M}/M_\odot$	$\chi_{\rm eff}$	q	Parameterized			SIM			PRP	
						TIGER	FTI	PCA	Phenom	EOB	LOSA	MDR	SSB
	GW190924_021846	$12.0^{+0.3}_{-0.4}$	$6.44^{+0.03}_{-0.02}$	$0.03^{+0.20}_{-0.08}$	$0.58^{+0.32}_{-0.30}$	$\checkmark_{\rm I}$	++	$\cdots$	$\cdots$	$\cdots$	$\cdots$	$\checkmark$	+
O3b	GW191109_010717	$17.2^{+0.5}_{-0.5}$	$60.1^{+9.8}_{-9.3}$	$-0.29^{+0.42}_{-0.31}$	$0.73^{+0.21}_{-0.24}$	$\not\checkmark_{\rm PI}$	$\cdots$	$\cdots$	$\cdots$	$\cdots$	$\cdots$	$\not\checkmark$	$\cdots$
	GW191129_134029	$13.1^{+0.2}_{-0.3}$	$8.49^{+0.06}_{-0.05}$	$0.06^{+0.16}_{-0.08}$	$0.63^{+0.31}_{-0.29}$	$\checkmark_{\rm I}$	++	$\cdots$	$\cdots$	$\cdots$	$\cdots$	$\checkmark$	+
	GW191204_171526	$17.5^{+0.2}_{-0.2}$	$9.69^{+0.05}_{-0.05}$	$0.16^{+0.08}_{-0.05}$	$0.69^{+0.25}_{-0.26}$	$\checkmark_{\rm I}$	++	$\checkmark$	$\checkmark$	$\cdots$	$\cdots$	$\checkmark$	+
	GW191215_223052	$11.2^{+0.3}_{-0.4}$	$24.9^{+1.5}_{-1.4}$	$-0.03^{+0.17}_{-0.21}$	$0.73^{+0.24}_{-0.27}$	$\checkmark$	$\cdots$	$\cdots$	$\cdots$	$\cdots$	$\cdots$	$\checkmark$	+
	GW191216_213338	$18.6^{+0.2}_{-0.2}$	$8.94^{+0.05}_{-0.05}$	$0.11^{+0.13}_{-0.06}$	$0.63^{+0.31}_{-0.29}$	$\checkmark$	++	$\checkmark$	$\checkmark$	$\cdots$	$\cdots$	$\checkmark$	+
	GW191222_033537	$12.5^{+0.2}_{-0.3}$	$51.0^{+7.2}_{-6.5}$	$-0.04^{+0.20}_{-0.25}$	$0.79^{+0.18}_{-0.32}$	$\checkmark_{\rm PI}$	$\cdots$	$\cdots$	$\cdots$	$\cdots$	$\cdots$	$\checkmark$	+
	GW200115_042309	$11.3^{+0.3}_{-0.5}$	$2.58^{+0.01}_{-0.01}$	$-0.15^{+0.24}_{-0.41}$	$0.243^{+0.432}_{-0.097}$	$\checkmark_{\rm I}$	++	$\cdots$	$\cdots$	$\cdots$	$\not\checkmark$	$\cdots$	$\cdots$
	GW200129_065458	$26.8^{+0.2}_{-0.2}$	$32.1^{+1.8}_{-2.6}$	$0.11^{+0.11}_{-0.16}$	$0.85^{+0.12}_{-0.41}$	$\checkmark$	++	$\cdots$	++	$\cdots$	$\cdots$	$\checkmark$	+
	GW200202_154313	$10.8^{+0.2}_{-0.4}$	$8.15^{+0.05}_{-0.05}$	$0.04^{+0.13}_{-0.06}$	$0.72^{+0.24}_{-0.31}$	$\checkmark_{\rm I}$	++	$\cdots$	$\cdots$	$\cdots$	$\cdots$	$\checkmark$	+
	GW200208_130117	$10.8^{+0.3}_{-0.5}$	$38.8^{+5.2}_{-4.8}$	$-0.07^{+0.22}_{-0.27}$	$0.73^{+0.23}_{-0.29}$	$\checkmark_{\rm PI}$	$\cdots$	$\cdots$	$\cdots$	$\cdots$	$\cdots$	$\checkmark$	+
	GW200219_094415	$10.7^{+0.3}_{-0.5}$	$43.7^{+6.3}_{-6.2}$	$-0.08^{+0.23}_{-0.29}$	$0.77^{+0.21}_{-0.32}$	$\checkmark_{\rm PI}$	$\cdots$	$\cdots$	$\cdots$	$\cdots$	$\cdots$	$\checkmark$	+
	GW200224_222234	$20.0^{+0.2}_{-0.2}$	$41.1^{+3.6}_{-3.8}$	$0.11^{+0.15}_{-0.15}$	$0.82^{+0.16}_{-0.26}$	$\checkmark_{\rm PI}$	$\cdots$	$\cdots$	$\cdots$	$\cdots$	$\cdots$	$\checkmark$	+
	GW200225_060421	$12.5^{+0.3}_{-0.4}$	$17.65^{+0.98}_{-1.97}$	$-0.12^{+0.17}_{-0.28}$	$0.73^{+0.23}_{-0.28}$	$\checkmark$	++	$\cdots$	$\cdots$	$\cdots$	$\cdots$	$\checkmark$	+
	GW200311_115853	$17.8^{+0.2}_{-0.2}$	$32.7^{+2.7}_{-2.8}$	$-0.02^{+0.16}_{-0.20}$	$0.82^{+0.16}_{-0.27}$	$\checkmark$	++	$\cdots$	$\cdots$	$\cdots$	$\cdots$	$\checkmark$	+
	GW200316_215756	$10.3^{+0.4}_{-0.7}$	$10.68^{+0.12}_{-0.12}$	$0.13^{+0.27}_{-0.10}$	$0.59^{+0.34}_{-0.38}$	$\checkmark_{\rm I}$	++	$\cdots$	$\checkmark$	$\cdots$	$\cdots$	$\not\checkmark$	$\cdots$
O4a	GW230518_125908	$14.2^{+0.2}_{-0.4}$	$2.943^{+0.004}_{-0.004}$	$-0.01^{+0.09}_{-0.11}$	$0.18^{+0.04}_{-0.03}$	$\checkmark_{\rm I}$	$\checkmark$	$\cdots$	$\cdots$	$\cdots$	$\cdots$	$\cdots$	$\cdots$
	GW230601_224134	$12.3^{+0.2}_{-0.3}$	$73.0^{+8.3}_{-11.8}$	$-0.03^{+0.27}_{-0.32}$	$0.69^{+0.26}_{-0.30}$	$\checkmark_{\rm PI}$	$\cdots$	$\cdots$	$\cdots$	$\cdots$	$\cdots$	$\checkmark$	$\checkmark$
	GW230605_065343	$10.5^{+0.3}_{-0.4}$	$14.44^{+0.28}_{-0.24}$	$0.06^{+0.16}_{-0.10}$	$0.65^{+0.31}_{-0.29}$	$\checkmark$	$\checkmark$	$\cdots$	$\cdots$	$\cdots$	$\cdots$	$\checkmark$	$\checkmark$
	GW230606_004305	$10.3^{+0.3}_{-0.4}$	$39.5^{+5.9}_{-5.8}$	$-0.11^{+0.26}_{-0.31}$	$0.70^{+0.27}_{-0.33}$	$\checkmark_{\rm PI}$	$\cdots$	$\cdots$	$\cdots$	$\cdots$	$\cdots$	$\checkmark$	$\checkmark$
	GW230609_064958	$9.8^{+0.3}_{-0.5}$	$40.1^{+5.7}_{-5.9}$	$-0.14^{+0.22}_{-0.27}$	$0.73^{+0.24}_{-0.30}$	$\checkmark_{\rm PI}$	$\cdots$	$\cdots$	$\cdots$	$\cdots$	$\cdots$	$\checkmark$	$\checkmark$
	GW230624_113103	$9.7^{+0.4}_{-0.5}$	$24.5^{+3.1}_{-2.4}$	$0.17^{+0.29}_{-0.25}$	$0.59^{+0.35}_{-0.29}$	$\checkmark_{\rm PI}$	$\cdots$	$\cdots$	$\cdots$	$\cdots$	$\cdots$	$\checkmark$	$\checkmark$
	GW230627_015337	$28.5^{+0.1}_{-0.1}$	$6.41^{+0.01}_{-0.01}$	$0.02^{+0.08}_{-0.03}$	$0.69^{+0.25}_{-0.21}$	$\checkmark$	$\checkmark$	$\checkmark$	$\cdots$	$\cdots$	$\cdots$	$\checkmark$	$\checkmark$
	GW230628_231200	$15.5^{+0.2}_{-0.3}$	$35.8^{+2.8}_{-2.7}$	$-0.01^{+0.16}_{-0.16}$	$0.85^{+0.14}_{-0.24}$	$\checkmark$	$\checkmark$	$\cdots$	$\cdots$	$\cdots$	$\cdots$	$\checkmark$	$\checkmark$
	GW230630_234532	$9.4^{+0.3}_{-0.5}$	$8.57^{+0.06}_{-0.09}$	$-0.04^{+0.16}_{-0.08}$	$0.67^{+0.29}_{-0.28}$	$\checkmark_{\rm I}$	$\cdots$	$\cdots$	$\cdots$	$\cdots$	$\cdots$	$\checkmark$	$\checkmark$
	GW230702_185453	$9.5^{+0.3}_{-0.5}$	$33.0^{+4.8}_{-3.9}$	$0.05^{+0.29}_{-0.26}$	$0.45^{+0.45}_{-0.25}$	$\checkmark_{\rm PI}$	$\cdots$	$\cdots$	$\cdots$	$\cdots$	$\cdots$	$\checkmark$	$\checkmark$
	GW230731_215307	$11.9^{+0.2}_{-0.3}$	$9.46^{+0.07}_{-0.06}$	$-0.05^{+0.11}_{-0.06}$	$0.76^{+0.22}_{-0.29}$	$\checkmark_{\rm I}$	$\checkmark$	$\cdots$	$\cdots$	$\cdots$	$\cdots$	$\checkmark$	$\checkmark$
	GW230811_032116	$12.8^{+0.3}_{-0.4}$	$33.3^{+3.0}_{-2.6}$	$0.02^{+0.18}_{-0.18}$	$0.63^{+0.31}_{-0.22}$	$\checkmark$	$\checkmark$	$\cdots$	$\cdots$	$\cdots$	$\cdots$	$\checkmark$	$\checkmark$
	GW230814_061920	$9.4^{+0.3}_{-0.5}$	77^{+12}_{-18}	$0.05^{+0.29}_{-0.28}$	$0.62^{+0.32}_{-0.29}$	$\checkmark_{\rm PI}$	$\cdots$	$\cdots$	$\cdots$	$\cdots$	$\cdots$	$\checkmark$	$\checkmark$
	GW230824_033047	$10.0^{+0.2}_{-0.4}$	$65.8^{+8.0}_{-12.7}$	$-0.00^{+0.23}_{-0.27}$	$0.71^{+0.26}_{-0.34}$	$\checkmark_{\rm PI}$	$\cdots$	$\cdots$	$\cdots$	$\cdots$	$\cdots$	$\checkmark$	$\checkmark$
	GW230904_051013	$10.2^{+0.3}_{-0.5}$	$9.06^{+0.06}_{-0.06}$	$0.05^{+0.15}_{-0.07}$	$0.68^{+0.29}_{-0.31}$	$\checkmark_{\rm I}$	$\cdots$	$\cdots$	$\cdots$	$\cdots$	$\cdots$	$\checkmark$	$\checkmark$
	GW230914_111401	$16.2^{+0.2}_{-0.3}$	$59.4^{+7.8}_{-11.3}$	$0.12^{+0.19}_{-0.20}$	$0.62^{+0.32}_{-0.26}$	$\checkmark_{\rm PI}$	$\cdots$	$\cdots$	$\cdots$	$\cdots$	$\cdots$	$\checkmark$	$\checkmark$
	GW230919_215712	$15.7^{+0.2}_{-0.3}$	$26.4^{+1.2}_{-1.2}$	$0.18^{+0.12}_{-0.13}$	$0.79^{+0.18}_{-0.25}$	$\checkmark$	$\checkmark$	$\cdots$	$\checkmark$	$\checkmark$	$\cdots$	$\checkmark$	$\checkmark$
	GW230920_071124	$10.1^{+0.3}_{-0.4}$	$35.8^{+4.1}_{-3.4}$	$0.00^{+0.22}_{-0.23}$	$0.75^{+0.22}_{-0.30}$	$\checkmark_{\rm PI}$	$\cdots$	$\cdots$	$\cdots$	$\cdots$	$\cdots$	$\checkmark$	$\checkmark$
	GW230922_020344	$11.8^{+0.3}_{-0.4}$	$38.2^{+3.6}_{-3.2}$	$0.03^{+0.20}_{-0.21}$	$0.75^{+0.22}_{-0.26}$	$\checkmark_{\rm PI}$	$\checkmark$	$\cdots$	$\cdots$	$\cdots$	$\cdots$	$\checkmark$	$\checkmark$
	GW230922_040658	$11.4^{+0.2}_{-0.4}$	105^{+15}_{-29}	$0.31^{+0.25}_{-0.32}$	$0.71^{+0.26}_{-0.43}$	$\checkmark_{\rm PI}$	$\cdots$	$\cdots$	++	$\cdots$	$\cdots$	$\checkmark$	$\checkmark$
	GW230924_124453	$12.9^{+0.2}_{-0.3}$	$31.7^{+2.4}_{-2.0}$	$0.02^{+0.18}_{-0.18}$	$0.81^{+0.17}_{-0.24}$	$\checkmark$	$\checkmark$	$\cdots$	$\cdots$	$\cdots$	$\cdots$	$\checkmark$	$\checkmark$

Table 1 *continued*

Table 1 *(continued)*

Run	Event Name	SNR	$(1+z)\mathcal{M}/M_\odot$	$\chi_{\rm eff}$	q	Parameterized			SIM			PRP	
						TIGER	FTI	PCA	Phenom	EOB	LOSA	MDR	SSB
	GW230927_043729	$10.5^{+0.2}_{-0.4}$	$41.0^{+4.3}_{-3.8}$	$0.01^{+0.20}_{-0.22}$	$0.80^{+0.18}_{-0.27}$	✓$_{\rm PI}$	⋯	⋯	⋯	⋯	⋯	✓	✓
	GW230927_153832	$19.7^{+0.2}_{-0.2}$	$20.14^{+0.41}_{-0.41}$	$0.03^{+0.08}_{-0.08}$	$0.75^{+0.21}_{-0.19}$	✓	✓	✓	⋯	⋯	⋯	✓	✓
	GW230928_215827	$8.9^{+0.4}_{-0.6}$	61^{+10}_{-14}	$0.40^{+0.20}_{-0.28}$	$0.56^{+0.35}_{-0.27}$	✓$_{\rm PI}$	⋯	⋯	⋯	⋯	⋯	✓	✓
	GW231001_140220	$9.6^{+0.3}_{-0.5}$	81^{+17}_{-20}	$-0.04^{+0.33}_{-0.35}$	$0.54^{+0.36}_{-0.26}$	✓$_{\rm PI}$	⋯	⋯	⋯	⋯	⋯	✓	✓
	GW231020_142947	$10.5^{+0.3}_{-0.4}$	$9.99^{+0.10}_{-0.10}$	$0.15^{+0.25}_{-0.12}$	$0.61^{+0.35}_{-0.40}$	✓$_{\rm I}$	✓	⋯	✓	✓	⋯	✓	✓
	GW231028_153006	$21.0^{+0.2}_{-0.2}$	107^{+10}_{-27}	$0.44^{+0.16}_{-0.20}$	$0.63^{+0.33}_{-0.35}$	✓$_{\rm PI}$	⋯	⋯	⋯	⋯	⋯	✓	✓
	GW231102_071736	$13.3^{+0.2}_{-0.3}$	$71.7^{+7.8}_{-10.5}$	$0.06^{+0.23}_{-0.22}$	$0.72^{+0.25}_{-0.27}$	✓$_{\rm PI}$	⋯	⋯	⋯	⋯	⋯	✓	✓
	GW231104_133418	$11.0^{+0.2}_{-0.4}$	$11.31^{+0.10}_{-0.10}$	$0.14^{+0.12}_{-0.07}$	$0.70^{+0.26}_{-0.31}$	✓$_{\rm I}$	✓	⋯	✓	✓	⋯	✓	✓
	GW231108_125142	$12.4^{+0.2}_{-0.3}$	$23.79^{+0.96}_{-0.97}$	$-0.08^{+0.13}_{-0.15}$	$0.75^{+0.22}_{-0.23}$	✓	✓	⋯	⋯	⋯	⋯	✓	✓
	GW231110_040320	$11.0^{+0.3}_{-0.4}$	$18.02^{+0.69}_{-0.48}$	$0.17^{+0.13}_{-0.12}$	$0.65^{+0.30}_{-0.25}$	✓	✓	⋯	✓	✓	⋯	✓	✓
	GW231113_200417	$10.1^{+0.3}_{-0.5}$	$9.82^{+0.08}_{-0.08}$	$0.13^{+0.14}_{-0.08}$	$0.65^{+0.31}_{-0.31}$	✓$_{\rm I}$	✓	⋯	✓	✓	⋯	✓	✓
	GW231114_043211	$9.8^{+0.3}_{-0.5}$	$14.61^{+0.37}_{-0.31}$	$0.08^{+0.22}_{-0.16}$	$0.36^{+0.27}_{-0.17}$	✓$_{\rm I}$	⋯	⋯	⋯	⋯	⋯	✓	✓
	GW231118_005626	$10.5^{+0.3}_{-0.5}$	$17.62^{+0.40}_{-0.54}$	$0.37^{+0.10}_{-0.11}$	$0.55^{+0.37}_{-0.22}$	✓	⋯	⋯	✓	⋯	⋯	✓	✓
	GW231118_090602	$10.9^{+0.4}_{-0.4}$	$10.53^{+0.12}_{-0.09}$	$0.08^{+0.36}_{-0.09}$	$0.56^{+0.38}_{-0.41}$	✓$_{\rm I}$	✓	⋯	✓	✓	⋯	✓	✓
	GW231123_135430	$20.7^{+0.2}_{-0.3}$	137^{+21}_{-27}	$0.31^{+0.25}_{-0.41}$	$0.74^{+0.22}_{-0.38}$	⋯	⋯	⋯	⋯	⋯	⋯	~~✓~~	~~✓~~
	GW231206_233134	$11.0^{+0.3}_{-0.4}$	$41.9^{+4.7}_{-4.9}$	$-0.09^{+0.22}_{-0.24}$	$0.81^{+0.17}_{-0.28}$	✓$_{\rm PI}$	⋯	⋯	⋯	⋯	⋯	✓	✓
	GW231206_233901	$21.0^{+0.1}_{-0.2}$	$36.1^{+2.3}_{-2.3}$	$-0.05^{+0.14}_{-0.15}$	$0.76^{+0.21}_{-0.25}$	✓	✓	⋯	⋯	⋯	⋯	✓	✓
	GW231213_111417	$9.7^{+0.2}_{-0.4}$	$44.4^{+7.2}_{-6.5}$	$0.06^{+0.24}_{-0.23}$	$0.79^{+0.19}_{-0.30}$	✓$_{\rm PI}$	⋯	⋯	⋯	⋯	⋯	✓	✓
	GW231223_032836	$8.8^{+0.3}_{-0.5}$	$55.0^{+9.3}_{-15.0}$	$-0.15^{+0.33}_{-0.37}$	$0.71^{+0.26}_{-0.41}$	✓$_{\rm PI}$	⋯	⋯	⋯	⋯	⋯	✓	✓
	GW231224_024321	$12.9^{+0.2}_{-0.3}$	$8.48^{+0.06}_{-0.06}$	$-0.01^{+0.08}_{-0.06}$	$0.79^{+0.19}_{-0.26}$	✓$_{\rm I}$	✓	⋯	⋯	⋯	⋯	✓	✓
	GW231226_101520	$33.7^{+0.1}_{-0.1}$	$39.8^{+1.6}_{-1.6}$	$-0.09^{+0.09}_{-0.10}$	$0.88^{+0.11}_{-0.19}$	✓	⋯	⋯	⋯	⋯	⋯	✓	✓

NOTE— Event selection table for the analyses in this paper, from O4a (Abac et al. 2026a) and the previous observing runs O1 (Abbott et al. 2016a), O2 (Abbott et al. 2019a), O3a (Abbott et al. 2021a, 2024), and O3b (Abbott et al. 2023), with binary parameters from each observing run's catalog paper. TIGER, FTI, and MDR results for GW170817 were published in Abbott et al. (2019b). The starred events GW151012 and GW170729 had previously been used for the indicated tests of GR in Abbott et al. (2016a, 2019c), but do not meet the current selection criteria. The O3a event GW190425 does meet the current selection criteria, but was previously excluded from most tests as a binary neutron star. A ✓ indicates an event meeting our selection criteria for an analysis and thus included in our results; only these have been used to generate the bounds on GR deviations presented in this paper. A ++ indicates previous results by the LVK exist, but are not used for the new bounds here, while a + indicates existing results in external works. A ⋯ indicates events not meeting selection criteria. For the TIGER tests, further subscripts I/PI indicate where the test is only applied to the inspiral/post-inspiral stages, respectively. A few events have ~~✓~~ signs, indicating they had originally met the selection criteria, but technical difficulties in their analysis prevented obtaining meaningful results.

(TIGER and FTI, both defined and described below) to place bounds on deviations in individual PN coefficients, and also illustrate how the posteriors on the PN coefficient deviations can be translated (with significant caveats) to the parameters in some alternative theories.

We also test for deviations in phenomenological post-inspiral coefficients with TIGER, in combinations of multiple PN coefficients using principal component analysis (PCA), and in the spin-induced multipole (SIM) PN coefficients.

Additionally, we place bounds on the line-of-sight acceleration (LOSA) of the source systems and on modifications to the propagation (PRP) of GWs to Earth, including in the GWs' dispersion relation (MDR), and of spacetime symmetry breaking (SSB) leading to anisotropic birefringence. The LOSA analysis is not a test of GR, but rather tests for astrophysics not included in the standard analyses performed in Abac et al. (2026a). However, the LOSA analysis is included in this paper as such effects could appear as a GR deviation in other tests. Similarly, the LOSA analysis is also sensitive to other deviations from the assumption of quasi-circular isolated binaries, including deviations from GR, and provides a test of deviations starting at -4PN (see Section 2.4) that is complementary to other analyses.

We apply these tests to the GW events from GWTC-4.0 that were observed with at least two detectors, and with a false-alarm rate of $\leq 10^{-3}\,\mathrm{yr}^{-1}$, as described in Paper I. These include 42 events from O4a, which are new, as well as some events from previous runs, O1 (Abbott et al. 2016a,b), O2 (Abbott et al. 2019a,b,c), O3a (Abbott et al. 2021b, 2024), and O3b (Abbott et al. 2023, 2025), which have been used for a subset of the tests, in particular in creating combined results. Table 1 details which events were analyzed by each test. Table 1 also provides each binary's redshifted chirp mass $(1+z)\mathcal{M}$, effective inspiral spin $\chi_{\rm eff}$, and mass ratio q, as convenient combinations of the masses and spins (Abac et al. 2025a).

The rest of this paper is organized as follows: Section 2 describes the parameterized tests of modifications in the generation of the GWs from the CBC systems, with the constraints on deviations in individual PN and post-inspiral coefficients given in Section 2.1 and the PCA multiparameter analysis given in Section 2.2, while Section 2.3 presents the SIM test and Section 2.4 the LOSA test. The propagation tests are given in Section 3 (MDR in Section 3.1 and SSB in Section 3.2). We provide final conclusions along with a summary of the bounds and some of their implications in Section 4. In Appendix A, we consider the effects of real detector noise on the TIGER reanalysis of GW190728_064510. In Appendix B, we discuss the check of waveform systematics (i.e., systematic biases due to waveform modeling uncertainties) for the TIGER analysis of GW231028_153006, while in Appendix C, we discuss how prior effects lead to the apparent GR deviation found in the MDR analysis of that event. Finally, in Appendix D, we discuss the waveform systematics found in the MDR analysis of GW231123_135430 (henceforth shortened to GW231123).

2. TESTS OF GW GENERATION

2.1. *FTI and TIGER: Single-parameter tests*

Alternative theories of gravity may lead to modifications of a binary's binding energy and angular momentum and the corresponding fluxes, which lead to changes in the orbital motion of the binary (e.g., Sotiriou & Barausse 2007; Yagi et al. 2012a; Mirshekari & Will 2013; Lang 2014, 2015; Julié 2018; Bernard et al. 2022; Shiralilou et al. 2022). This means that the inspiral portion of the GW signal emitted by the binary differs from GR. Such deviations from GR can be captured by introducing extra parameters in the waveform. In this section, we focus on constraining deviations from GR by introducing parametric deviations in the inspiral, post-inspiral, and merger–ringdown part of a waveform model. We will focus on deviations in the frequency domain GW phase, since GW observations are less sensitive to deviations in the amplitude (see, e.g., Cutler & Flanagan 1994).

The GW signal from the early inspiral of compact binaries can be well described using the PN formalism (Blanchet 2024). In the PN approximation, the waveform is expanded in powers of dimensionless velocity v/c, where $\mathcal{O}([v/c]^n)$ relative to the leading order is referred to as the $(n/2)$PN order. Given the intrinsic parameters of a binary, the coefficients at each PN order are uniquely determined in GR. Measuring these coefficients by allowing them to differ from their GR value can therefore be used as a null test of GR (Blanchet & Sathyaprakash 1994, 1995; Arun et al. 2006a,b; Yunes & Pretorius 2009; Mishra et al. 2010; Li et al. 2012a,b). Although many alternative theories of gravity admit a PN expansion and can therefore be captured in this form, this is not always the case. For example, abrupt changes in the waveform such as dynamical scalarization do not admit a PN expansion (Sampson et al. 2014; Khalil et al. 2019). However, such a null test may still be able to detect such deviations from GR.

The frequency domain phase of the GW signal during early inspiral can be obtained from the PN expanded time domain waveform using the stationary phase approximation (Sathyaprakash & Dhurandhar 1991; Cutler & Flanagan 1994; Buonanno et al. 2009). For quasi-circular, spin-aligned binaries, it has the form

$$\Psi_{\ell m}(f) = 2\pi f t_c - \phi_c - \frac{\pi}{4} + \frac{3c^5}{128\eta v^5}\frac{|m|}{2}\sum_{n=0}^{7}\left(\psi_n + \psi_{nl}\log\frac{v}{c}\right)\frac{v^n}{c^n}, \quad (1)$$

where $v = [2\pi G(1+z)Mf/|m|]^{1/3}$ with f the GW frequency, M the total mass, η the symmetric mass ratio, z the redshift, and t_c, ϕ_c the time and phase at coalescence (Abac et al. 2025a). The coefficients ψ_n and ψ_{nl} (where the l denotes the coefficients of the logarithmic terms) are the $(n/2)$PN coefficients and depend on the masses and spins of the binary. The subscript ℓm denotes the (ℓ, m) multipole in the spherical harmonic decomposition of the waveform. The PN coefficients are fully known up to 4.5PN (Blanchet et al. 2023), but we only include the ones up to 3.5PN here since we do not test for higher orders.

Deviations from GR can then be modeled by introducing parametric deviations to the non-spinning part of the PN coefficients in GR $\psi_i^{\rm GR,NS}$, i.e., of the form

$$\psi_i \to (1 + \delta\hat{\varphi}_i)\psi_i^{\rm GR,NS} + \psi_i^{\rm GR,S}, \quad (2)$$

where $\delta\hat{\varphi}_i$ is the deviation parameter and $\psi_i^{\rm GR,S}$ is the spin-dependent part of the PN coefficient in GR. This is the same parameterization that was previously used (Abbott et al. 2016b, 2019b,c, 2021b, 2025; Sänger et al. 2026), and avoids possible singularities when the spin-dependent terms cancel with the non-spinning terms. Since the spin terms are still included in the GR part of the model, excluding the spin terms from the normalization of the deviations does not lead to any problems even for highly spinning systems. The full set of inspiral parameters that we constrain is then

$$\{\delta\hat{\varphi}_{-2}, \delta\hat{\varphi}_0, \delta\hat{\varphi}_1, \delta\hat{\varphi}_2, \delta\hat{\varphi}_3, \delta\hat{\varphi}_4, \delta\hat{\varphi}_{5l}, \delta\hat{\varphi}_6, \delta\hat{\varphi}_{6l}, \delta\hat{\varphi}_7\}\,. \quad (3)$$

The non-logarithmic 2.5PN term is degenerate with the coalescence phase, so it cannot be constrained. In GR, the -1PN and 0.5PN terms vanish, so we instead treat $\delta\hat{\varphi}_{-2}$ and $\delta\hat{\varphi}_1$ as absolute deviations with a normalization factor equal to the

0PN coefficient. All other deviation parameters are fractional deviations relative to the GR values.

We use two different frameworks to constrain these inspiral deviation parameters. They use a different approach for how exactly the corrections are added to the GR waveform, and differ in the underlying GR waveform model used. Using two different implementations of the parameterized inspiral test with two different GR waveform models makes the test more robust against waveform systematics coming from approximations made in the models.

The first framework is called the Flexible Theory-Independent (FTI) method (Mehta et al. 2023) and can use any frequency-domain, aligned-spin GR waveform as a baseline model. In this work, we use the SEOBNRv5HM_ROM (Pompili et al. 2023) waveform approximant for BBHs. For NSBHs (only GW230518_125908 in O4a), we use SEOBNRv4_ROM_NRTidalv2_NSBH (Dietrich et al. 2019; Matas et al. 2020). Previous papers used SEOBNRv4_ROM (Bohé et al. 2017) for both BBHs and NSBHs, as well as SEOBNRv4HM_ROM (Cotesta et al. 2020) for a few BBHs, and additionally used SEOBNRv4_ROM_NRTidalv2 (Dietrich et al. 2019) for the BNSs GW170817. In FTI, the beyond GR corrections are added to the phase of an inspiral–merger–ringdown frequency-domain waveform. The frequency-domain phase is computed for the inspiral part and then smoothly tapered off to zero towards merger–ringdown so that the post-inspiral part of the signal remains the same as in GR. The tapering happens using a windowing function that is centered around a tapering frequency, which is a free parameter of the model together with the window width. We choose the tapering frequency to be the frequency at the peak of the $(2,2)$ multipole $f_{\rm tape} = f^{22}_{\rm peak}$ (using the fit from Bohé et al. 2017) and the window width to be one GW cycle $\mathcal{N}_{\rm GW} = 1$.

The settings used for FTI in previous papers (Abbott et al. 2016b, 2019b,c, 2021b, 2025) were different than those employed here. Specifically, the choice of the tapering frequency changed from $f_{\rm tape} = 0.35 f^{22}_{\rm peak}$ in GWTC-3.0 to $f_{\rm tape} = 1.0 f^{22}_{\rm peak}$ in this work. The motivation for increasing the tapering frequency is that this captures more of the late inspiral, which is especially important for higher PN orders and more massive systems (Mehta et al. 2023). Since the bounds obtained depend on the tapering frequency used, it is not possible to directly compare the GWTC-3.0 and O4a bounds. Typically, the increase in tapering frequency leads to tighter bounds on higher PN coefficients (up to a factor of ~ 3) since more of the late inspiral is considered in the analysis, as illustrated in Mehta et al. (2023). For low total-mass systems like BNSs, the tapering frequency lies outside the sensitive band of the detectors and therefore does not significantly influence the results. Only new events from O4a were analyzed with the updated FTI model, so any results obtained by combining events only use the events marked with a ✓ in Table 1.

In the second framework, the Test Infrastructure for GEneral Relativity (TIGER; Agathos et al. 2014; Meidam et al. 2018; Roy et al. 2026), the parameterized deviations are directly added to the PN phase coefficients in the IMRPhenomXAS (Pratten et al. 2020) waveform model. This means that it can only be used by waveforms in that family, and the corrections are propagated to the spin-precessing waveform with higher order multipole moments IMRPhenomXPHM_SpinTaylor (IMRPhenomXPHM for brevity; Pratten et al. 2021; Colleoni et al. 2025b), which is used in this work. However, the corrections do not affect the spin precession. By implementing the corrections directly into the PN coefficients of the model, a smooth connection to the post-inspiral part of the waveform is guaranteed by construction. Previous versions of TIGER used the same construction for the IMRPhenomPv2 (Hannam et al. 2014; Bohé et al. 2016; Husa et al. 2016; Khan et al. 2016) and IMRPhenomPv3HM (Khan et al. 2019, 2020) waveform models.

The TIGER framework also allows for parameterized deviations in the post-inspiral part of the waveform, similarly to Cornish et al. (2011). The IMRPhenomXAS waveform has analytical expressions for the GW phase in the intermediate and merger–ringdown regimes which contain coefficients that can be parameterized much like the inspiral PN coefficients. The main difference is that the post-inspiral coefficients come from calibrating the waveform to numerical relativity (NR) simulations in GR instead of from analytical results. The parameters $\delta\hat{b}_1, \delta\hat{b}_2, \delta\hat{b}_3, \delta\hat{b}_4$ capture deviations in the NR-calibrated coefficients in the intermediate regime, and the parameters $\delta\hat{c}_1, \delta\hat{c}_2, \delta\hat{c}_4, \delta\hat{c}_\ell$ capture deviations in the merger–ringdown calibration coefficients (Pratten et al. 2020; Roy et al. 2026).

In this section, we vary only one deviation parameter

$$\delta\hat{p}_i \in \left\{ \underbrace{\delta\hat{\varphi}_{-2}, \delta\hat{\varphi}_0, \ldots, \delta\hat{\varphi}_7}_{\text{Inspiral}}, \underbrace{\delta\hat{b}_1, \ldots, \delta\hat{b}_4}_{\text{Intermediate}}, \underbrace{\delta\hat{c}_1, \delta\hat{c}_2, \delta\hat{c}_4, \delta\hat{c}_\ell}_{\text{Merger-ringdown}} \right\} \tag{4}$$

at a time. This is sufficient to detect and constrain deviations from GR, even when the deviations are present in multiple PN orders (Sampson et al. 2013; Meidam et al. 2018; Perkins & Yunes 2022). Testing for multiple deviation parameters at the same time would lead to less informative posteriors due to correlations between the parameters (Abbott et al. 2016b; Gupta et al. 2020). In Section 2.2, such a multi-parameter test is performed using the principal component analysis approach. For both FTI and TIGER, we use priors that are uniform in $\delta\hat{p}_i$ and symmetric around zero. For the TIGER analyses, we adopt the following prior ranges: $\delta\hat{\varphi}_{-2} \in [-0.1, 0.1]$, $\delta\hat{\varphi}_{0,1,2,3} \in [-5, 5]$, $\delta\hat{\varphi}_{4,5\ell,6} \in [-20, 20]$, $\delta\hat{\varphi}_{6\ell,7} \in [-30, 30]$, and for the post-inspiral parameters, $[-20, 20]$. We use the following prior ranges for FTI: $\delta\hat{\varphi}_{-2} \in [-1, 1]$ ($[-0.01, 0.01]$ for GW230518_125908) and $\delta\hat{\varphi}_i \in [-20, 20]$ for all other parameters. These broad priors are chosen to avoid prior-railing issues (i.e., significant posterior probability density right up to at least one prior boundary), which often arise from degeneracies between the deviation parameters and the GR parameters. Since the priors we use are wide enough to avoid truncating the posterior, the exact choice of range does not impact the

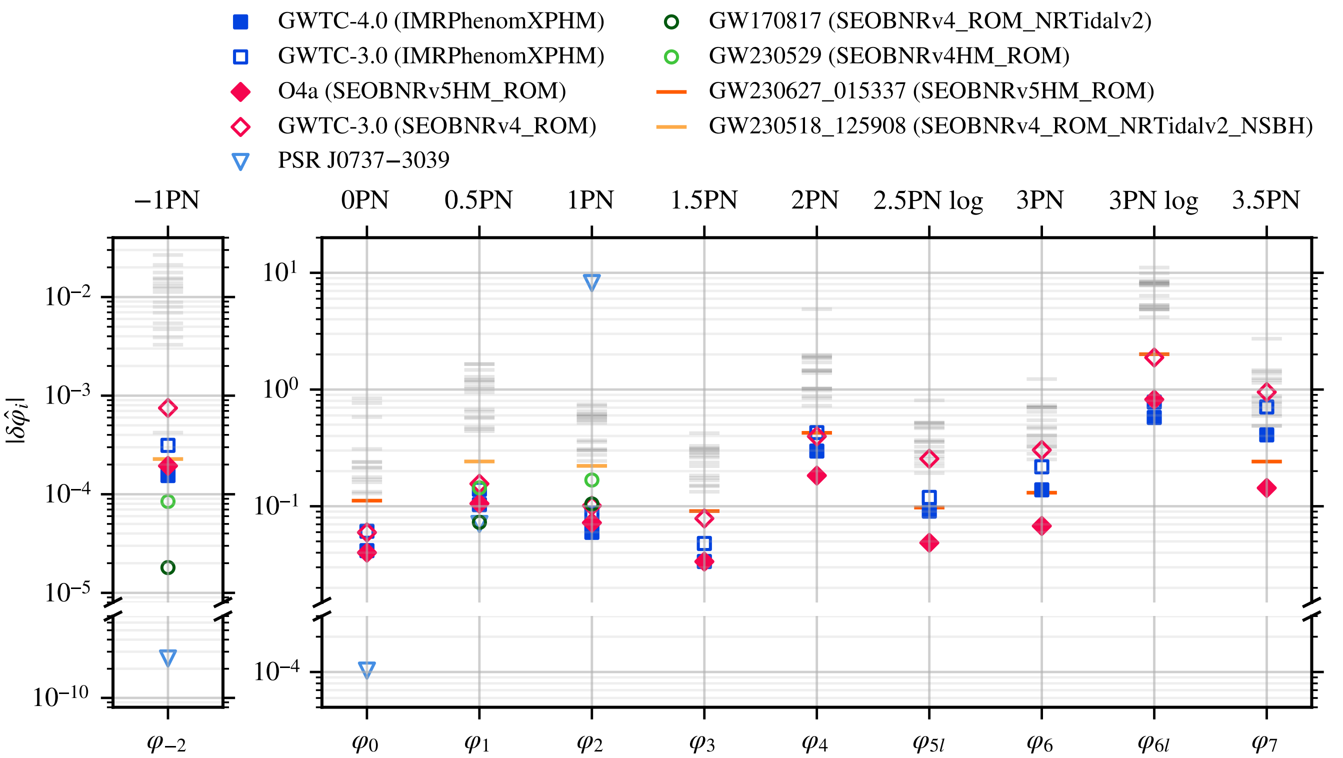

Figure 1. Results for the magnitudes of the inspiral deviation coefficients (from −1PN to 3.5PN) in terms of 90% upper limits, compared with previous combined results from GWTC-3.0 (Abbott et al. 2025), including the updates to use the IMRPHENOMXPHM waveform model for the TIGER results. The horizontal stripes mark the results from individual events obtained with the SEOBNRV5HM_ROM waveform model using the FTI analysis. Marginalizing over all results from O4a (GWTC-3.0), while assuming that all events share the same values for the violation coefficients, results in the filled (unfilled) red diamonds for the SEOBNRV5HM_ROM (SEOBNRV4_ROM) waveform model. These bounds cannot be directly compared due to changes in the tapering frequency and waveform model used in the analysis. Marginalizing over all results from GWTC-4.0 (GWTC-3.0) for the TIGER analysis using the IMRPHENOMXPHM waveform model results in the filled (unfilled) blue squares. The dark and light orange stripes highlight BBH GW230627_015337 and NSBH GW230518_125908, respectively, when they give the best individual event constraints on the inspiral parameters. The green circles show the bounds obtained with BNS GW170817 (Abbott et al. 2019b) and NSBH GW230529 (Sänger et al. 2026) when competitive; those two events are not included in the combined bounds. The blue upside-down triangles indicate bounds obtained with the double pulsar J0737−3039 (Kramer et al. 2021) when competitive. Starting from 1.5PN the pulsar bounds get much worse than the bounds from GWs and are therefore not shown.

constraints on deviation parameters, though it does impact the values of Bayes factors (quoted below for TIGER).

The FTI test is only applied to events that have a significant inspiral signal. The inspiral part of the signal is in this case defined in the frequency domain as the frequencies up to the tapering frequency used. The selection criteria are then a signal-to-noise ratio (SNR) of at least 10 in the inspiral and at least 5 GW cycles in the inspiral to ensure there is enough inspiral signal. The inspiral SNR and cycles are calculated using the maximum likelihood parameters from the GR analysis (Abac et al. 2026a) with IMRPHENOMXPHM. In the TIGER analysis, we impose an SNR threshold of greater than 6 in the inspiral part of the signal to select an event for testing inspiral phasing coefficients. An identical criterion is applied in the post-inspiral regime to determine whether an event qualifies for the analysis of post-inspiral phasing coefficients. Following the prescription of the IMRPHENOMXAS model, we use the $(2, 2)$ multipole frequency at the minimum energy circular orbit (MECO; Cabero et al. 2017) to divide the waveform between the inspiral and post-inspiral regimes. (There are small corrections to the MECO used to obtain the exact end-of-inspiral frequency in IMRPHENOMXAS, but these are less than a 3% correction for the range of mass ratios and spins allowed by our priors.) This prescription gives an end-of-inspiral frequency that is between 1.4 and 3.6 times smaller than the one used by FTI, with the largest differences occurring for negative effective inspiral spins (defined in Abac et al. 2025a). The median SNR values are computed using posterior samples obtained from the standard GR analysis with the IMRPHENOMXPHM model.

For the TIGER part, we also analyze the GWTC-3.0 events using the new IMRPHENOMXPHM-based framework (Roy et al. 2026). We keep the same event-selection criteria as in the GWTC-2.0 tests of GR paper (Abbott et al. 2021b).

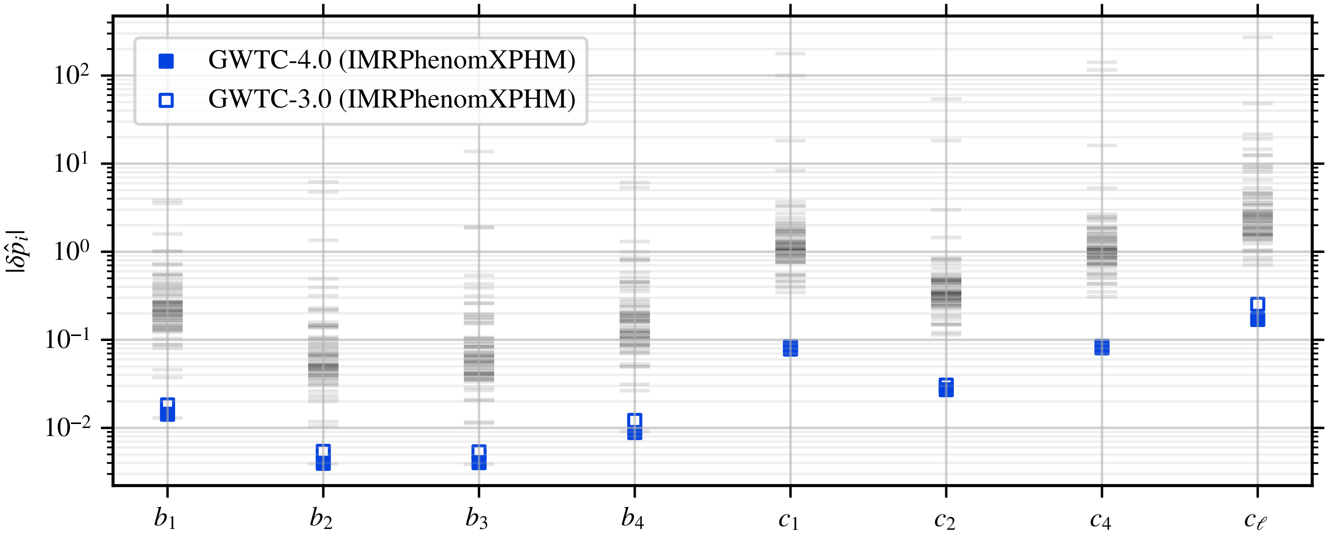

Figure 2. Results for the magnitudes of the post-inspiral deviation coefficients using TIGER. The horizontal stripes mark the results from individual events obtained with the IMRPHENOMXPHM waveform model. Marginalizing over all analyzed events in GWTC-4.0 (GWTC-3.0), while assuming that all events share the same values for the violation coefficients, results in the filled (unfilled) blue squares.

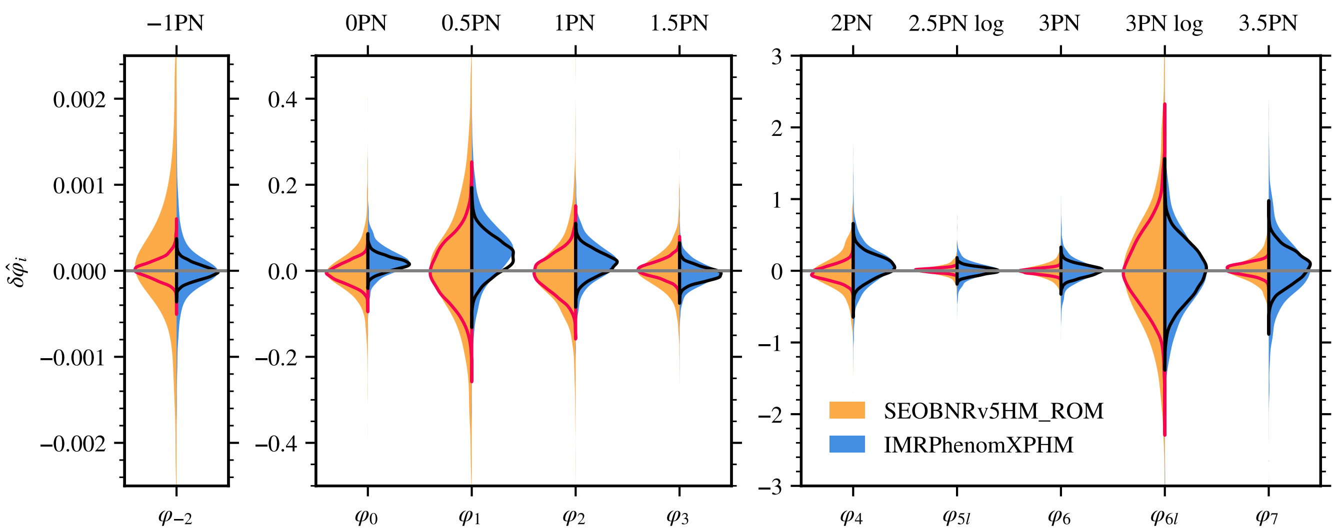

Figure 3. The constraints on the GR violation parameters in the inspiral, marginalized over all analyzed events, in orange on the left for the SEOBNRV5HM_ROM waveform model (FTI analysis) and in blue on the right for the IMRPHENOMXPHM waveform model (TIGER analysis). Consistency of GR corresponds to vanishing parameters (the horizontal line). Assuming independent violation parameters between events, using a hierarchical analysis, results in the filled probability densities. Instead, assuming that the violation parameters share the same values between different events leads to the unfilled distributions.

GW170809 was not included in the GWTC-2.0 TIGER inspiral analysis. This event does not meet the selection criteria when using IMRPHENOMPV2, but it passes them when using the IMRPHENOMXPHM posterior samples from GWTC-2.1 (Abbott et al. 2024). However, we leave its possible inclusion in the TIGER inspiral analysis to a future publication. GW191109_010717 was excluded from the combined analysis despite meeting the post-inspiral selection criteria. We found apparent deviations for this event, similar to the findings reported in the GWTC-3.0 tests of GR paper (Abbott et al. 2025), with the apparent tension explained as being driven by data-quality issues in both LIGO detectors rather than by genuine departures from GR. For GW190728_064510, we find apparent tension in the lower-PN coefficients when analyzing it using the IMRPHENOMXPHM version of TIGER. However, we also find similar behavior when analyzing simulated signals added to real-noise and conclude that the apparent tension is likely caused by noise-induced fluctuations that the analysis including higher multipole moments is more sensitive to rather than evidence for a departure from GR. This is further discussed in Appendix A.

The results for the inspiral deviation parameters $\delta\hat{\varphi}_i$ are consistent with GR for all events analyzed. There are two events where GR is outside the 90% credible interval for some parameters for FTI. For the parameters with the largest deviations, GR is still found within the 92.7% credible interval for GW230628_231200 and the 98.2% credible interval for GW231110_040320. However, for GW230628_231200, TIGER finds the GR value within the 90% credible interval for the inspiral parameters, though it is found outside that interval for some post-inspiral parameters, but still within the 94.3% credible interval. For GW231110_040320, TIGER finds that GR lies outside the 90% credible interval for all the inspiral parameters except -1PN, and for all of the intermediate parameters. However, GR is still found within the 98.9% credible interval. Additionally, the TIGER Bayes factors prefer GR for both events for all the deviation parameters. In general, we expect to find GR outside the 90% credible interval for a few events due to noise fluctuations, given the number of events under consideration.

For four of the events, namely GW230518_125908, GW231020_142947, GW231104_133418, and GW231113_200417, we were unable to obtain constraints on the 0PN deviation parameter for FTI. These are all low-mass events with low SNR where strong correlations between $\delta\hat{\varphi}_0$ and the chirp mass lead to problems in the analysis (Sänger et al. 2026). The higher tapering frequency in FTI, compared to the lower end-of-inspiral frequency in TIGER, implies that this degeneracy is stronger for FTI. The TIGER results do not show this issue for these events, except for GW230518_125908 and one O3b event, GW200115_042309. This is likely because the lower cutoff frequency leaves a few unmodified GW cycles in band that break the degeneracy. The exceptional behavior in these two events is specifically due to a strong degeneracy between $\delta\hat{\varphi}_0$ and the chirp mass, leading to a significantly larger chirp mass compared to the GR case and, consequently, to an apparent deviation in the 0PN term with a positive value, as seen in Sänger et al. (2026). The FTI analysis of GW200115_042309 in Abbott et al. (2025) also exhibits a degeneracy with the chirp mass, resulting in a bias in the posterior distribution of the 0PN deviation parameter. Since a lower tapering frequency was used in that analysis, the bias was less severe, and the event was not excluded from the combined analysis.

The deviation parameters at other PN orders can also show significant correlations with the intrinsic parameters. How strong these correlations are depends on the PN order and where in parameter space the system is. In particular, the correlations are strongest at the order a given parameter first appears, so $\delta\hat{\varphi}_2$ for the mass ratio and $\delta\hat{\varphi}_3$ for spins in addition to $\delta\hat{\varphi}_0$ and the chirp mass. However, these correlations are not as strong as is the case for the $\delta\hat{\varphi}_0$–chirp mass degeneracy for low mass systems, and higher SNR events usually show smaller correlations. We therefore do not experience any

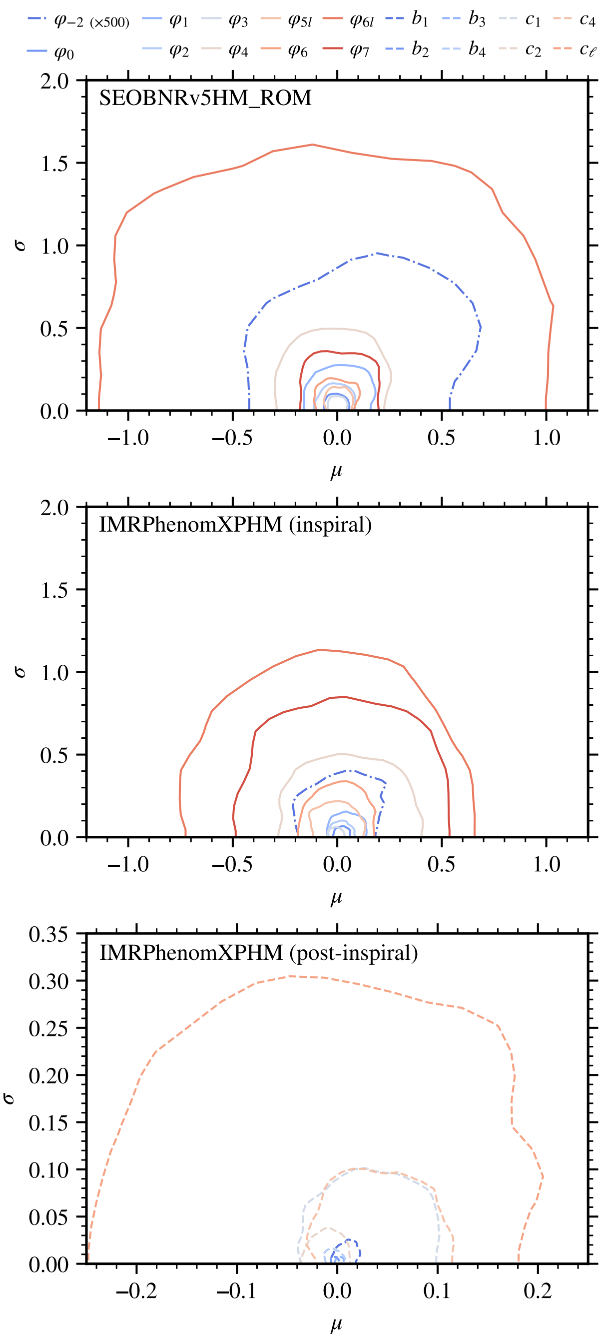

Figure 4. Inferred hyperparameters μ and σ of the GR violation coefficients. For each testing coefficient, the contours mark 90% credible regions. The inspiral parameters for the two waveform models SEOBNRv5HM_ROM (using the FTI analysis) and IMRPhenomXPHM (using the TIGER analysis) are considered in the top and middle panel respectively. The bottom panel shows the post-inspiral parameters for the IMRPhenomXPHM waveform model. All contours enclose the GR expectation of $\mu = \sigma = 0$; the $\delta\hat{\varphi}_{-2}$ values are rescaled $\times 500$ to improve visibility.

problems with sampling for other PN deviation parameters or higher mass systems.

TIGER finds the GR value near the boundary of 90% credibility for the high-mass event GW231028_153006, where the GR analysis (Abac et al. 2026a) finds significant systematic modeling uncertainties. As discussed in Appendix B, we find that the largest shifts away from GR (for the intermediate coefficients) are likely attributable to waveform modeling uncertainties, but the smaller shifts for the merger–ringdown coefficients seem instead to be attributable primarily to a prior effect.

In Figure 1, we show the 90% upper bounds on the magnitude of the PN deviation parameters in the inspiral; the analogous plot for the TIGER post-inspiral coefficients is Figure 2. The bounds for individual events obtained with FTI are shown as grey stripes. We highlight the event GW230627_015337, which is the BBH signal that gives the best constraints. This event is particularly good for inspiral tests of GR because its low masses means there is a long inspiral while it also has a relatively high SNR of $28.5^{+0.1}_{-0.1}$. We also show the bounds for the BNS GW170817 (Abbott et al. 2019b) and NSBH GW230529_181500 (abbreviated to GW230529; Sänger et al. 2026) for comparison when their bounds are competitive. GW230529 does not meet the selection criteria for inclusion in this paper because it was detected by only one detector and therefore is excluded from the combined results we present here. The high-SNR single-detector event GW230814_230901 (Abac et al. 2026d) is not shown, however, since its bounds do not stand out compared to those of other events, though the more recent even higher-SNR event GW250114 (Abac et al. 2025b) from the second part of the fourth observing run (O4b) does provide even better constraints on its own (Abac et al. 2026e).

We also show the combined bounds for both FTI and TIGER obtained under the assumption that deviations have the same value for each event. When combining events, we exclude the BNS GW170817 due to the different nature of its source. For comparison, we also include the combined FTI and TIGER results from previous catalogs. For TIGER, we plot the updated results from the reanalysis of GWTC-3.0 using the IMRPhenomXPHM version of TIGER (Roy et al. 2026), though there are no TIGER results in the GWTC-3.0 paper (Abbott et al. 2025). All combined bounds improve with the largest improvements seen for FTI for the high-PN parameters. As discussed before, the change in tapering frequency is contributing to this improvement. The list of events included in the combined bounds is different between FTI and TIGER, making it impossible to directly compare the combined bounds between the two. The differences between the bounds for individual events from FTI and TIGER should be seen as an estimate for the systematic uncertainties that can be expected from inspiral tests, with FTI pushing the transition from inspiral to post-inspiral to the highest possible frequency and TIGER providing more conservative bounds. The best bound from GWs at -1PN is still from GW170817, and is an order of magnitude better than the combined constraints from O4a (FTI) or GWTC-4.0 (TIGER).

It is also possible to put constraints on the PN deviation parameters using binary pulsars (Yunes & Hughes 2010; Nair & Yunes 2020). The best overall bound on dipole radiation comes from the double pulsar PSR J0737$-$3039A/B (Kramer et al. 2021), with a 90% upper bound corresponding to $|\delta\hat{\varphi}_{-2}| \leq 2.6 \times 10^{-10}$. This double pulsar also puts the most stringent constraint on deviations from GR at Newtonian order with $|\delta\hat{\varphi}_0| \leq 1.0 \times 10^{-4}$. At 0.5PN, the double pulsar bound is $|\delta\hat{\varphi}_1| \leq 7.0 \times 10^{-2}$, which is on par with the bound from GW170817. From 1PN onwards the bounds from the double pulsar are less constraining than the bounds from GWs. The bounds from PSR J0737$-$3039A/B are shown as blue upside-down triangles in Figure 1.

The combined posteriors for the inspiral deviation parameters are shown in Figure 3 (unfilled violins) and are consistent with GR at the 90% credible level for all parameters. The combined posteriors are dominated by GW230627_015337 because of its tight constraints. The posteriors for this event are centered around zero, a trait inherited by the displayed combined posteriors. This is reflected in the GR quantiles shown in Table 2 being between 40% and 60%. Here the GR quantile is defined as the fraction of samples with $\delta\hat{\varphi}_i < 0$, so a posterior perfectly centered on GR gives a quantile of 50%. We also combined the posteriors from the different events using a hierarchical approach to get the combined posteriors shown in Figure 3 (filled violins). This approach allows the deviation parameters to take independent values for each event, modeling their distribution as a Gaussian described by a mean μ and standard deviation σ. We again see that the posteriors are consistent with GR at the 90% credible level for all PN deviation parameters. The 90% contours for the hyperparameters μ and σ of the hierarchical approach are shown in Figure 4 for each PN deviation parameter. GR corresponds to $\mu = \sigma = 0$, which is enclosed by the contours for all inspiral parameters. The medians, 90% credible intervals, and GR quantiles for all $\delta\hat{\varphi}_i$ and both approaches to combine results are listed in Table 2, as well as the medians and 90% credible intervals for μ and the 90% upper limits on σ.

Figure 2 shows the 90% upper bounds on the magnitude of the post-inspiral deviation parameters obtained with TIGER for each O4a event (grey stripes). The blue squares are the bounds obtained by combining all events assuming that deviations have the same value for each event. Figure 5 shows the combined posteriors for the post-inspiral parameter obtained with both the restricted (unfilled violins) and hierarchical (filled violins) approaches. The 90% contours for the hyperparameters of the hierarchical analysis are shown in the bottom panel of Figure 4. Table 2 gives the median and 90% credible intervals on the post-inspiral deviation parameters for the combined constraints using both approaches, as well as the medians and 90% credible intervals for μ and the 90% upper limits on σ. All results for the TIGER post-inspiral parameters are consistent with GR at the 90% credible level.

The improvement in the combined post-inspiral TIGER constraints from GWTC-3.0 to GWTC-4.0 is not as significant as that found for the inspiral coefficients. The combined post-inspiral constraints are mostly dominated by the

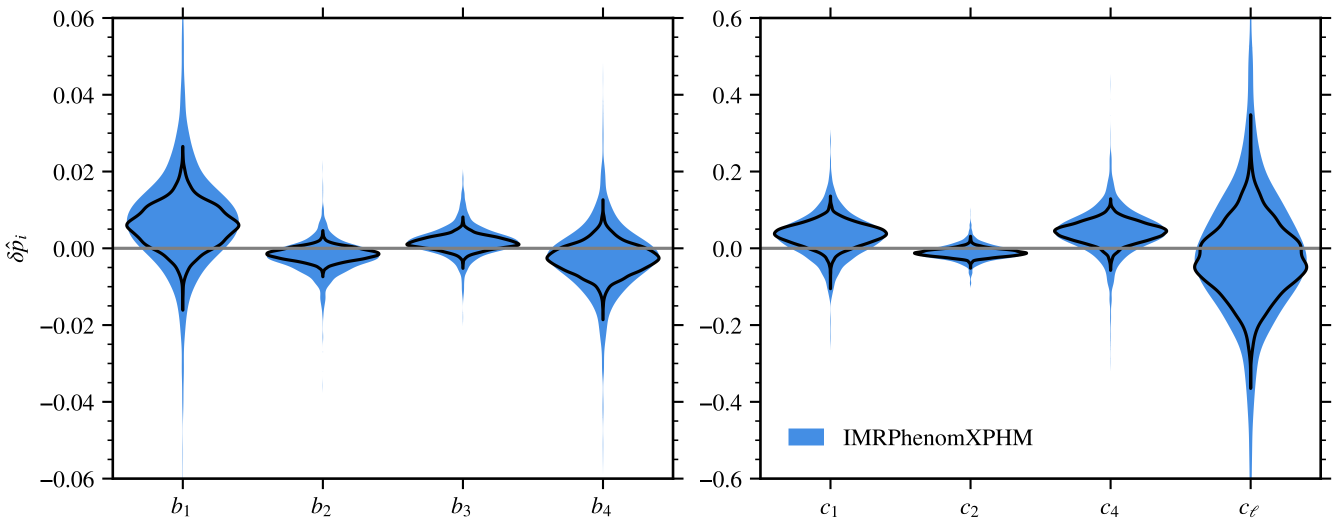

Figure 5. The constraints on the GR violation parameters in the post-inspiral using TIGER, marginalized over all analyzed events in GWTC-4.0. Consistency of GR corresponds to vanishing parameters (the horizontal line). Assuming independent violation parameters between events, using a hierarchical analysis, results in the colored probability densities. Instead, assuming that the violation parameters share the same values between different events leads to the unfilled distributions.

O3a events GW190412 and GW190814, which provide the strongest bounds among the analyzed events for most coefficients. Thus, the addition of O4a events does not lead to a large improvement, even though 31 out of the 66 events in the combined analysis are from O4a. For the TIGER inspiral coefficients, the improvement is instead largely driven by the O4a events GW230518_125908 and GW230627_015337, which enable significantly tighter constraints on several PN coefficients. If these two events are removed from the combined inspiral analysis, the improvement becomes comparable to what is found for the post-inspiral analysis.

A useful framework for interpreting agnostic PN deformation tests is the parameterized post-Einsteinian (ppE) formalism, which provides a systematic description of leading deviations from general relativity in the gravitational waveform phase and amplitude (Yunes & Pretorius 2009; Cornish et al. 2011). In this approach, deviations are introduced as power-law corrections at specific PN orders, allowing one to connect agnostic constraints on PN coefficients to a broad class of modified gravity theories.

To provide intuition for the meaning of the agnostic constraints on deviations in the PN coefficients we have obtained, we thus follow the ppE formalism and perform event-by-event illustrative mappings of the inferred PN deformation posteriors onto parameters appearing in selected modified gravity theories, with the translation for the event that provides the best result for each mapping given in Table 3. The example theories considered are: scalar–tensor theories with an evolving scalar field (Jacobson 1999; Horbatsch & Burgess 2012), Einstein–dilaton–Gauss–Bonnet (EdGB; Gross & Sloan 1987; Kanti et al. 1996), dynamical Chern–Simons (dCS; Alexander & Yunes 2009), Einstein–Maxwell with black hole charge, and dirty black holes or pseudo-complex GR (Hess & Greiner 2009; Caspar et al. 2012; Hess 2016; Maimon et al. 2025).

These mappings should not be interpreted as theory-specific statistical constraints, but rather as illustrative translations of agnostic deviations into the language of particular models, obtained under simplifying assumptions (e.g., leading-order modifications and no deviations in the merger-ringdown phase).

Importantly, each mapping is performed independently for each GW event using the corresponding posterior samples of both intrinsic binary parameters and the agnostic PN deformation parameter, with consistent reweighting to account for prior differences.

In order to map a PN parameter constraint to a parameter in a given theory, we map use the posteriors of the PN coefficient constraint along with the intrinsic parameters for each analyzed O4a event and the PN expressions derived to leading order in Yagi et al. (2012a) for EdGB, Yagi et al. (2012a,b) for dCS gravity, Khalil et al. (2018) for Einstein–Maxwell with black hole charge, Nielsen & Birnholtz (2018) for pseudo-complex GR, and Horbatsch & Burgess (2012); Yunes et al. (2016) for scalar–tensor theories with an evolving scalar field.

The mapping on theories we quote in Table 3 are the 90% result for the O4a GW event that gives the tightest translation on a given parameter. For comparison, we also provide existing bounds or illustrative translations on each theory. Current constraints on scalar–tensor theories come from observations of the quasar OJ 287 (Horbatsch & Burgess 2012). For EdGB gravity and Einstein–Maxwell, the strongest bound arises from the low-mass, long-inspiral signal GW230529 (Sänger et al. 2026, not included here because it is a single-detector event). For dCS gravity, the current bound of 8.5 km comes from combining NICER observations of a pulsar with the NS tidal deformability inferred from the binary NS event GW170817 (Silva et al. 2021).

Table 2. Results from parametrized tests of GW generation

p_i	pipeline	waveform	Hierarchical				Restricted	
			μ	σ	$\delta\hat{\varphi}_i$	$Q_{\rm GR}$	$\delta\hat{\varphi}_i$	$Q_{\rm GR}$
φ_{-2} $(\times 500)$	FTI	EOB	$0.06^{+0.47}_{-0.27}$	< 0.66	$0.05^{+0.81}_{-0.57}$	40%	$0.01^{+0.10}_{-0.08}$	44%
	TIGER	Phenom	$-0.00^{+0.17}_{-0.13}$	< 0.31	$-0.00^{+0.32}_{-0.28}$	52%	$-0.01^{+0.07}_{-0.07}$	57%
φ_0	FTI	EOB	$0.00^{+0.05}_{-0.04}$	< 0.08	$0.00^{+0.09}_{-0.09}$	54%	$-0.01^{+0.04}_{-0.04}$	59%
	TIGER	Phenom	$0.02^{+0.03}_{-0.03}$	< 0.05	$0.02^{+0.06}_{-0.05}$	22%	$0.02^{+0.03}_{-0.02}$	14%
φ_1	FTI	EOB	$0.01^{+0.13}_{-0.12}$	< 0.22	$0.01^{+0.24}_{-0.24}$	46%	$0.00^{+0.11}_{-0.11}$	50%
	TIGER	Phenom	$0.05^{+0.07}_{-0.07}$	< 0.12	$0.05^{+0.13}_{-0.14}$	23%	$0.03^{+0.07}_{-0.07}$	20%
φ_2	FTI	EOB	$-0.01^{+0.07}_{-0.07}$	< 0.13	$-0.01^{+0.13}_{-0.13}$	55%	$-0.01^{+0.06}_{-0.07}$	57%
	TIGER	Phenom	$0.02^{+0.05}_{-0.05}$	< 0.07	$0.02^{+0.08}_{-0.08}$	30%	$0.02^{+0.04}_{-0.04}$	26%
φ_3	FTI	EOB	$0.00^{+0.04}_{-0.03}$	< 0.07	$0.00^{+0.08}_{-0.08}$	51%	$0.00^{+0.03}_{-0.03}$	43%
	TIGER	Phenom	$-0.01^{+0.03}_{-0.03}$	< 0.05	$-0.01^{+0.05}_{-0.05}$	61%	$-0.01^{+0.03}_{-0.03}$	69%
φ_4	FTI	EOB	$-0.02^{+0.21}_{-0.19}$	< 0.40	$-0.02^{+0.45}_{-0.43}$	54%	$-0.03^{+0.16}_{-0.15}$	62%
	TIGER	Phenom	$0.06^{+0.25}_{-0.25}$	< 0.40	$0.07^{+0.45}_{-0.45}$	37%	$0.06^{+0.24}_{-0.25}$	34%
φ_{5l}	FTI	EOB	$0.01^{+0.05}_{-0.05}$	< 0.11	$0.01^{+0.13}_{-0.12}$	45%	$0.01^{+0.04}_{-0.05}$	40%
	TIGER	Phenom	$0.00^{+0.09}_{-0.11}$	< 0.17	$0.01^{+0.18}_{-0.21}$	46%	$0.00^{+0.08}_{-0.09}$	52%
φ_6	FTI	EOB	$0.00^{+0.09}_{-0.08}$	< 0.15	$0.00^{+0.18}_{-0.18}$	51%	$-0.01^{+0.06}_{-0.06}$	58%
	TIGER	Phenom	$0.00^{+0.14}_{-0.13}$	< 0.26	$0.00^{+0.28}_{-0.29}$	50%	$0.00^{+0.13}_{-0.14}$	50%
φ_{6l}	FTI	EOB	$-0.04^{+0.79}_{-0.81}$	< 1.23	$-0.01^{+1.45}_{-1.40}$	51%	$0.01^{+0.83}_{-0.75}$	49%
	TIGER	Phenom	$-0.04^{+0.54}_{-0.54}$	< 0.86	$-0.04^{+0.94}_{-1.00}$	54%	$0.00^{+0.55}_{-0.60}$	50%
φ_7	FTI	EOB	$0.01^{+0.15}_{-0.14}$	< 0.29	$0.01^{+0.33}_{-0.34}$	47%	$0.03^{+0.11}_{-0.12}$	38%
	TIGER	Phenom	$0.03^{+0.38}_{-0.39}$	< 0.66	$0.02^{+0.77}_{-0.78}$	48%	$0.06^{+0.35}_{-0.35}$	40%
b_1 $(\times 10)$	TIGER	Phenom	$0.08^{+0.11}_{-0.10}$	< 0.19	$0.07^{+0.22}_{-0.18}$	23%	$0.06^{+0.09}_{-0.09}$	13%
b_2 $(\times 10)$	TIGER	Phenom	$-0.02^{+0.03}_{-0.03}$	< 0.06	$-0.02^{+0.06}_{-0.07}$	76%	$-0.01^{+0.02}_{-0.03}$	83%
b_3 $(\times 10)$	TIGER	Phenom	$0.02^{+0.04}_{-0.03}$	< 0.06	$0.02^{+0.07}_{-0.06}$	26%	$0.01^{+0.03}_{-0.03}$	18%
b_4 $(\times 10)$	TIGER	Phenom	$-0.03^{+0.07}_{-0.08}$	< 0.12	$-0.02^{+0.13}_{-0.14}$	65%	$-0.03^{+0.06}_{-0.06}$	78%
c_1	TIGER	Phenom	$0.03^{+0.05}_{-0.06}$	< 0.08	$0.03^{+0.09}_{-0.09}$	25%	$0.04^{+0.04}_{-0.05}$	9%
c_2	TIGER	Phenom	$-0.01^{+0.02}_{-0.02}$	< 0.03	$-0.01^{+0.03}_{-0.03}$	75%	$-0.01^{+0.02}_{-0.01}$	89%
c_4	TIGER	Phenom	$0.04^{+0.05}_{-0.06}$	< 0.08	$0.04^{+0.08}_{-0.09}$	17%	$0.04^{+0.04}_{-0.04}$	5%
c_ℓ	TIGER	Phenom	$-0.02^{+0.17}_{-0.16}$	< 0.24	$-0.02^{+0.29}_{-0.27}$	56%	$-0.03^{+0.15}_{-0.14}$	64%

NOTE—Combined constraints on the deviation parameters obtained by marginalizing over all analyzed events in GWTC-4.0 using the analyses FTI (which uses the SEOBNRv5HM_ROM waveform) and TIGER (which uses the IMRPhenomXPHM and IMRPhenomPv2 waveforms). Hierarchical (restricted) constraints are obtained under the assumption that deviation coefficients can (cannot) vary across the observed events. The one-sided quantile corresponding to the GR value for the distributions plotted in Figures 3 and 5 is indicated by $Q_{\rm GR}$. For hierarchical constraints, we also provide the mean μ and standard deviation σ of the inferred hyperdistribution. For $\delta\hat{\varphi}_i$ and μ, we report the median as well as the 90%-credible intervals, while for σ we only present 90% upper bounds. We scale the φ_{-2} and b_i entries to display the bounds with only two decimal places (for b_1 and b_4 without rounding up). For φ_{-2}, we use the same scaling as in Figure 4.

The expression from Horbatsch & Burgess (2012) used to obtain the translation to the evolution of the scalar field in the scalar–tensor case requires $\epsilon_{\rm ST} = 2Gm_1|\dot{\phi}|/c^3 \ll 1$. While $|\dot{\phi}|$ in our translation is large in units of $\rm s^{-1}$, the 90% upper bound on $\epsilon_{\rm ST}$ is 0.077 and 0.070 for TIGER and FTI respectively, which are smaller than the value of 0.13 for the primary of OJ 287 used to obtain the constraints in Horbatsch & Burgess (2012). The much better constraints on $|\dot{\phi}|$ from OJ 287 are due to its much larger total mass (its primary's mass is $\sim 10^{10} M_\odot$). Additionally, the assumptions made in obtaining the frequency-domain dephasing used in the translation assume that the dipole radiation is a small perturbation to the quadrupole radiation (as discussed in, e.g., Yunes & Pretorius 2009), but this is also the case here: The 90% upper

Table 3. Illustrative mappings of agnostic constraints on PN coefficients onto parameters of selected modified gravity theories for the event that gives the best result for each mapping

Theory	φ_i	Parameter	FTI mapping	TIGER mapping	Existing constraint/mapping
Scalar–tensor	φ_{-2}	$\lvert\dot{\phi}\rvert$ [s^{-1}]	1.1×10^3	1.1×10^3	10^{-6} (Horbatsch & Burgess 2012)
Einstein–dilaton–Gauss–Bonnet	φ_{-2}	$\sqrt{\alpha_{\rm EdGB}}$ [km]	0.98	1.07	0.28 (Sänger et al. 2026)
Einstein–Maxwell	φ_{-2}	$\zeta = \left\lvert \frac{q_1}{m_1} - \frac{q_2}{m_2} \right\rvert$	0.047	0.052	0.024 (Gao et al. 2024)
pseudo-complex GR $n = 2$	φ_4	b_c/b	0.34	0.15	0.10 (FTI), 0.07 (TIGER)†
pseudo-complex GR $n = 3$	φ_6	b_c/b	0.25	0.07	0.05 (FTI), 0.05 (TIGER)†

NOTE— The values shown are mappings of posteriors on agnostic PN deformation parameters (from FTI and TIGER analyses) into 90% credibility results for parameters in modified gravity theories for the event that gives the best result for each mapping. These mappings are performed independently for each O4a event using posterior samples for the intrinsic binary parameters along with the agnostic PN deformation parameter, and includes consistent prior reweighting. The results therefore reflect how agnostic constraints project onto theory parameters under simplifying assumptions, rather than a joint or theory-specific inference. Specifically the binary parameters used for the translations involving φ_{-2} are those of GW230518_125908, which provide the best results, while for pseudo-complex GR, GW230627_015337 provides the best results for all but TIGER φ_6, where GW230919_215712 provides the best result, so those events' parameters are used. Additionally, for pseudo-complex GR, we give the best illustrative translations for O3b events, for comparison, using the results from Abbott et al. (2025) for FTI and our reanalysis in this paper for TIGER. The O3b translations come from GW191204_171526, except for FTI φ_4, which comes from GW191216_213338. We mark those entries as a dagger to call attention to their status as only illustrative translations, compared to the bounds given for other theories. All these translations should not be interpreted as statistical constraints on the underlying theories, nor as exclusions. In particular, real modified gravity theories generically induce correlated deviations across multiple PN coefficients and modify the merger–ringdown signal, effects not included in this mapping. The table is therefore intended only to provide intuition about the agnostic PN bounds we have obtained by showing how they would translate to the parameters of some commonly considered alternative theories, together with constraints on those parameters from the literature. For pseudo-complex GR, larger values correspond to better constraints and a b_c/b bound above 1 rules out horizonless objects for that n in this model (Maimon et al. 2025).

bounds on the ratio of the leading dipole to quadrupole energy fluxes are 0.062 and 0.053 for TIGER and FTI at the low-frequency cutoff of 20 Hz and decrease at higher frequencies. The GW event that gives rise to the tightest value for $|\dot{\phi}|$ is GW230518_125908, whose source is likely an NSBH. We assume that the NS secondary has a vanishing scalar charge, maximizing the amount of dipolar radiation emitted by the system.

Similarly, the PN expressions used for dCS and EdGB gravity are derived under the perturbative assumption that the dimensionless coupling $\zeta_{\rm dCS,EdGB} = 16\pi\alpha^2_{\rm dCS/EdGB}/\left(Gm_2/c^2\right)^4 \ll 1$ throughout the inspiral (Yagi et al. 2012a), where we have evaluated this quantity using m_2, since that sets the smallest length scale in the binary. Evaluating this condition for each theory, we find that although the translation for EdGB gravity satisfies the small-coupling requirement within the 90% credible region with a value for $\zeta_{\rm EdGB}$ of $\mathcal{O}(10^{-3})$, the dCS translation does not. Indeed, the dCS mapping gives a value ~ 4 times larger than the best current bounds on the theory (Silva et al. 2021), but the 90% upper bound on small-coupling parameter is $\mathcal{O}(10^4)$. As a result, the perturbative waveform is not self-consistent for the systems considered, and any inferred PN-to-theory translation for dCS gravity would lie outside the regime of validity of the effective field theory expansion. We therefore do not report a dCS entry in Table 3. In order to obtain constraints for dCS that are within small-coupling approximation from GW observations, one would need a low-mass binary with at least one rapidly spinning object.

The values given in Table 3 are for the purposes of illustration, and there are several caveats to them being directly taken as constraints on the specific theories. To begin with, a given modified gravity theory will give deviations in multiple PN parameters, while the analyses consider each PN parameter deviation in isolation. In addition, these analyses make use of the merger–ringdown signal, but without taking into account how a specific theory would modify that portion of the GW signal from GR. For instance, Johnson-McDaniel et al. (2022) analyzes phenomenological non-GR signals with FTI and TIGER, finding that these methods can yield constraints on a PN deviation parameter that are much smaller than the true deviation. Thus, these mappings will not be equivalent to those obtained with an analysis that assumes a specific theory.

2.2. *FTI and TIGER: Multiparameter PN coefficient tests with PCA*

The parametrized tests of GR aim to identify potential deviations by modifying the GW phasing with dimensionless deviation parameters. This approach is implemented in the FTI and TIGER frameworks, as discussed before. Focusing

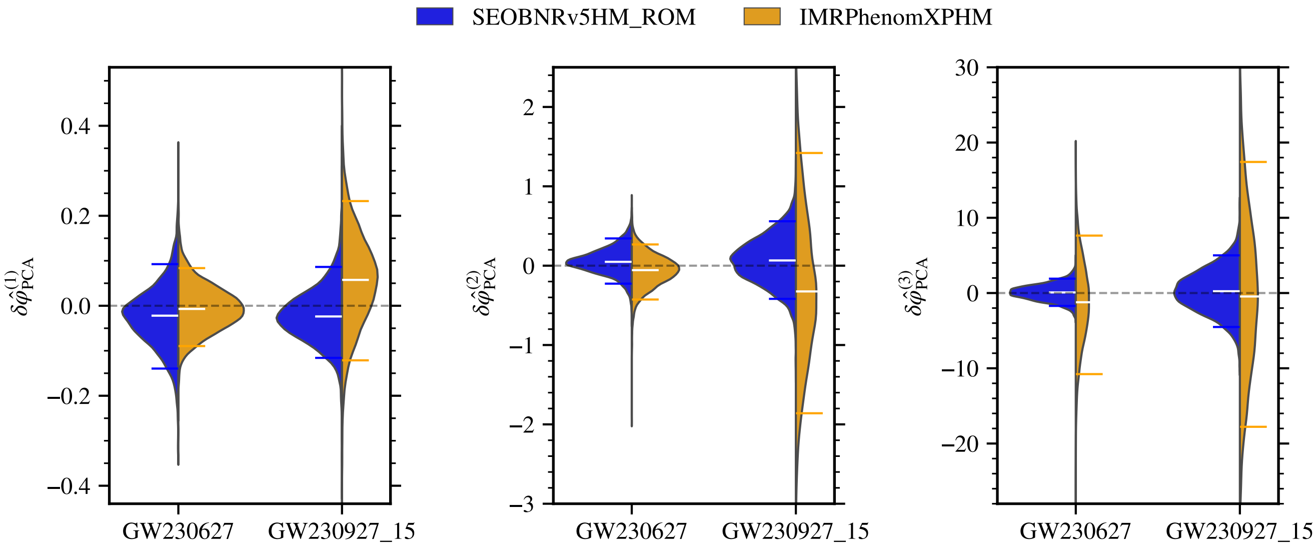

Figure 6. Violin plots showing the posterior probability distribution of the first three leading PCA parameters, from the O4a events listed in the PCA column of Table 1 (GW230627_015337 and GW230927_153832, abbreviated as GW230627 and GW230927_15), passing the selection criteria described in Section 2.2. In each violin plot, the colored horizontal bars and the horizontal white solid line denote the 90% credible intervals and the posterior median, respectively. We mark the GR value of zero with dashed grey lines.

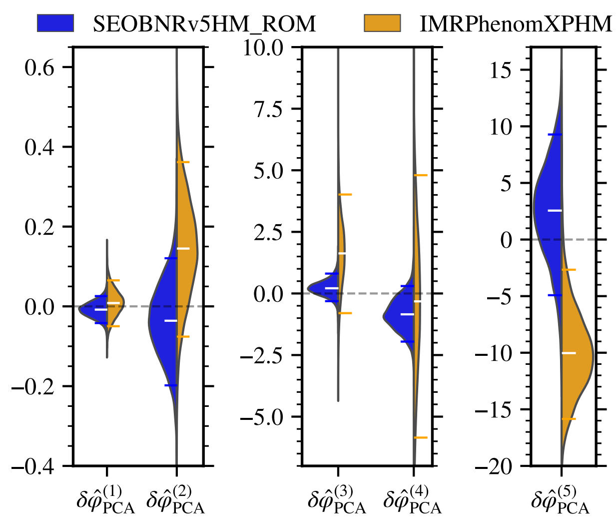

Figure 7. The joint posterior probability distributions on the first five leading PCA parameters from all the selected GWTC-4.0 events are shown. The joint bounds are obtained through the marginalized-likelihood multiplication technique. The markers have the same meaning as in Figure 6. All PCA parameters are statistically consistent with GR at the 90% credible level, except for the fifth parameter in the TIGER framework. This deviation may stem from instrumental noise features or from waveform-modeling systematic uncertainties.

on the inspiral part of the GW signal, the null parametrization $\delta\hat{\varphi}_i$ is introduced at each PN order, with i denoting the PN index, in Equation (2). Considering the inspiral phase up to the 3.5PN order with non-vanishing PN coefficients in GR gives rise to eight deviation parameters, i.e., by dropping $\delta\hat{\varphi}_{-2}$ and $\delta\hat{\varphi}_1$ in Equation (3). However, all the deviation parameters are not measured simultaneously since such *multi-parameter* tests give rise to uninformative posteriors. This is caused by the correlations between the deviation parameters and other GR parameters, which can be mitigated by increasing detector network sensitivity (Gupta et al. 2020; Datta et al. 2021) or by basing the parametrization on the radiative multipole moments (Kastha et al. 2018, 2019; Mahapatra 2024; Mahapatra & Kastha 2024; Mahapatra et al. 2024). While deviation from GR can occur at any PN order and hence the eight deviation parameters should be measured simultaneously, to avoid the aforementioned problem with uninformative posteriors, the FTI and TIGER analyses each perform eight *single parameter* tests, where only one deviation parameter is measured with the others being consistent with GR. However, we will instead use principal component analysis (PCA; Arun & Pai 2013; Pai & Arun 2013; Saleem et al. 2022; Shoom et al. 2023; Datta et al. 2024; Mahapatra et al. 2025) to identify the best-measured linear combinations of a set of PN deviation parameters. The bounds so obtained are more constraining than the single parameter tests since they contain the information from multiple PN orders.

In a multi-parameter test, along with the 15 GR parameters, the six deviation parameters, introduced from 1.5PN to 3.5PN, are included:

$$\{\delta\hat{\varphi}_3, \delta\hat{\varphi}_4, \delta\hat{\varphi}_{5\ell}, \delta\hat{\varphi}_6, \delta\hat{\varphi}_{6\ell}, \delta\hat{\varphi}_7\}\,, \tag{5}$$

with the assumption that $\{\delta\hat{\varphi}_0, \delta\hat{\varphi}_1, \delta\hat{\varphi}_2\}$, the leading-order PN deviation parameters, are consistent with GR. While current GW detectors are sensitive enough to distinguish lower-order fractional deviations from intrinsic binary parameters

Table 4. Combined constraints on the leading five PCA parameters from all selected GWTC-4.0 events

$\delta\hat{\varphi}^{(k)}_{\rm PCA}$	Median & 90% errors		GR quantile	
	FTI	TIGER	FTI	TIGER
$\delta\hat{\varphi}^{(1)}_{\rm PCA}$	$-0.01^{+0.04}_{-0.03}$	$0.01^{+0.06}_{-0.06}$	66%	41%
$\delta\hat{\varphi}^{(2)}_{\rm PCA}$	$-0.04^{+0.16}_{-0.16}$	$0.14^{+0.22}_{-0.22}$	64%	14%
$\delta\hat{\varphi}^{(3)}_{\rm PCA}$	$0.21^{+0.60}_{-0.52}$	$1.63^{+2.39}_{-2.43}$	24%	14%
$\delta\hat{\varphi}^{(4)}_{\rm PCA}$	$-0.85^{+1.15}_{-1.10}$	$-0.32^{+5.12}_{-5.53}$	88%	54%
$\delta\hat{\varphi}^{(5)}_{\rm PCA}$	$2.56^{+6.72}_{-7.48}$	$-10.03^{+7.36}_{-5.82}$	28%	98%

NOTE—We give the median, 90% credible intervals, and the GR quantile, i.e., $P(\delta\hat{\phi}^{(i)}_{\rm PCA} < 0)$, of the combined PCA posteriors.

in single-parameter tests for some events, in particular distinguishing 0PN and 1PN deviations from chirp mass and mass ratio, this is not the case for multi-parameter tests. Moreover, the -1PN and 0PN deviations are already well-constrained by binary pulsar measurements (Yunes & Hughes 2010; Nair & Yunes 2020; Kramer et al. 2021). Of course, constraints on the -1PN coefficient from BNSs are not directly applicable to BBH signals, since there are theories in which BHs scalarize (leading to dipole radiation at -1PN) and NSs do not (Yagi et al. 2012a, 2016). However, GW230529, whose source has at least one BH, has also placed fairly tight constraints on the -1PN coefficient (Sänger et al. 2026). Thus, our analysis focuses on a six-dimensional test with fractional deviation parameters ranging from 1.5PN to 3.5PN (Mahapatra et al. 2025). This results in a 21-dimensional parameter space; hence, these analyses are computationally expensive. After obtaining the marginalized posteriors on the six deviation parameters, we post-process the posteriors using PCA to transition to a new basis. This new basis is a linear combination of the original deviation parameters with suitable weights, expressed as

$$\delta\hat{\varphi}^{(k)}_{\rm PCA} = \sum_i \alpha^{ki}\delta\hat{\varphi}_i\,, \tag{6}$$

where the summation index runs over the six deviation parameters in Equation (5). The coefficient α^{ki} corresponds to elements of the transformation matrix that diagonalizes the covariance matrix (Arun & Pai 2013; Pai & Arun 2013; Saleem et al. 2022; Datta et al. 2024; Mahapatra et al. 2025). Hence, shifting to the PCA basis reduces the correlations and provides better constraints. The PN coefficients that contribute relatively more to the observed inspiral signal have better-constrained fractional deviation parameters and therefore contribute dominantly to the leading informative PCA components, making the PCA method sensitive to the relative normalization of the different deviation parameters. PCA has inherent sign ambiguity because the direction of eigenvectors is not uniquely determined; their signs can be flipped without affecting the variance they explain. To resolve this, we adopt a sign convention where each eigenvector and each principal component is adjusted so that the largest element is always positive (Mahapatra et al. 2025).

We implement the PCA on GW events observed during the O4a run that meet specific selection criteria and constrain the deviations from GR. Due to the high computational cost of multi-parameter runs, we use strict selection criteria of inspiral SNR ≥ 14.5 and detector-frame chirp mass $(1+z)\mathcal{M} < 20.5M_\odot$ to ensure longer inspiral signals. The inspiral SNR in the FTI and TIGER frameworks is defined in Section 2.1. For chirp mass, we use the median of the chirp mass posterior from the GR analysis with IMRPhenomXPHM. Imposing this criterion results in two qualifying events from O3a (GW190412 and GW190814), two from O3b (GW191204_171526 and GW191216_213338), and two from O4a (GW230627_015337 and GW230927_153832) selected for PCA analysis in both the FTI and TIGER frameworks.

We perform a multi-parameter run on the selected events using the parametrized extension of the SEOBNRv5HM_ROM waveform for FTI and the IMRPhenomXPHM waveform for TIGER, as in the single-parameter analyses in Section 2.1. Both waveforms give consistent results in the PCA basis. In Figure 6, we show the violin plots of the posterior probability distributions for the first three leading PCA parameters corresponding to the selected O4a events. The results from PCA analysis on the O3a and O3b events are presented in Mahapatra et al. (2025). We restrict our attention to the first three PCA parameters since they carry the most information. The higher-order PCA parameters receive relatively larger contributions from those original deviation parameters that have uninformative posteriors (i.e., are dominated by the priors). Consequently, the higher-order PCA parameters, which have wide posteriors, are not considered. We find that for both events, the posteriors are consistent with GR at the 90% credible level for all PCA parameters within both the FTI and TIGER frameworks.

To combine information from multiple events, we use the marginalized-likelihood multiplication technique applied to the original deviation parameters (Saleem et al. 2022; Mahapatra et al. 2025), where the likelihoods are constructed by sampling from six-dimensional kernel density estimator fits using a Gaussian mixture model (as implemented in SCIKIT-LEARN; Pedregosa et al. 2011). Subsequently, we apply PCA to the combined posteriors of the original deviation parameters in order to obtain the PCA parameters for multiple events. We find that higher PCA parameters for multiple events contain useful information, even though they do not for the individual events: The leading three PCA parameters in the FTI framework and the leading two in the TIGER framework are informative in all individual event analyses, as the Jensen–Shannon (JS) divergence (Lin 1991) between the posterior and prior distributions exceeds 0.1 bit. An exception is GW230627_015337 in the TIGER framework, where the JS divergence for the third PCA parameter also exceeds 0.1 bit. However, in the joint analysis, the leading five PCA parameters are informative, with the JS divergence exceeding 0.1 bit in both frameworks.

The combined posterior probability distributions on the first five leading PCA parameters from all the GW events passing the selection criteria are displayed in Figure 7. The median values, 90% credible intervals, and GR quantiles for combined PCA posteriors are listed in Table 4. The combined posterior distributions of the PCA parameters are statistically consistent with GR within the 90% credible interval, except for the fifth PCA parameter in the TIGER framework. The fifth PCA parameter in the TIGER framework exhibits a significant offset from zero, with a GR quantile of 98%. Furthermore, the fourth PCA parameter in the FTI framework, as well as the second and third PCA parameters in the TIGER framework, are offset from zero. These offsets are all driven by the event GW190814 (Abbott et al. 2020b), for which we observed a similar offset in the PCA posteriors (Mahapatra et al. 2025). If GW190814 is excluded from the combined results, they do not have any notable offsets from zero. The deviations found for GW190814 could possibly be caused by noise artifacts present in the data or by systematic errors from the waveform model and parameterization framework (Mahapatra et al. 2025). The difference between the FTI and TIGER results is an estimate of the latter. We deduce a joint bound (at 90% credibility) on the leading PCA parameter to be $-0.01^{+0.04}_{-0.03}$ ($0.01^{+0.06}_{-0.06}$) in the FTI (TIGER) framework, consistent with GR predictions. The loud O4b event GW250114 (Abac et al. 2025b) also provides tight constraints on the first two PCA parameters (Abac et al. 2026e).

2.3. *Spin-induced multipole moment coefficient null test*

The gravitational field of a spinning object includes contributions from the object's quadrupole and higher multipole moments, which arise from rotationally induced deformations. These higher-order contributions leave unique imprints on gravitational waveforms, encoding the values of the spin-induced multipole moments of the binary's constituent objects. For black holes, these moments take specific values that are uniquely determined by the mass and spin, as dictated by the no-hair conjecture (Carter 1971; Hansen 1974). Inferring the values of these moments from their imprints on gravitational waveforms can allow one to distinguish exotic compact objects from black holes. In this analysis, we model the spin-induced quadrupole moment of each compact object using the parameterization

$$Q_i = -\kappa_i \chi_i^2 m_i^3, \tag{7}$$

where Q_i, representing the quadrupole-moment scalar, appears in the leading-order 2PN term in the GW phase and κ_i encodes the response of the object's shape to its spin for object $i = 1, 2$. Here m_i and χ_i are the mass and the dimensionless spin of the compact object i. Along with the 2PN leading-order term, we also include the spin-induced quadrupole-moment terms at 3PN in the binary inspiral phase (Arun et al. 2009; Mishra et al. 2016). For a given family of exotic compact objects, the value of κ_i, the dimensionless spin-induced quadrupole-moment coefficient, is primarily determined by the mass of the compact object, with a subdominant dependence on the object's spin, but the value can be significantly different for different classes of exotic compact objects.

For Kerr black holes, the value is $\kappa_{\rm BH} = 1$ (Carter 1971; Hansen 1974); for other compact stars, the value of κ is different due to the stars' internal structure. For models of spinning neutron stars, κ can vary between $\sim$2 and $\sim$14 (Pappas & Apostolatos 2012a,b; Harry & Hinderer 2018). For available models of spinning boson stars, κ can have values of $\sim$10–150 (Ryan 1997), and κ can even be negative for exotic stars such as gravastars (Uchikata & Yoshida 2016). One expects any compact object that has a spin-induced quadrupole different from that of a black hole to have a nonzero tidal deformability (e.g., Sennett et al. 2017; Johnson-McDaniel et al. 2020; Pacilio et al. 2020; Narikawa et al. 2021) as well as differences in the tidal heating (Cardoso et al. 2017; Maselli et al. 2018; Datta & Bose 2019; Datta et al. 2020; Chia et al. 2025) and modifications to the merger–ringdown part of the signal compared to that from an BBH. However, including these effects is not essential for the effectiveness of the null test presented here. While we do not explicitly test signals from non-black hole objects, the measurement of the spin-induced quadrupole coefficient κ from GW data serves as a physics-motivated null test: deviations from the Kerr prediction $\kappa = 1$ may indicate the presence of exotic compact objects or deviations from GR.

The coefficients κ_i represent the primary and secondary components' spin-induced quadrupole moment parameters for a spinning compact binary system. Although we include the 3PN spin-quadrupole contributions in our waveform model, the estimation of individual spin-induced quadrupole parameters κ_1 and κ_2 remains challenging due to their strong correlations with the component masses and spins. In principle, higher-order corrections beyond 3PN could help disentangle these parameters. Given the current detector sensitivities, at least the additional 3.5PN term (where the spin-induced octupole first enters Marsat 2015) does not significantly improve constraints, which remain broad. For this reason, we limit our analysis to the leading and next-to-leading spin-quadrupole terms. However, with a combination of κ_i values one can proceed further (Krishnendu et al. 2017, 2019a,b; Abbott et al. 2021b; Divyajyoti et al. 2024). We consider the symmetric and anti-symmetric combinations of κ_i,

$$\kappa_{\rm s} = \frac{\kappa_1 + \kappa_2}{2}, \tag{8}$$

$$\kappa_{\rm a} = \frac{\kappa_1 - \kappa_2}{2}. \tag{9}$$

For binary black holes in general relativity, $\kappa_{\rm s} = 1$ and $\kappa_{\rm a} = 0$. In this analysis, we assume $\kappa_{\rm a} = 0$ in order to construct a more constraining null test for the Kerr nature of compact objects by measuring deviations from the expected value via $\kappa_{\rm s} = 1 + \delta\kappa_{\rm s}$. This assumption simplifies the parameter space and enhances our ability to detect deviations from the black hole prediction, though it does not capture possible asymmetries in the spin-induced quadrupole moments of the two components. However, for the loud O4b event GW241011 (Abac et al. 2025c), whose source was an unequal-mass binary,

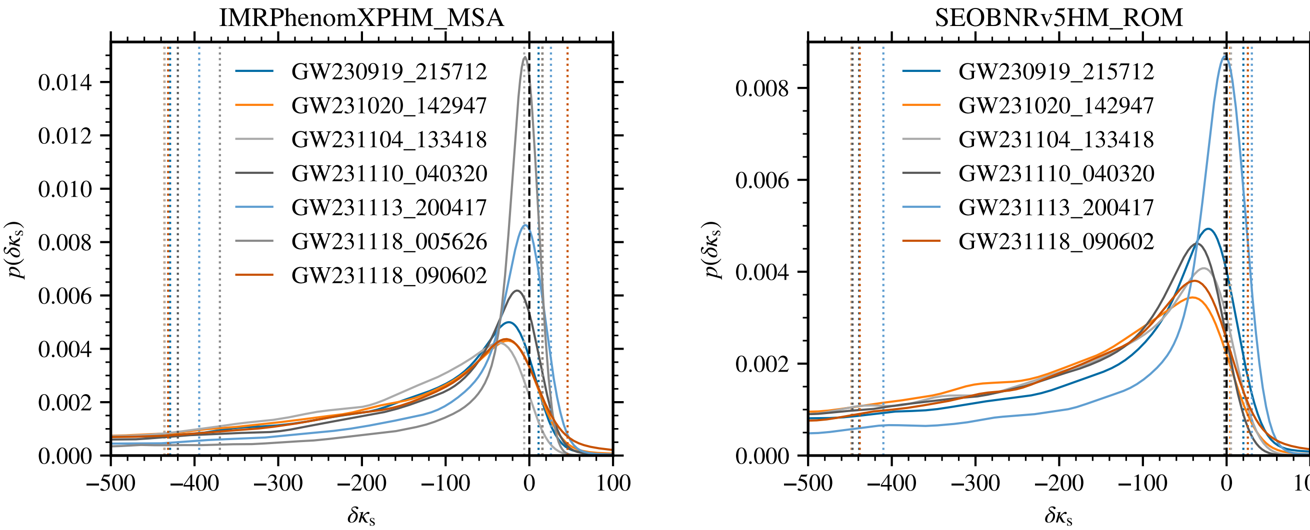

Figure 8. The posterior probability distribution on the spin-induced quadrupole moment parameter $\delta\kappa_s$ using the IMRPHENOMXPHM_MSA (left panel) and SEOBNRv5HM_ROM (right panel) waveform models. The black dashed vertical line indicates the BBH value ($\delta\kappa_s = 0$). The colored vertical lines show the 90% symmetric bounds on $\delta\kappa_s$ calculated from the individual events assuming a uniform prior ranging between $[-500, 500]$ on $\delta\kappa_s$.

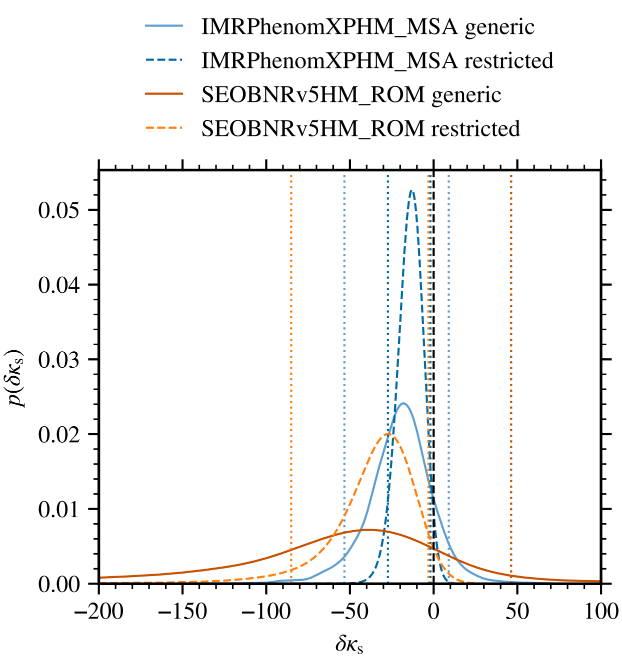

Figure 9. Joint posterior probability distribution on the spin-induced quadrupole moment parameter $\delta\kappa_s$ from the GWTC-4.0 events. Bounds obtained by multiplying the likelihoods (restricted) and by hierarchically combining events (generic) are shown. The analysis is performed assuming a uniform prior ranging between $[-500, 500]$ on $\delta\kappa_s$. The dashed line indicates the BBH value of $\delta\kappa_s$, while the dotted lines mark the 90% symmetric credible intervals. The BBH value is found slightly outside of the 90% credible interval for the restricted results, due to correlations with $\chi_{\rm eff}$.

we have been able to constrain deviations in κ_1, allowing it and κ_2 to vary independently.

We introduce the parameterized deviations $\delta\kappa_s$ to the inspiral phase for both the IMRPHENOMXPHM_MSA and SEOBNRv5HM_ROM waveform models, similar to the introduction of generic deviations of PN coefficients for these waveform models in Section 2.1. Here IMRPHENOMXPHM_MSA denotes that we use the version of this model in which precession is modeled using a multiscale analysis (Pratten et al. 2021), which was previously studied on GWTC-3.0 events (Divyajyoti et al. 2024), instead of the SpinTaylor variant used throughout the rest of this paper.

We apply selection criteria based on the measurability of $\delta\kappa_s$, requiring that the posterior distribution is sufficiently constrained to distinguish potential deviations from the black hole value $\kappa_s = 1$. For the IMRPHENOMXPHM_MSA analysis, we require (i) an inspiral network SNR of at least 6 and (ii) $\chi_{\rm eff} > 0$ at the 90% credible level. To compute the combined bounds, we include events reported in Abbott et al. (2021b) that satisfy both selection criteria. This results in a total of seven events from O4a and eight events from GWTC-3.0. The event selection criterion on $\chi_{\rm eff}$ is stricter than the one imposed for GWTC-3.0, so GW200129_065458 is no longer selected for this test.

Besides the spin-induced quadrupole-moment test previously used in Abbott et al. (2021b), we also employ a new test based on the FTI framework used for parameterized inspiral tests (see Section 2.1). For this version of the test, the corrections due to $\delta\kappa_s$ are added at 2PN and 3PN in the frequency-domain phase during inspiral (Mehta et al. 2023). In order to only apply the corrections to the inspiral portion of the waveform, the corrections are tapered off towards the merger-ringdown, which is left the same as in GR, as described in

Section 2.1. This test uses the SEOBNRv5HM_ROM waveform model and is applied only to events that satisfy the FTI event selection criteria of having an inspiral SNR of at least 10 and at least 5 GW cycles in the inspiral. Additionally, as for the IMRPhenomXPHM_MSA analysis, we require that zero effective inspiral spin $\chi_{\rm eff} = 0$ is outside the 90% credible interval of the GR posterior. Overall, six events from O4a pass these selection criteria.

Figure 8 shows the posterior distributions of $\delta\kappa_{\rm s}$ for individual events. They are derived under the assumption of a uniform prior on $\delta\kappa_{\rm s}$ between $[-500, 500]$. As the parameter $\delta\kappa_{\rm s}$ is correlated with $\chi_{\rm eff}$, individual events constrain positive values of $\delta\kappa_{\rm s}$ more strongly for positive effective inspiral spin and often have a long tail for negative $\delta\kappa_{\rm s}$ (Krishnendu et al. 2019b). Since most events observed have small but positive $\chi_{\rm eff}$ (Abac et al. 2025d), it is expected that the combined posterior and the 90% bounds will have more stringent constraints on positive values of $\delta\kappa_{\rm s}$ than negative values.

The combined posterior distribution on $\delta\kappa_{\rm s}$ from all selected GW events is shown in Figure 9. The 90% credible interval on $\delta\kappa_{\rm s}$ from the hierarchical analysis is $\delta\kappa_{\rm s} = -19^{+28}_{-34}$ for IMRPhenomXPHM_MSA and $\delta\kappa_{\rm s} = -49^{+95}_{-176}$ for SEOBNRv5HM_ROM. When restricted to the positive prior region, this analysis places a 90% credibility constraint of $\delta\kappa_{\rm s} < 26$ for IMRPhenomXPHM_MSA and $\delta\kappa_{\rm s} < 127$ for SEOBNRv5HM_ROM. The combined IMRPhenomXPHM_MSA bounds are tighter than the SEOBNRv5HM_ROM ones because the GWTC-3.0 events have not yet been included in the SEOBNRv5HM_ROM analysis, due to computational constraints. However, the IMRPhenomXPHM_MSA and SEOBNRv5HM_ROM results for individual events in Figure 8 agree quite well.

The distribution hyperparameters are just consistent with the null hypothesis ($\mu = \sigma = 0$), with $\mu = -19^{+20}_{-22}$ and $\sigma < 25$ for IMRPhenomXPHM_MSA, and with $\mu = -51^{+53}_{-128}$ and $\sigma < 119$ for SEOBNRv5HM_ROM. Both μ and the population-marginalized posterior in Figure 9 inherit the asymmetry of the individual events, which tend to be skewed toward $\delta\kappa_{\rm s} < 0$. This explains why the results are marginally consistent with the null hypothesis and suggests that negative values of $\delta\kappa_{\rm s}$ are harder to constrain.

The dashed curves in Figure 9 shows the joint-likelihood posterior obtained under the assumption that all events share a common value of $\delta\kappa_{\rm s}$. Within this framework, we obtain $\delta\kappa_{\rm s} = -14^{+12}_{-14}$ for IMRPhenomXPHM_MSA and $\delta\kappa_{\rm s} = -32^{+29}_{-53}$ for SEOBNRv5HM_ROM. The combined results of the restricted analysis are not consistent with $\delta\kappa_{\rm s} = 0$ at the 90% credible level due to the correlation with $\chi_{\rm eff}$, just like the hierarchical results. When restricted to positive values, the constraint becomes $\delta\kappa_{\rm s} < 5.7$ for IMRPhenomXPHM_MSA and $\delta\kappa_{\rm s} < 13$ for SEOBNRv5HM_ROM.

Overall, the results are consistent with BBHs described by GR.

2.4. *LOSA: Line-of-Sight Acceleration*

Motion of a CBC relative to a GW detector will cause the signal to be Doppler shifted. Uniform (constant velocity) motion will cause a constant Doppler shift, the measurement of which is perfectly degenerate with the intrinsic mass of the CBC following the mass–redshift degeneracy in GW signals (Abac et al. 2025a). However, a CBC moving with a *time-varying* relative velocity caused, e.g., by a constant LOSA a such as due to a nearby supermassive black hole, will cause a -4PN modulation (Vijaykumar et al. 2023; Tiwari et al. 2026) at the leading order: the strength of this modulation is proportional to the magnitude of the LOSA. Tiwari et al. (2026) discusses how LOSA compares to other effects like repeated lensing by a supermassive black hole.

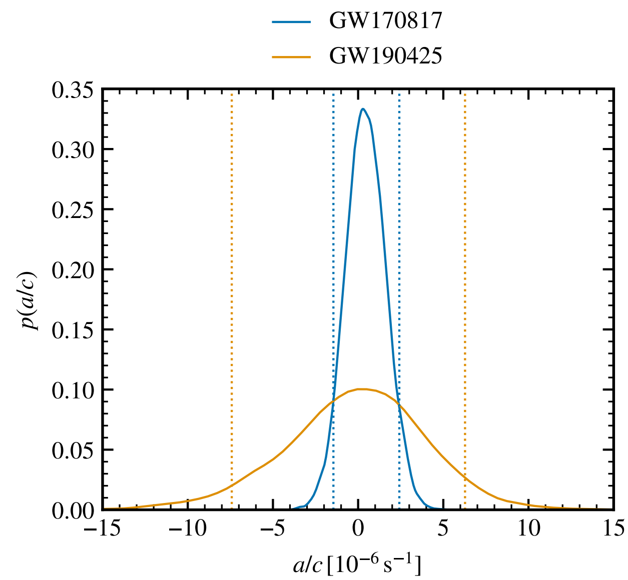

Figure 10. The posterior probability distributions for events satisfying the LOSA selection criteria. The colored dotted lines represent the 90% credible levels.

The modulated inspiral GW waveform in the frequency domain can be written as

$$\tilde{h}(f) = \tilde{h}_{\rm non-acc}(f)\left(1 + \frac{\Delta\mathcal{A}_{\rm LOSA}}{\mathcal{A}_{\rm non-acc}}\right) e^{i\Delta\Psi_{\rm LOSA}}, \quad (10)$$

where $\tilde{h}_{\rm non-acc}(f)$ is the waveform without the effects of LOSA, $\Delta\mathcal{A}_{\rm LOSA}/\mathcal{A}_{\rm non-acc} \propto a/v^8$ is the modulation in the amplitude, and $\Delta\Psi_{\rm LOSA} \propto a/v^{13}$ is the phase correction due to LOSA. Here $v = [\pi G(1+z)Mf]^{1/3}$ is the binary's orbital velocity, where z is the binary's redshift and M is its total mass. The phase correction contains contributions from point-particle, aligned spin, and tidal effect terms (Vijaykumar et al. 2023; Tiwari et al. 2026).

The LOSA corrections have been derived assuming $|a/c|t_{\rm sd} \ll 1$, where $t_{\rm sd}$ is the signal duration in the detector's sensitive band, so we can linearize in $|a/c|t_{\rm sd}$. Additionally, the current setup of phase corrections due to LOSA only has corrections to the dominant $(2, \pm2)$ multipoles of the waveform and does not include contributions from precessing spins. For a precessing binary, the aligned spin LOSA corrections are computed using the spin components at the reference frequency.

We impose a set of selection criteria (Tiwari et al. 2026) to identify events to which to apply the LOSA analysis, where we evaluate these criteria using the intrinsic parameters of the binary based on the GR analyses (Abac et al. 2026a), in addition to using the LOSA results themselves in the final two a posteriori criteria:

1. We ensure that the median of the redshifted total mass $(1+z)M$ of the CBC is $\leq 10\,M_\odot$, since lower-mass binaries have longer signals in the detectors sensitive band, with many cycles at relatively small v, which give the best constraints on the LOSA.

2. We ensure the median value of mass ratio $q \geq 0.25$, to avoid biased LOSA recovery due to higher multipole content.

3. We ensure the median value of $\chi_\mathrm{p} \leq 0.4$, to avoid biased LOSA recovery due to precession, since the LOSA corrections used are only for aligned spins.

4. After we perform LOSA inference on the events passing the above selection criteria, we calculate the quantity $|a/c|t_\mathrm{sd}$ to ensure it is ≤ 0.01 at the 90% credible level. Here we compute t_sd using the Newtonian-order expression for the time to coalescence, $5G(1+z)Mc^5/(256\eta v^8)$ (e.g., Buonanno et al. 2009), starting from the low frequency used in the analysis.

We use precessing waveforms IMRPhenomXP_MSA (Pratten et al. 2021) and IMRPhenomXP_NRTidalv2 (Colleoni et al. 2025a) as the base waveforms for BBHs and BNSs, respectively, while we use IMRPhenomNSBH (Thompson et al. 2020), which is non-precessing, for NSBHs.

Among the O4 events, we find GW230518_125908 to have a total redshifted mass very close to the cutoff, so the first selection criteria is only satisfied for the results using some waveform models. We thus restrict consideration to the IMRPhenomNSBH analysis, where we found that the median total mass of GW230518_125908 is slightly above the threshold. However, three pre-O4 events fulfilled the first three selection criteria regardless of the waveform model used in the analysis, namely GW170817, GW190425, and GW200115_042309. We find GW170817 and GW190425 to also fulfill the fourth criterion and to be non-accelerating (see Figure 10): a/c is constrained to be $0.42^{+2.00}_{-1.87} \times 10^{-6}\,\mathrm{s}^{-1}$ for GW170817 and $-0.01^{+6.29}_{-7.40} \times 10^{-6}\,\mathrm{s}^{-1}$ for GW190425. We also find that GW200115_042309 is consistent with zero LOSA at slightly less than 90% credibility. However, the GW200115_042309 results fail criterion four, so we cannot claim a reliable constraint on LOSA, and thus do not provide quantitative results for that event.

3. TESTS OF GW PROPAGATION

This section is dedicated to plausible modification (beyond GR) of the GW signal as it propagates between the source and the detector. As discussed in Abbott et al. (2019c), we assume that GR accurately models the generation of GWs near the source in its local wave zone (Thorne 1980), or that the deviations from GR during the generation or due to nonlinearity of the field in the near zone are not observable. This is an excellent assumption in many cases. For instance, for the massive graviton, the combined constraints from propagation mean that the Yukawa length scale λ_g that determines the corrections to the Newtonian potential is $\lambda_g/r \gtrsim 10^{11}$ times the maximum separation of the binary r in the sensitive band of ground-based detectors, thus leading to corrections to the binary's GR dynamics from a massive graviton that are of order $r^2/(2\lambda_g^2) \lesssim 10^{-22}$ (bounds on m_g from individual events would lead to corrections at most an order of magnitude higher). We also assume that the GW signal is described sufficiently accurately by two (tensorial) polarizations similar to GR. In Section 3.1, we consider a phenomenological model where the modification in the propagation of GW is caused by a modification to the dispersion relation. In Section 3.2, we consider modifications in GW signal caused by the difference in propagation of each polarization. For both of the above tests, the modification to the GR waveform scales with the distance to the source. As such, GWTC-4.0, containing many events at $> 1\,\mathrm{Gpc}$ (Abac et al. 2026a), is well suited to improve constraints on the modified propagation theories.

The companion paper focusing on the inference of cosmological parameters with GWTC-4.0 (Abac et al. 2025e), also constrains a broad class of theoretical models that allow for violations of GR. In that work, we concentrate on a specific effect often referred to as GW friction, which manifests itself as a modification of the GW amplitude and thus alters the inferred luminosity distance. We place constraints on the ratio of gravitational-wave to electromagnetic luminosity distances by using the distribution of source-frame BBH masses and assuming luminal GW propagation, finding results consistent with GR.

3.1. *Tests of a modified GW dispersion relation*

GR predicts that the gravitational interaction (graviton) propagates with the speed of light, and the corresponding energy-momentum relation takes a simple form $E^2 = p^2c^2$. However, in the case of massive graviton and Lorentz invariance violating theories of gravity, we have a modified dispersion relation (MDR) with an extra term:

$$E^2 = p^2c^2 + A_\alpha p^\alpha c^\alpha, \tag{11}$$

where the phenomenological parameter A_α governs the strength of the violation and α controls the frequency dependence of the dispersion (Will 1998; Mirshekari et al. 2012). The modified dispersion causes different frequency components of the signal to travel with different group velocities, changing the morphology of the signal, which can be expressed as a frequency-dependent phase modification of the GR waveform $\tilde{h}(f) = \tilde{h}_\mathrm{GR}(f)\exp(i\delta\Psi(f))$, with the modification (Ezquiaga et al. 2022):

$$\delta\Psi(f) = -\frac{\pi D_\alpha h^{\alpha-2}(1+z)^{\alpha-1}}{c} A_\alpha f^{\alpha-1}\,. \tag{12}$$

Here h is the Planck constant, z is the redshift of the source, and D_α is a modified distance parameter, defined by:

$$D_\alpha = \frac{c(1+z)^{1-\alpha}}{H_0} \int_0^z \frac{(1+\bar{z})^{\alpha-2}}{\sqrt{\Omega_{\rm m}(1+\bar{z})^3 + \Omega_\Lambda}} {\rm d}\bar{z} \,, \quad (13)$$

where H_0 is the Hubble constant, $\Omega_{\rm m}$ is the matter density parameter, and Ω_Λ is the dark energy density parameter. Here, we use the ΛCDM cosmological model given in Abac et al. (2025a). As such, we neglect the radiation density in the expression for our distance parameter.

Previous tests of MDR performed by the LVK (Abbott et al. 2017, 2019c, 2021b, 2025) quoted the results using the particle velocity, for which the constraints on A_α are $1-\alpha$ times larger than those obtained with the group velocity for $\alpha \neq 1$; for $\alpha = 1$ the particle velocity yields a deviation with a different frequency dependence than the group-velocity results. Ezquiaga et al. (2022) showed that the phase modification obtained using the group velocity is consistent with that obtained through the Wentzel–Kramers–Brillouin approach (Beltrán Jiménez et al. 2020), which is why we use the group-velocity expressions here.

The MDR given in Equation (11) provides a simple phenomenological parametrization to a broad class of modified theories. Different values of α describe the leading dispersive effect in different non-GR theories. Particular predictions correspond to $\alpha = 0$ (massive graviton; Will 1998), $\alpha = 2.5$ (multi-fractal spacetime; Calcagni 2010), $\alpha = 3$ (doubly special relativity; Amelino-Camelia 2002), and $\alpha = 4$ (Hořava–Lifshitz and extra dimensional theories; Hořava 2009; Sefiedgar et al. 2011).

Following the phenomenological approach, we test $\alpha \in \{-3, -2, -1, 0, 0.5, 1.5, 2.5, 3, 3.5, 4\}$. The case $\alpha = 2$ is excluded, as this choice is equivalent to changing the overall speed of GW propagation and results in no dispersion. Compared with GWTC-3.0, we drop the test of $\alpha = 1$; in this case the GW group velocity is equal to the speed of light at leading order and the amplitude $A_{\alpha=1}$ cannot be constrained (Baka et al. 2026). However, we now also include negative values of α, which can result from a dark energy phase transition (de Rham & Melville 2018; Baker et al. 2022; Harry & Noller 2022).

We have introduced two novelties in the analysis after GWTC-3.0 (Abbott et al. 2025). First, we use IMRPhenomXPHM for the underlying GR waveform. Second, for each value of α, we sample in the effective amplitude parameter $A_{\rm eff}$ (which decouples the sampling parameter from the choice of cosmology) and reweight the final result to a prior flat in A_α, instead of sampling separately for the positive and negative values of A_α using the logarithm of an effective wavelength parameter (Abbott et al. 2019c; Baka et al. 2026). For $\alpha = 0$, we additionally sample in the effective graviton mass (Baka et al. 2026). For the combined bounds on the graviton mass, we opt to transform the A_0 posterior to a prior flat in graviton mass (Baka et al. 2026), to ensure consistency between between our bounds on A_0 and m_g.

Contrary to the tests of GW generation, where the deviation from GR is expected to depend on the parameters of each individual source, we assume that the modification in the propagation of the gravitational waves themselves is universal to all events, and independent of their SNR or parameters. Therefore, we do not perform a hierarchical analysis as in Section 2. Instead, we just apply kernel density estimation to the A_α posteriors and combine the posteriors from different events by multiplying together the individual likelihoods (which are proportional to the posteriors as the priors were chosen to be flat) and renormalizing the result. Finally, we estimate bounds on the amplitude parameters using the combined results.

We use all 43 events analyzed for MDR in GWTC-3.0 (Abbott et al. 2025), as well as all new BBH events in GWTC-4.0 that pass the general selection criteria described in Section 1. BNS and NSBH events are excluded due to computational constraints, as these signals have long durations. Additionally, these relatively nearby events provide limited information on dispersion, with only loosely constrained posteriors, as demonstrated for GW170817 (Abbott et al. 2019b). We exclude GW230518_125908 due to its likely NSBH nature. Although we analyzed GW231123, we omit it from our combined analysis due to significant waveform systematic uncertainties (Abac et al. 2025f), which led to an apparent GR violation when analyzed with the IMRPhenomXPHM waveform model. We give details of our studies of the systematic errors from waveform modeling for this event and MDR in Appendix D.

Therefore, we include 40 new events from O4a in our combined analysis. In Baka et al. (2026), the authors reanalyze the GWTC-3.0 data using all of the improvements described above and provide a more detailed explanation of the methods. All comparisons to the GWTC-4.0 results are made with respect to these reanalyzed GWTC-3.0 results, to ensure that any differences are driven only by the inclusion of results from the new mergers, and not by changes in methodology.

Figure 11 shows the violin plots describing the combined bounds on the amplitude parameters A_α. The shaded gray region shows the result for 43 events from GWTC-3.0 (Abbott et al. 2025; Baka et al. 2026), while the blue posteriors show the result for the 83 cumulative events in GWTC-4.0 (i.e., after adding the events from O4a). Overall, the new results are more constraining than those from GWTC-3.0 and more consistent with the GR prediction (zero) for positive values of α. On average, the new posteriors are narrower by a factor 1.96 compared to the factor of 1.39 improvement expected from the multiplication of Gaussian distributions. Although for $\alpha = -3$ and $\alpha = -2$ cases, GR lands outside the central 90% credible interval, this is driven primarily by GW231028_153006 for which prior effects lead to the apparent GR violations. The deviations disappear if this event is excluded and therefore we find no evidence for dispersion of GWs. See Appendix C for details about the prior effects for GW231028_153006.

In Table 5 we summarize the data from Figure 11. For each tested value of α, we report the 5% and 95% quantiles together with the quantile at which GR was found, $Q_{\rm GR} = P(A_\alpha < 0)$. These values show the difference in width of

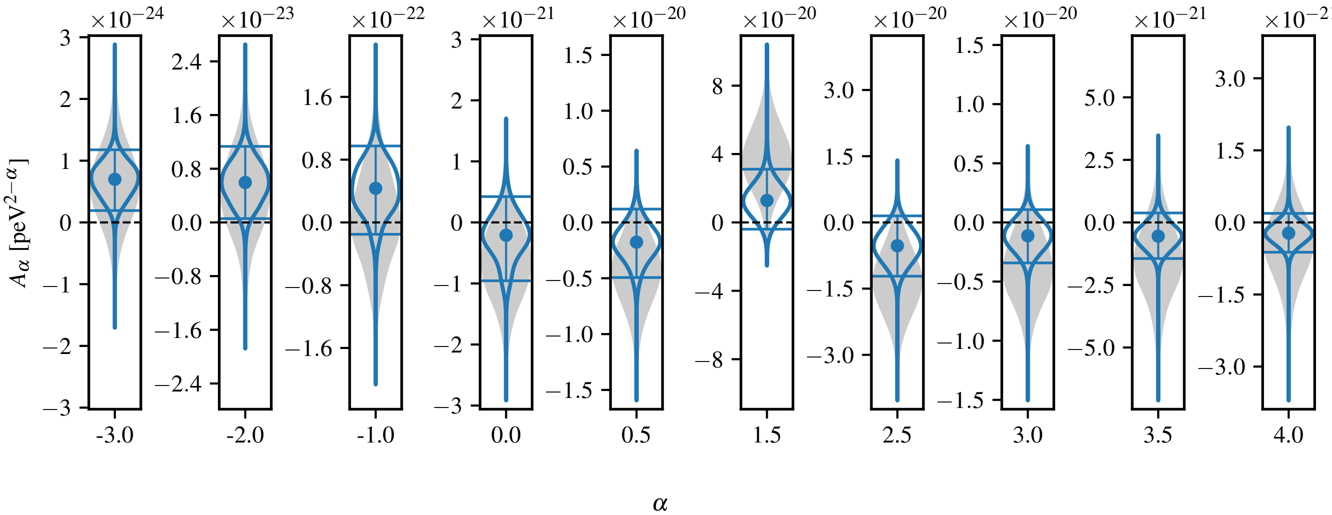

Figure 11. Posteriors on the MDR amplitude parameters A_α. Results from GWTC-3.0 (Abbott et al. 2025; Baka et al. 2026) are indicated by a shaded light-gray area, while the new results in GWTC-4.0 are represented by blue curves. The error bars indicate 90% credible intervals. The significant shifts away from zero for $\alpha = -3, -2$ are driven by prior effects for GW231028_153006.

Table 5. Combined results for the MDR analysis

	$\bar{m}_g$	$\bar{A}_{-3.0}$		$\bar{A}_{-2.0}$		$\bar{A}_{-1.0}$		$\bar{A}_{0.0}$		$\bar{A}_{0.5}$	
	90% $[10^{-23}]$	90% $[10^{-84}]$	$Q_{\rm GR}$ %	90% $[10^{-71}]$	$Q_{\rm GR}$ %	90% $[10^{-58}]$	$Q_{\rm GR}$ %	90% $[10^{-45}]$	$Q_{\rm GR}$ %	90% $[10^{-39}]$	$Q_{\rm GR}$ %
GWTC-3.0	2.23	$-0.38 - 1.59$	15.7	$-0.53 - 1.42$	22.3	$-0.86 - 1.04$	45.5	$-1.63 - 0.41$	84.1	$-9.40 - 0.66$	92.2
GWTC-4.0	1.92	$0.19 - 1.18$	1.1	$0.06 - 1.13$	3.4	$-0.15 - 0.97$	10.3	$-0.96 - 0.42$	71.7	$-4.94 - 1.20$	84.8
		$\bar{A}_{1.5}$		$\bar{A}_{2.5}$		$\bar{A}_{3.0}$		$\bar{A}_{3.5}$		$\bar{A}_{4.0}$	
		$[10^{-26}]$	%	$[10^{-14}]$	%	$[10^{-9}]$	%	$[10^{-3}]$	%	$[10^{3}]$	%
GWTC-3.0		$0.95 - 6.83$	1.3	$-2.50 - -0.11$	96.4	$-8.53 - 0.95$	90.4	$-3.89 - 0.85$	85.0	$-1.69 - 0.64$	75.3
GWTC-4.0		$-0.40 - 3.11$	10.5	$-1.22 - 0.15$	90.0	$-3.42 - 1.08$	79.8	$-1.44 - 0.38$	84.2	$-0.62 - 0.19$	82.5

NOTE—We compare the results for GWTC-4.0 with those for GWTC-3.0 (Abbott et al. 2025; Baka et al. 2026). The table shows 90% credible intervals for the dimensionless graviton mass $\bar{m}_g = m_g/(\mathrm{eV}/c^2)$ and the dimensionless amplitude parameters $\bar{A}_\alpha = A_\alpha/\mathrm{eV}^{2-\alpha}$. We also include the quantiles of the GR hypothesis $Q_{\rm GR} = P(A_\alpha < 0)$. The significant shifts away from zero for $\alpha = -3, -2$ are driven by prior effects for GW231028_153006.

the marginalised posteriors and consistency with GR between GWTC-3.0 and its extension to GWTC-4.0.

We applied a special treatment for $\alpha = 0$, which can be interpreted as giving the dispersion due to a massive graviton, and obtained the 90% upper bound on the graviton mass, 1.92×10^{-23} eV$/c^2$. The new result gives a factor of 1.16 improvement compared to the GWTC-3.0 bound 2.23×10^{-23} eV$/c^2$ (Abbott et al. 2025; Baka et al. 2026). The bound on the graviton mass from planetary ephemerides is 1.01×10^{-24} eV$/c^2$ at the 99.7% confidence level (Mariani et al. 2023), which is an order of magnitude better than our constraint. However, these results are complementary, since they use different set of observations (GW versus astrometry) and focus on different phenomenologies (wave propagation versus orbital motion).

3.2. *Tests of anisotropic birefringence from the Standard Model Extension*

The effective field theory referred to as the Standard Model Extension (SME) is a phenomenological framework for deriving observational constraints of SSB, such as violations of Lorentz invariance and charge–parity–time (CPT) symmetry (Colladay & Kostelecký 1998; Kostelecký 2004). For GWs, Lorentz and CPT violation can result in anisotropic and dispersive propagation. One particular prediction of SME is birefringence, which can cause the two polarizations to travel at different speeds in vacuum.

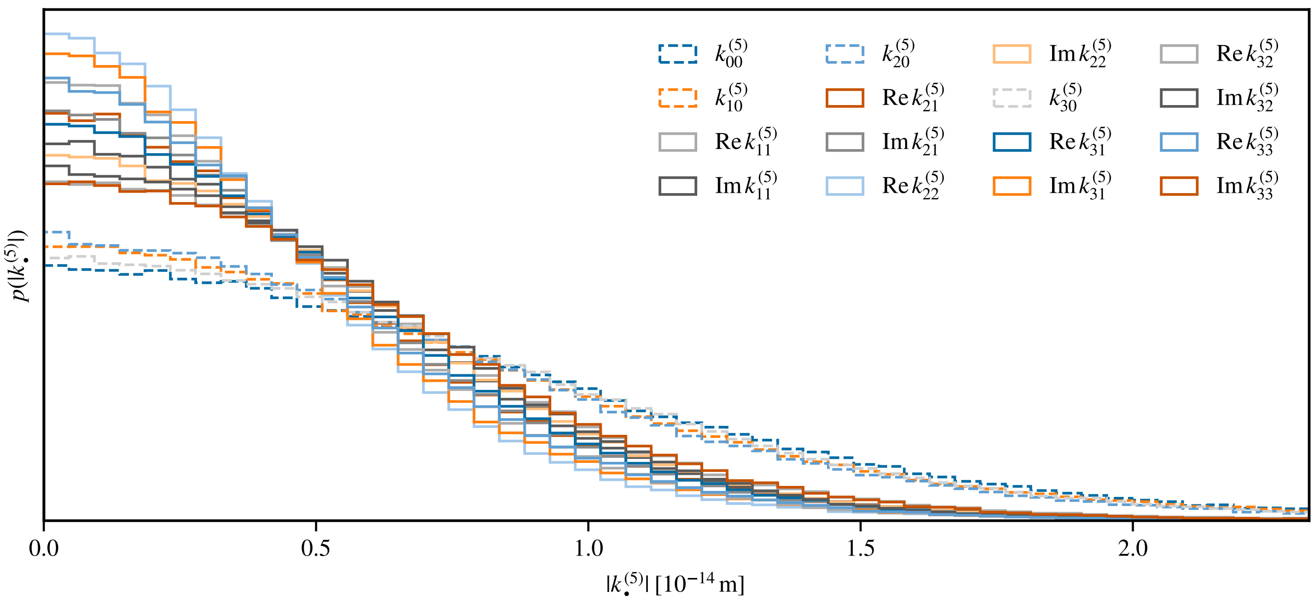

Figure 12. The combined posterior probability on the 16 anisotropic dispersion and birefringence coefficients $k^{(5)}_{\ell m}$ from O4a. We highlight the $m = 0$ coefficients, which have weaker constraints that the others.

Within the SME's gravity sector, all symmetry-breaking operators that appear in the Lagrangian are associated with a certain mass dimension d. Operators at higher mass dimensions are suppressed by larger powers of the natural energy scale (Kostelecký & Mewes 2016). For gauge-invariant theories that allow SSB, the leading order manifestation of anisotropic birefringence appears at mass-dimension $d = 5$. This introduces a frequency-dependent birefringent dispersion relation (Kostelecký & Mewes 2016; Mewes 2019), which changes the frequency-domain waveform,

$$\tilde{h}_+(f) = \tilde{h}_+^{\mathrm{GR}}(f)\cos\left(\beta f^2\right) - \tilde{h}_\times^{\mathrm{GR}}(f)\sin\left(\beta f^2\right), \quad (14)$$

$$\tilde{h}_\times(f) = \tilde{h}_+^{\mathrm{GR}}(f)\,\sin\left(\beta f^2\right) + \tilde{h}_\times^{\mathrm{GR}}(f)\cos\left(\beta f^2\right). \quad (15)$$

Here $\tilde{h}_+^{\mathrm{GR}}(f)$ and $\tilde{h}_\times^{\mathrm{GR}}(f)$ are the polarization components in GR and β is the deviation parameter directly related to the symmetry breaking operators that appear in the SME Lagrangian at $d = 5$:

$$\beta = \frac{4\pi^2}{c}\left|k^{(5)}_{\mathrm{eff}}\right|\tau(z)\,, \quad k^{(5)}_{\mathrm{eff}} = \sum_{\ell,m} Y_{\ell m}(\hat{\boldsymbol{n}})\,k^{(5)}_{\ell m}\,, \quad (16)$$

$$\tau(z) = \int_0^z \frac{1+\bar{z}}{H_0\sqrt{\Omega_{\mathrm{m}}(1+\bar{z})^3+\Omega_\Lambda}}\,\mathrm{d}\bar{z}\,. \quad (17)$$

where the superscript (5) denotes parameters related to dimension $d = 5$ and the parameters $k^{(5)}_{\ell m}$ often appear as $k^{(5)}_{(V)\,\ell m}$ in other papers (Kostelecký & Mewes 2016; O'Neal-Ault et al. 2021; Haegel et al. 2023). Here $\ell = 0, 1, \ldots, d-2 = 3$ and $-\ell \leq m \leq \ell$, while $\hat{\boldsymbol{n}}$ is the direction of the source in spherical polar coordinates centered on the Earth and $\tau(z)$ is the effective propagation time associated with cosmological redshift z, where we use the cosmological model given in Abac et al. (2025a). Similarly to MDR, we only consider the propagation effect and neglect any modifications in the GWs that could arise during their generation.

Since CBC sources are isotropically distributed over the sky (Essick et al. 2023), we have sufficiently many GW detections to extract all 16 $k^{(5)}_{\ell m}$ parameters to determine all the degrees of freedom possible in $d = 5$ symmetry breaking operators in the Lagrangian.

We place a uniform prior on $k^{(5)}_{\mathrm{eff}}\tau(z)$ and use IMRPhenomXPHM as the baseline GR waveform model. We then derive the posteriors on $k^{(5)}_{\mathrm{eff}}$ and perform the singular value decomposition of the matrix of spherical harmonics to obtain the posteriors of the 16 $k^{(5)}_{\ell m}$ parameters we are interested in. While we do not have uniform priors on the individual $k^{(5)}_{\ell m}$ parameters, we have checked that we obtain almost identical results when placing a uniform prior on $k^{(5)}_{\mathrm{eff}}$. These post-processing details can be found in Haegel et al. (2023), which provides the limits obtained from 45 events in GWTC-3.0. However, there were some typographic errors in their calculations, and the actual constraint is $(Y_{00}(\hat{\boldsymbol{n}}))^2$ times the original constraint, which is about one order of magnitude tighter. We do not provide results on GWTC-3.0, awaiting re-analysis with the updated Bilby implementation.

Figure 12 shows the marginalized posteriors of the absolute values of the 16 $k^{(5)}_{\ell m}$ coefficients from 40 events in O4a. Here we omit GW231123 from the combined results due to the waveform modeling uncertainties discussed in Abac et al. (2025f) and also illustrated for MDR in Appendix D. For GW231028_153006, the SSB analysis finds the same prior-driven shifts away from GR found by MDR (see Appendix C), and we thus include this event in the combined results, as does

Table 6. Combined results for the SSB analysis

$\lvert k_{ij}^{(5)}\rvert$ [10^{-14}m]	90%
$\lvert k_{00}^{(5)}\rvert$	1.52
$\lvert k_{10}^{(5)}\rvert$	1.46
$\lvert \mathrm{Re}\, k_{11}^{(5)}\rvert$	1.05
$\lvert \mathrm{Im}\, k_{11}^{(5)}\rvert$	0.98
$\lvert k_{20}^{(5)}\rvert$	1.39
$\lvert \mathrm{Re}\, k_{21}^{(5)}\rvert$	0.95
$\lvert \mathrm{Im}\, k_{21}^{(5)}\rvert$	0.94
$\lvert \mathrm{Re}\, k_{22}^{(5)}\rvert$	0.81
$\lvert \mathrm{Im}\, k_{22}^{(5)}\rvert$	0.99
$\lvert k_{30}^{(5)}\rvert$	1.42
$\lvert \mathrm{Re}\, k_{31}^{(5)}\rvert$	0.95
$\lvert \mathrm{Im}\, k_{31}^{(5)}\rvert$	0.85
$\lvert \mathrm{Re}\, k_{32}^{(5)}\rvert$	0.87
$\lvert \mathrm{Im}\, k_{32}^{(5)}\rvert$	0.98
$\lvert \mathrm{Re}\, k_{33}^{(5)}\rvert$	0.88
$\lvert \mathrm{Im}\, k_{33}^{(5)}\rvert$	1.05

NOTE—We give the 90% upper bounds for the magnitudes of all 16 $k_{\ell m}^{(5)}$ SSB coefficients from the O4a marginalized posteriors in Figure 12.

MDR. The posteriors for all parameters peak at zero, which corresponds to GR. In Table 6 we summarize the data from Figure 12. Compared to the original GWTC-3.0 results in Haegel et al. (2023), the constraints from just O4a are about a factor of two tighter, after accounting for the correction mentioned above. These are thus the current best constraints on these coefficients—see Table D51 in Kostelecký & Russell (2026), which also shows results from other studies that have obtained more constraining illustrative bounds by varying the coefficients one at a time, though this procedure is only valid for the purposes of illustration.

4. CONCLUSIONS

We have presented the results of eight tests of GR or physics beyond isolated, quasi-circular binaries, four of which are new (and one, TIGER, has been significantly updated), all testing various parameterized modifications to GR, and placing constraints on such deviations.

Overall, our tests find that the signals conform to our expectations from GR. We provide highlights of the bounds and improvements in Table 1 of Paper I. In particular, we improve the constraints on deviations in the PN coefficients compared to GWTC-3.0 by up to a factor of 5.5 (where some of this improvement is due to an increase in the tapering frequency used by FTI, as discussed in Section 2.1). We also provide illustrative translations (with caveats) of the PN coefficient constraints to constraints on a variety of alternative theories in Table 3. The loudest event during O4a, GW230814_230901, can by itself place a tight bound on some PN deviations (Abac et al. 2026d), but it is excluded from this paper's analysis because it is a single-detector event; even without it, the PN coefficient constraints obtained from the full catalog are better. However, the loud O4b event GW250114 (Abac et al. 2025b) provides even better constraints than the full catalog (Abac et al. 2026e). Additionally, the MDR analysis updates the bound on the graviton mass to $m_g \leq 1.92 \times 10^{-23}$ eV$/c^2$ at 90% credibility.

Since we apply these tests to 91 events in GWTC-4.0, statistically a few should display apparent deviations from GR expectations. Of the 42 O4a events covered in this paper, this occurred for four events, namely GW230628_231200, GW231028_153006, GW231110_040320, and GW231123, which showed some deviations. The last three of these produced results with GR outside the 90% credible interval for the MDR test, though for GW231028_153006 this is due to priors, as discussed in Appendix C. The deviations for GW231110_040320 are only slight, and the Bayes factors still favor GR, while the deviations for GW231123 can be attributed to waveform systematics, as discussed in Appendix D, though alternative explanations such as wave-optics lensing have also been raised (Abac et al. 2025f). TIGER also finds deviations for GW231028_153006 for most post-inspiral coefficients but the Bayes factors still favor GR (FTI does not analyze this event), while both FTI and TIGER find deviations for GW231110_040320. Both FTI and TIGER find GR outside the 90% credible interval for GW230628_231200.

For events before O4, the tests in this paper find GR inside the 90% credible interval for all but GW190814 (Abbott et al. 2020b), where the TIGER and PCA analyses find GR to be outside the 90% credible interval for some parameters. FTI also finds minor shifts away from zero for some parameters (though GR is still in the 90% credible interval), which studies in Mehta et al. (2023) attribute to properties of the noise around the time of the event. Inclusion of GW190814 in the PCA combined results for TIGER also leads to shifts away from zero for some parameters, with the largest shift in the fifth PCA parameter, with a 98% GR quantile, while there are no notable shifts for any PCA parameters if GW190814 is excluded from the combined results.

Our analyses find consistency with GR in these tests for all other events. For all other tests, we find such consistency for the entire GWTC-4.0 catalog, though the SIM analyses find that GR is slightly outside the 90% credible interval in the combined results, due to correlations with the effective inspiral spin. The few events that met the criteria for the LOSA test are consistent with zero LOSA.

In summary, almost all events analysed were found to be consistent with the expectations of GR. In those few cases where the results were not seen to be consistent, likely causes of the inconsistency were identified which are likely sufficient to explain these apparent deviations, given the large number of events analysed, without requiring violations of GR. Continued improvement in waveform modeling and detector sensitivities as well as the analysis of additional events will further clarify the situation.

We thus expect to place even better constraints on deviations from GR with the analysis of additional events from the remainder of the fourth observing run and from future observing runs (Abbott et al. 2020a).[1] Additionally, improvements in analyses will also lead to better constraints, particularly performing tests for specific alternative theories, where inspiral–merger–ringdown waveform models have started to be developed and applied to data (Julié et al. 2025; Liu & Yunes 2025), improving on analyses that place constraints using either the inspiral (Nair et al. 2019; Perkins et al. 2021; Lyu et al. 2022; Perkins & Yunes 2022) or ringdown (Silva et al. 2023; Chung & Yunes 2025; Maenaut et al. 2026) alone.

All strain data analyzed in this paper are available from the Gravitational Wave Open Science Center (Abac et al. 2026f). The data and scripts used to prepare the figures and tables are available at LIGO Scientific, Virgo, and KAGRA Collaboration (2026a).

ACKNOWLEDGEMENTS

This material is based upon work supported by NSF's LIGO Laboratory, which is a major facility fully funded by the National Science Foundation. The authors also gratefully acknowledge the support of the Science and Technology Facilities Council (STFC) of the United Kingdom, the Max-Planck-Society (MPS), and the State of Niedersachsen/Germany for support of the construction of Advanced LIGO and construction and operation of the GEO 600 detector. Additional support for Advanced LIGO was provided by the Australian Research Council. The authors gratefully acknowledge the Italian Istituto Nazionale di Fisica Nucleare (INFN), the French Centre National de la Recherche Scientifique (CNRS) and the Netherlands Organization for Scientific Research (NWO) for the construction and operation of the Virgo detector and the creation and support of the EGO consortium. The authors also gratefully acknowledge research support from these agencies as well as by the Council of Scientific and Industrial Research of India, the Department of Science and Technology, India, the Science & Engineering Research Board (SERB), India, the Ministry of Human Resource Development, India, the Spanish Agencia Estatal de Investigación (AEI), the Spanish Ministerio de Ciencia, Innovación y Universidades, the European Union NextGenerationEU/PRTR (PRTR-C17.I1), the ICSC - CentroNazionale di Ricerca in High Performance Computing, Big Data and Quantum Computing, funded by the European Union NextGenerationEU, the Comunitat Autonòma de les Illes Balears through the Conselleria d'Educació i Universitats, the Conselleria d'Innovació, Universitats, Ciència i Societat Digital de la Generalitat Valenciana and the CERCA Programme Generalitat de Catalunya, Spain, the Polish National Agency for Academic Exchange, the National Science Centre of Poland and the European Union - European Regional Development Fund; the Foundation for Polish Science (FNP), the Polish Ministry of Science and Higher Education, the Swiss National Science Foundation (SNSF), the Russian Science Foundation, the European Commission, the European Social Funds (ESF), the European Regional Development Funds (ERDF), the Royal Society, the Scottish Funding Council, the Scottish Universities Physics Alliance, the Hungarian Scientific Research Fund (OTKA), the French Lyon Institute of Origins (LIO), the Belgian Fonds de la Recherche Scientifique (FRS-FNRS), Actions de Recherche Concertées (ARC) and Fonds Wetenschappelijk Onderzoek - Vlaanderen (FWO), Belgium, the Paris Île-de-France Region, the National Research, Development and Innovation Office of Hungary (NKFIH), the National Research Foundation of Korea, the Natural Sciences and Engineering Research Council of Canada (NSERC), the Canadian Foundation for Innovation (CFI), the Brazilian Ministry of Science, Technology, and Innovations, the International Center for Theoretical Physics South American Institute for Fundamental Research (ICTP-SAIFR), the Research Grants Council of Hong Kong, the National Natural Science Foundation of China (NSFC), the Israel Science Foundation (ISF), the US-Israel Binational Science Fund (BSF), the Leverhulme Trust, the Research Corporation, the National Science and Technology Council (NSTC), Taiwan, the United States Department of Energy, and the Kavli Foundation. The authors gratefully acknowledge the support of the NSF, STFC, INFN and CNRS for provision of computational resources.

This work was supported by MEXT, the JSPS Leading-edge Research Infrastructure Program, JSPS Grant-in-Aid for Specially Promoted Research 26000005, JSPS Grant-in-Aid for Scientific Research on Innovative Areas 2402: 24103006, 24103005, and 2905: JP17H06358, JP17H06361 and JP17H06364, JSPS Core-to-Core Program A. Advanced Research Networks, JSPS Grants-in-Aid for Scientific Research (S) 17H06133 and 20H05639, JSPS Grant-in-Aid for Transformative Research Areas (A) 20A203: JP20H05854, the joint research program of the Institute for Cosmic Ray Research, University of Tokyo, the National Research Foundation (NRF), the Computing Infrastructure Project of the Global Science experimental Data hub Center (GSDC) at KISTI, the Korea Astronomy and Space Science Institute (KASI), the Ministry of Science and ICT (MSIT) in Korea, Academia Sinica (AS), the AS Grid Center (ASGC) and the National Science and Technology Council (NSTC) in Taiwan under grants including the Science Vanguard Research Program, the Advanced Technology Center (ATC) of NAOJ, and the Mechanical Engineering Center of KEK.

Additional acknowledgements for support of individual authors may be found in the following document:
https://dcc.ligo.org/LIGO-M2300033/public.

[1] LVK observing run plans https://observing.docs.ligo.org/plan

The following open-source software has been used:
Calibration of the Laser Interferometer Gravitational-Wave Observatory (LIGO) strain data was performed with a GstLAL-based calibration software pipeline (Viets et al. 2018). Calibration of the Virgo strain data is performed with C-based software (Acernese et al. 2022). Data-quality products and event-validation results were computed using the DMT (Zweizig 2006), DQR (LIGO Scientific Collaboration and Virgo Collaboration 2018), DQSEGDB (Fisher et al. 2021), GWDETCHAR (Macleod et al. 2021a), HVETO (Smith et al. 2011), IDQ (Essick et al. 2020), Omicron (Robinet et al. 2020) and PythonVirgoTools (Virgo Collaboration 2021) software packages and contributing software tools. Analyses in this catalog relied upon the LALSuite software library (LIGO Scientific, Virgo, and KAGRA Collaboration 2026b; Wette 2020). The detection of the signals and subsequent significance evaluations in this catalog were performed with the GstLAL-based inspiral software pipeline (Messick et al. 2017; Sachdev et al. 2019; Hanna et al. 2020; Cannon et al. 2021), with the MBTA pipeline (Adams et al. 2016; Aubin et al. 2021), and with the PyCBC (Usman et al. 2016; Nitz et al. 2017; Davies et al. 2020) and the cWB (Klimenko et al. 2004, 2011, 2016) packages. Estimates of the noise spectra and glitch models were obtained using BayesWave (Cornish & Littenberg 2015; Littenberg et al. 2016; Cornish et al. 2021; Gupta & Cornish 2024). Noise subtraction for one candidate was also performed with GWSUBTRACT (Davis et al. 2022). Source-parameter estimation was performed with the Bilby and ParallelBilby libraries (Ashton et al. 2019; Romero-Shaw et al. 2020; Smith et al. 2020) using the Dynesty nested sampling package (Speagle 2020). FTI, TIGER, SIM, LOSA, MDR, and SSB waveforms used for testing GR were generated using BilbyTGR (Ashton et al. 2025b). PESummary was used to postprocess and collate parameter-estimation results (Hoy & Raymond 2021). The various stages of the parameter-estimation analysis were managed with the Asimov library (Williams et al. 2023) together with CBCFlow (Ashton et al. 2025a). Plots were prepared with Matplotlib (Hunter 2007), SEABORN (Waskom 2021), and GWpy (Macleod et al. 2021b). NumPy (Harris et al. 2020), SCIKIT-LEARN (Pedregosa et al. 2011), and SciPy (Virtanen et al. 2020) were used in the preparation of the manuscript.

APPENDIX

In these Appendices, we discuss apparent GR deviations found for various events and either the TIGER or MDR analyses. Specifically, we discuss the effects of noise on GW190728_064510 in the TIGER reanalysis with IMRPhenomXPHM (Appendix A), as well as systematic errors from waveform modeling for the events GW231028_153006 for the TIGER and MDR analyses (Appendices B and C) and GW231123 for the MDR analysis (Appendix D). See Abac et al. (2025f) for studies of waveform-driven systematic uncertainties in standard parameter estimation for GW231123.

A. TIGER AND GW190728_064510

In the TIGER analysis of GW190728_064510 using the IMRPhenomXPHM model, we find that the GR value lies outside the 90% credible interval for the lower PN terms, in particular from 0PN to 1.5PN, as shown by the orange violin plots in Figure 13. The posterior distributions of the deviation parameters also exhibit bimodal features. However, the $\log_{10}$ Bayes factors in favor of the beyond GR hypothesis over the GR hypothesis are negative for all deviation parameters, except for the 0PN and 0.5PN cases, where the values are positive but small, with $\log_{10} \mathcal{B} < 0.2$.

Also, the TIGER analysis of this event using the IMRPhenomPv2 model was reported in the GWTC-2.0 tests of GR (Abbott et al. 2021b). In that analysis, no apparent deviation was found, although strong bimodal features were present for several deviation parameters, with one mode consistent with GR and another mode shifted away from the GR value. To understand whether the differences with the IMRPhenomXPHM results are driven primarily by the improved treatment of precession or by the inclusion of higher-order modes, we additionally analyze this event using the IMRPhenomXP_SpinTaylor model (henceforth just IMRPhenomXP), which includes the updated precession treatment but not higher-order modes. We find a similar bimodal structure. However, the posteriors obtained with IMRPhenomPv2 and IMRPhenomXP are not fully consistent.

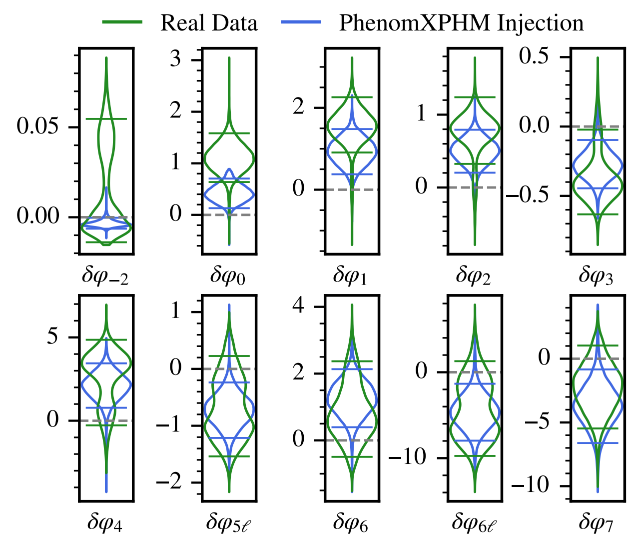

Figure 13. Results from the TIGER test on the inspiral part of the signal GW190728_064510, including the real data and real-noise injection studies, one with IMRPhenomXPHM, based on the maximum-likelihood sample from the GR analysis. All TIGER analyses were carried out using the same waveform model as the baseline.

Table 7. Comparison of the GR quantiles, $Q_{\rm GR} = P(\delta\hat{\varphi}_i < 0)$, for the TIGER analysis of GW190728_064510 and the corresponding real noise injection

Parameter	Real event	Injection
$\delta\varphi_{-2}$	40.3%	94.0%
$\delta\varphi_0$	0.3%	0.7%
$\delta\varphi_1$	1.4%	0.6%
$\delta\varphi_2$	3.8%	0.7%
$\delta\varphi_3$	93.5%	99.2%
$\delta\varphi_4$	9.2%	1.1%
$\delta\varphi_{5\ell}$	87.0%	99.1%
$\delta\varphi_6$	14.7%	1.2%
$\delta\varphi_{6\ell}$	87.4%	98.1%
$\delta\varphi_7$	87.6%	97.6%

NOTE—The injection was performed 18 s after the event merger time and generated using the maximum-likelihood sample from the IMRPHENOMXPHM analysis. The TIGER analyses were carried out with the same waveform.

Since the IMRPHENOMXP result still shows a GR-consistent mode, while this mode is significantly suppressed in the IMRPHENOMXPHM analysis, the comparison suggests that the apparent deviation in the lower PN coefficients is mainly associated with the inclusion of higher-order modes.

To investigate whether the apparent tension with GR is driven by waveform systematics, we first perform a zero-noise injection analysis (i.e., we analyze simulated observations with no noise added) using IMRPHENOMXPHM and the event PSDs released with GWTC-2.1 (Abbott et al. 2024). The injection waveform is generated using the maximum-likelihood sample from a new IMRPHENOMXPHM_SPINTAYLOR analysis of this event. (Here we do not abbreviate the name of the waveform model to emphasize the difference compared to the IMRPHENOMXPHM_MSA version used in the GWTC-2.1 parameter-estimation analysis.) We do not observe any comparable deviation or bias in the posterior distributions of the deviation parameters.

We then perform a set of injections in real detector noise around the event time. The median detector-frame component masses of GW190728_064510 are $15.1\,M_\odot$ and $9.1\,M_\odot$, and the standard parameter-estimation analysis was performed using a 16 s data segment. To avoid overlap with the data segment used to analyze the event, we choose nearby integer-second offsets somewhat randomly, injecting the signal 20 s before and 18 s after the merger time. These choices place the injections close to the event time while keeping the corresponding data segments non-overlapping with the event segment. As described above, we use the same injection parameters and waveform model for these injections. For the injection performed 20 s before the event, the posteriors of the deviation parameters are consistent with the GR value.

However, for the injection performed 18 s after the event, we find qualitatively similar biases to those seen in the real event analysis, with the GR value lying outside the 90% credible intervals for several deviation parameters, as shown in Figure 13. The shifts are not identical to those in the real event, and in some lower PN cases the real event posteriors show larger apparent deviations. This is expected, since the injection probes only one nearby realization of real detector noise and is not intended to reproduce the exact noise fluctuation present at the event time. Instead, it demonstrates that real detector noise for GW190728_064510 like event can produce apparent deviations with comparable character.

Table A lists the GR quantiles, $Q_{\rm GR} = P(\delta\hat{\varphi}_i < 0)$, for the PN deviation coefficients considered in this analysis. Except for the 0PN coefficient, the real noise injection shows GR quantiles that are comparable to, or more extreme than, those of the real event, supporting the interpretation that such apparent deviations can arise from detector noise fluctuations. We also find that the $\log_{10}$ Bayes factors are positive for the 0.5PN, 1PN, and 3PN logarithmic deviation parameters, but all remain below 0.4.

A similar injection study was performed in previous work using NR waveforms injected into 21 different stretches of real detector noise and recovered with the previous version of TIGER (based on IMRPHENOMPv2; Meidam et al. 2018). Figure 8 of Meidam et al. (2018) shows the 90% credible intervals of the deviation parameters. In several cases, the GR value lies outside, or close to the edge of, the 90% credible interval. In particular, simulation number 20 shows behavior that is qualitatively consistent with our findings for GW190728_064510.

We therefore conclude that the apparent deviations observed for GW190728_064510 are most likely caused by a particular realization of detector noise rather than by waveform systematics or evidence for a genuine violation of GR. The weak Bayes-factor support for the beyond-GR hypotheses further supports this interpretation. Thus, while GW190728_064510 shows interesting behavior in the lower PN coefficients, the result is consistent with noise-induced fluctuations and does not provide evidence for a departure from GR.

B. TIGER AND GW231028_153006

As the GR analysis of GW231028_153006 found potential waveform systematic uncertainties (Abac et al. 2026a), we highlight the TIGER results for this event. This event only passes the criteria for TIGER analysis with post-inspiral parameters. For all intermediate parameters and two merger–ringdown parameters, the GR value lies at the edge of the 90% credible interval, as shown in the orange violin plot in Figure 14. However, the Bayes factor in favor of the beyond-GR model against the GR model is negative for all deviation parameters; specifically, all $\log_{10}$ Bayes factor values are less than -1.2.

To investigate whether the apparent tension with GR is driven by waveform uncertainties, we perform a zero-noise injection analysis using the NRSUR7DQ4 model (Varma et al. 2019), which directly interpolates numerical-relativity simu-

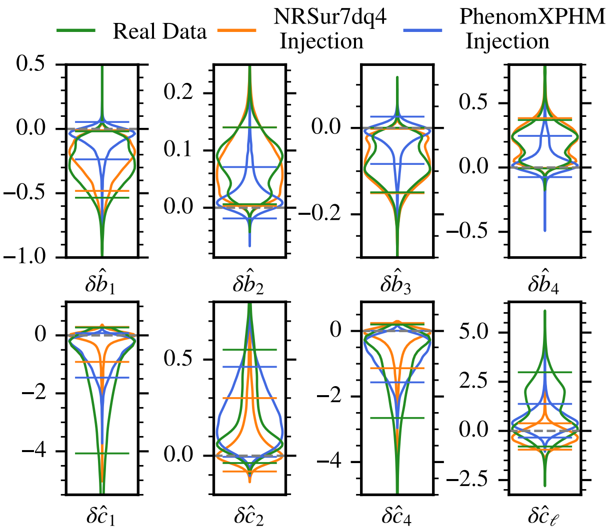

Figure 14. Results from the TIGER test on the intermediate and merger–ringdown portion of the signal GW231028_153006, including the real data and two zero-noise injection studies, one with NRSUR7DQ4 and one with IMRPHENOMXPHM, both based on the maximum-likelihood sample from the GR analysis. All TIGER analyses were carried out using the IMRPHENOMXPHM waveform model as the baseline.

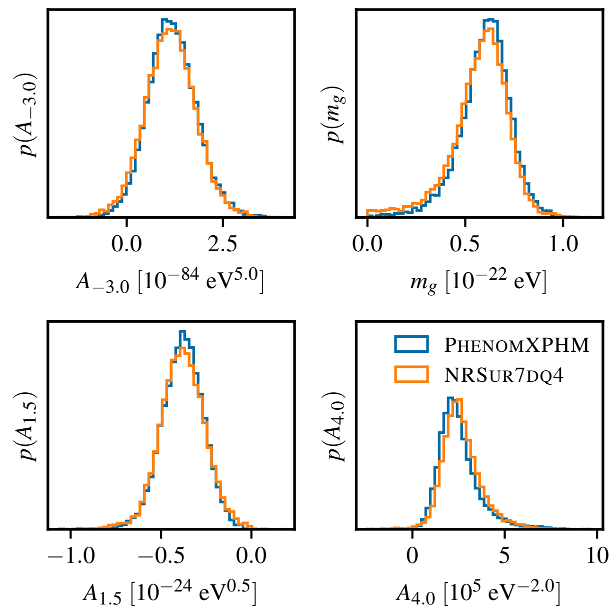

Figure 15. Representative posteriors for the MDR amplitude parameters A_α and the graviton mass m_g for GW231028_153006. Inference using both the IMRPHENOMXPHM and NRSUR7DQ4 waveform models does not show any significant systematic uncertainties. We instead find that this shift away from GR is due to a prior effect.

lations, avoiding the approximations used to construct IMRPHENOMXPHM. The injection waveform is generated from the maximum-likelihood sample of the NRSUR7DQ4 GR analysis for this event (Abac et al. 2026a). The same injection study for the MDR analysis is presented in Appendix C. As shown in Figure 14, the posteriors of the deviation parameters from the injection analysis are consistent with those from the real data. In particular, the GR value for the posterior of intermediate parameters is also found at the edge of the 90% credible interval. Since the TIGER baseline model is IMRPHENOMXPHM, the apparent tension may be driven by the choice of waveform model used in the injection simulations.

To further investigate the degeneracy between the deviation parameter and the GR parameters, we performed a zero-noise injection study using the maximum-likelihood sample from the IMRPHENOMXPHM GR analysis of this event. This approach avoids systematics arising from the choice of waveform models. The blue violin plots in Figure 14 show the posterior distributions of the deviation parameters. For the intermediate parameters, the GR values are recovered within the 90% credible intervals. However, for the merger–ringdown parameters, the GR values lie at the edge of the intervals. We find that the masses and spins are strongly correlated with the deviation parameter. In particular, the spin magnitude of the injection parameters is nearly unity, while the recovery with the TIGER model shows reduced consistency at high spin values for some deviation parameters. Moreover, the posteriors of the mass-related parameters differ significantly from those obtained with the GR model. Therefore, we conclude that while the shifts away from GR seen in the intermediate coefficients are primarily due to waveform uncertainties, the results for the merger–ringdown parameters are partly due to a strong degeneracy between the deviation parameter and the GR parameters, not by physics beyond GR.

C. MDR AND GW231028_153006

Of the 40 new events contributing to the improved bounds on the dispersion amplitudes A_α, GW231028_153006 is the least consistent with GR. Since the GR analysis identified potential waveform systematic uncertainties for this event, we performed an additional analysis using the more accurate NRSUR7DQ4 waveform model. Representative posteriors are shown in Figure 15. The posteriors are consistent across waveform models, indicating that our initial analysis with IMRPHENOMXPHM is reliable.

To better understand the apparent tension with GR, we analyzed a NRSUR7DQ4 injection into zero noise, based on the maximum-likelihood sample from the GR analysis of this event. In Figure 16, we show the inferred posterior distribution of the graviton mass m_g for this injection, compared to the result from the analysis of the actual data. The posteriors agree and both exhibit a peak in m_g away from zero, even though the injected signal is consistent with GR.

This can be attributed to a degeneracy between m_g and other binary parameters: the inferred parameters differ from those of the injection, yet the corresponding waveforms remain similar. We quantify this similarity using the mismatch between two

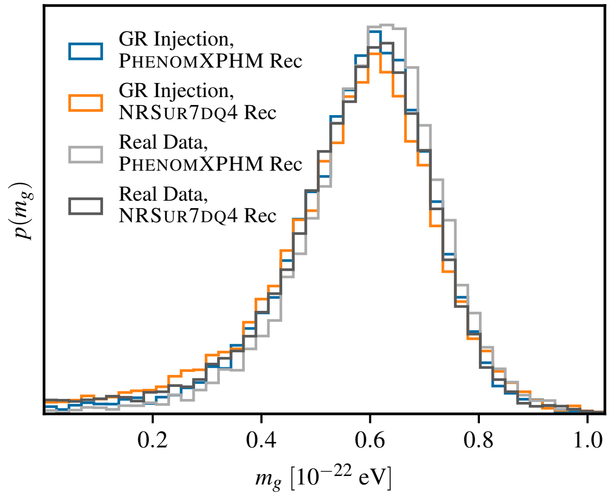

Figure 16. Graviton-mass posterior for GW231028_153006 both for real data and NRSur7dq4 injections into zero noise based on the maximum-likelihood sample from GR analysis. Both are analyzed with IMRPhenomXPHM and NRSur7dq4 waveform models. We thus find that this shift away from GR is due to a prior effect.

templates h_1 and h_2, defined as (Cutler & Flanagan 1994):

$$\mathrm{MM} = 1 - \left| \frac{\langle h_1 | h_2 \rangle}{\sqrt{\langle h_1 | h_1 \rangle \langle h_2 | h_2 \rangle}} \right|, \tag{C1}$$

where $\langle \cdot | \cdot \rangle$ denotes the noise-weighted inner product and a mismatch of 0 corresponds to identical templates. Comparing the injected signal with the waveform corresponding to the maximum-posterior sample, we find a low mismatch of $\mathrm{MM} = 0.0054$. While the likelihood near both the injection point and the maximum-posterior sample is similar, the prior density at the maximum-posterior location is higher by a factor of 3.31×10^5. Consequently, samples near the maximum-posterior point dominate, and GR-consistent solutions lie at the edge of the posterior distribution.

D. MDR AND GW231123

While GW231123 passed the MDR selection criteria, this event shows significant issues with waveform systematic uncertainties (Abac et al. 2025f). As the MDR analysis with IMRPhenomXPHM showed an apparent GR violation, we reanalyzed the data with the NRSur7dq4 waveform model to check if waveform uncertainties are responsible. NRSur7dq4 is a surrogate model that shows better agreement than IMRPhenomXPHM with numerical-relativity simulations for systems with similar total mass to GW231123 (Abac et al. 2025f). The results show significant discrepancies in the inferred posteriors of the amplitude parameters A_α and the graviton mass m_g; we show a few examples in Figure 17. The use of the NRSur7dq4 waveform model shifts the posteriors so that the GR value of 0 is included in the posterior mass. For $\alpha \leq 0$, the posteriors are unimodal and centered near zero. For $\alpha \in \{0.5, 1.5, 2.5\}$, the posteriors have multiple peaks but still show consistency with GR. For $\alpha \geq 3$, the

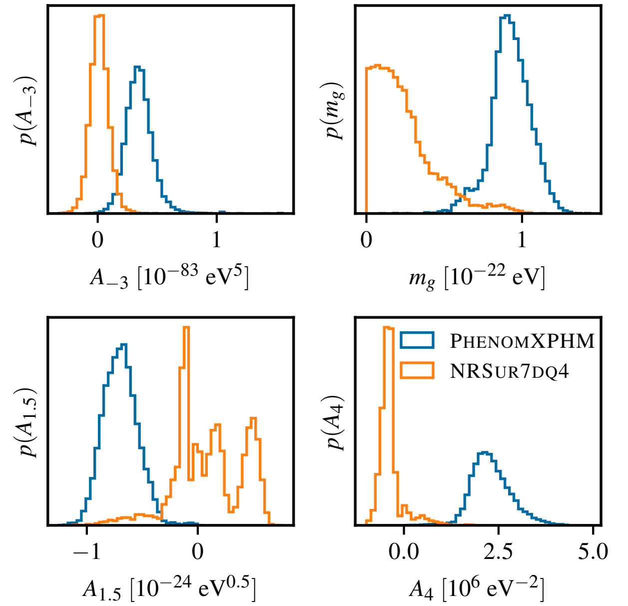

Figure 17. Representative posteriors for the MDR amplitude parameters A_α and the graviton mass m_g for GW231123. We find a large discrepancy in the results between those obtained using IMRPhenomXPHM and NRSur7dq4.

Table 8. $\mathcal{B}^{\mathrm{MDR}}_{\mathrm{GR}}$ comparison for GW231123

	XPHM $\log_{10} \mathcal{B}^{\mathrm{MDR}}_{\mathrm{GR}}$	NRSur $\log_{10} \mathcal{B}^{\mathrm{MDR}}_{\mathrm{GR}}$
$\alpha = -3.0$	-0.5	-2.5
$\alpha = -2.0$	-0.3	-2.5
$\alpha = -1.0$	0.1	-2.5
m_g	1.0	-1.3
$\alpha = 0.0$	0.2	-2.4
$\alpha = 0.5$	0.3	-2.2
$\alpha = 1.5$	0.8	-1.2
$\alpha = 2.5$	1.0	-0.6
$\alpha = 3.0$	1.0	-0.5
$\alpha = 3.5$	1.1	-0.2
$\alpha = 4.0$	1.8	0.1

Note—We give the values of the log Bayes factor $\mathcal{B}^{\mathrm{MDR}}_{\mathrm{GR}}$ in favor of MDR over GR for GW231123 analyzed with the IMRPhenomXPHM and NRSur7dq4 waveform models and consider a selection of different dispersion models (different values of α). The m_g row denotes the analysis with a prior uniform in the graviton mass. Each entry compares analyses performed with the same waveform model.

posteriors are almost unimodal, with a small peak near 0 and a larger peak further away. The inferred amplitude parameter A_α is closer to 0 and with the opposite sign compared to the IMRPhenomXPHM results.

In Table 8, we compare how the Bayes factors $\mathcal{B}^{\rm MDR}_{\rm GR}$ in favor of MDR over GR vary depending on the waveform used. For IMRPhenomXPHM, the Bayes factor shows a preference for MDR for $\alpha > -2$, despite its larger prior volume compared to GR (due to one additional parameter and an expanded prior range for the chirp mass to avoid railing). In the NRSur7dq4 analysis, GR is generally preferred over MDR, except for the $\alpha = 4$ case, where there is a small preference for MDR, though the uncertainty on the Bayes factors has a standard deviation of ~ 0.2.

Due to these issues with the waveform systematic uncertainties, we have excluded GW231123 from the combined bounds on GW dispersion.

REFERENCES

Abac, A. G., Abouelfettouh, I., Acernese, F., et al. 2025a, ApJL, 995, L18, doi: 10.3847/2041-8213/ae0c06

—. 2025b, PhRvL, 135, 111403, doi: 10.1103/kw5g-d732

—. 2025c, ApJL, 993, L21, doi: 10.3847/2041-8213/ae0d54

—. 2025d. https://arxiv.org/abs/2508.18083

—. 2025e. https://arxiv.org/abs/2509.04348

—. 2025f, ApJL, 993, L25, doi: 10.3847/2041-8213/ae0c9c

—. 2026a, ApJL, 1004, L22, doi: 10.3847/2041-8213/ae2c74

—. 2026b. https://arxiv.org/abs/2603.19019

—. 2026c. https://arxiv.org/abs/2603.19021

—. 2026d, ApJL, 1004, L23, doi: 10.3847/2041-8213/ae2ad3

—. 2026e, PhRvL, 136, 041403, doi: 10.1103/6c61-fm1n

—. 2026f, ApJ, 1004, 232, doi: 10.3847/1538-4357/ae211e

Abbott, B. P., Abbott, R., Abbott, T. D., et al. 2016a, PhRvX, 6, 041015, doi: 10.1103/PhysRevX.6.041015

—. 2016b, PhRvL, 116, 221101, doi: 10.1103/PhysRevLett.116.221101

—. 2017, PhRvL, 118, 221101, doi: 10.1103/PhysRevLett.118.221101

—. 2019a, PhRvX, 9, 031040, doi: 10.1103/PhysRevX.9.031040

—. 2019b, PhRvL, 123, 011102, doi: 10.1103/PhysRevLett.123.011102

—. 2019c, PhRvD, 100, 104036, doi: 10.1103/PhysRevD.100.104036

—. 2020a, LRR, 23, 3, doi: 10.1007/s41114-020-00026-9

Abbott, R., Abbott, T. D., Abraham, S., et al. 2020b, ApJL, 896, L44, doi: 10.3847/2041-8213/ab960f

—. 2021a, PhRvX, 11, 021053, doi: 10.1103/PhysRevX.11.021053

—. 2021b, PhRvD, 103, 122002, doi: 10.1103/PhysRevD.103.122002

Abbott, R., Abbott, T. D., Acernese, F., et al. 2023, PhRvX, 13, 041039, doi: 10.1103/PhysRevX.13.041039

—. 2024, PhRvD, 109, 022001, doi: 10.1103/PhysRevD.109.022001

Abbott, R., Abe, H., Acernese, F., et al. 2025, PhRvD, 112, 084080, doi: 10.1103/PhysRevD.112.084080

Acernese, F., Agathos, M., Ain, A., et al. 2022, CQGra, 39, 045006, doi: 10.1088/1361-6382/ac3c8e

Adams, T., Buskulic, D., Germain, V., et al. 2016, CQGra, 33, 175012, doi: 10.1088/0264-9381/33/17/175012

Agathos, M., Del Pozzo, W., Li, T. G. F., et al. 2014, PhRvD, 89, 082001, doi: 10.1103/PhysRevD.89.082001

Alexander, S., & Yunes, N. 2009, PhR, 480, 1, doi: 10.1016/j.physrep.2009.07.002

Amelino-Camelia, G. 2002, Nature, 418, 34, doi: 10.1038/418034a

Arun, K. G., Buonanno, A., Faye, G., & Ochsner, E. 2009, PhRvD, 79, 104023, doi: 10.1103/PhysRevD.79.104023

Arun, K. G., Iyer, B. R., Qusailah, M. S. S., & Sathyaprakash, B. S. 2006a, PhRvD, 74, 024006, doi: 10.1103/PhysRevD.74.024006

—. 2006b, CQGra, 23, L37, doi: 10.1088/0264-9381/23/9/L01

Arun, K. G., & Pai, A. 2013, IJMPD, 22, 1341012, doi: 10.1142/S0218271813410125

Ashton, G., Hübner, M., Lasky, P. D., et al. 2019, ApJS, 241, 27, doi: 10.3847/1538-4365/ab06fc

Ashton, G., Udall, R., & Yarbrough, Z. 2025a, CBC Workflow. https://github.com/Rhiannon-Udall/cbcflow

Ashton, G., Talbot, C., Roy, S., et al. 2025b, Bilby TGR, v0.2, Zenodo, doi: 10.5281/zenodo.15676285

Aubin, F., Brighenti, F., Chierici, R., et al. 2021, CQGra, 38, 095004, doi: 10.1088/1361-6382/abe913

Baka, T., Cirok, B., Haris, K., Noller, J., & Krishnendu, N. V. 2026, PhRvD, 113, 064064, doi: 10.1103/bgvh-c1wj

Baker, T., Calcagni, G., Chen, A., et al. 2022, JCAP, 08, 031, doi: 10.1088/1475-7516/2022/08/031

Beltrán Jiménez, J., Ezquiaga, J. M., & Heisenberg, L. 2020, JCAP, 04, 027, doi: 10.1088/1475-7516/2020/04/027

Bernard, L., Blanchet, L., & Trestini, D. 2022, JCAP, 08, 008, doi: 10.1088/1475-7516/2022/08/008

Blanchet, L. 2024, LRR, 27, 4, doi: 10.1007/s41114-024-00050-z

Blanchet, L., Faye, G., Henry, Q., Larrouturou, F., & Trestini, D. 2023, PhRvL, 131, 121402, doi: 10.1103/PhysRevLett.131.121402

Blanchet, L., & Sathyaprakash, B. S. 1994, CQGra, 11, 2807, doi: 10.1088/0264-9381/11/11/020

—. 1995, PhRvL, 74, 1067, doi: 10.1103/PhysRevLett.74.1067

Bohé, A., Hannam, M., Husa, S., et al. 2016, PhenomPv2 - Technical Notes for LAL Implementation, Tech. Rep. LIGO-T1500602, LIGO Project. https://dcc.ligo.org/LIGO-T1500602/public

Bohé, A., Shao, L., Taracchini, A., et al. 2017, PhRvD, 95, 044028, doi: 10.1103/PhysRevD.95.044028
Buonanno, A., Iyer, B. R., Ochsner, E., Pan, Y., & Sathyaprakash, B. S. 2009, PhRvD, 80, 084043, doi: 10.1103/PhysRevD.80.084043
Cabero, M., Nielsen, A. B., Lundgren, A. P., & Capano, C. D. 2017, PhRvD, 95, 064016, doi: 10.1103/PhysRevD.95.064016
Calcagni, G. 2010, PhRvL, 104, 251301, doi: 10.1103/PhysRevLett.104.251301
Cannon, K., Caudill, S., Chan, C., et al. 2021, SoftX, 14, 100680, doi: 10.1016/j.softx.2021.100680
Cardoso, V., Franzin, E., Maselli, A., Pani, P., & Raposo, G. 2017, PhRvD, 95, 084014, doi: 10.1103/PhysRevD.95.084014
Carter, B. 1971, PhRvL, 26, 331, doi: 10.1103/PhysRevLett.26.331
Caspar, G., Schonenbach, T., Hess, P. O., Schafer, M., & Greiner, W. 2012, IJMPE, 21, 1250015, doi: 10.1142/S0218301312500152
Chandrasekhar, S. 1965, ApJ, 142, 1488, doi: 10.1086/148432
Chia, H. S., Zhou, Z., & Ivanov, M. M. 2025, PhRvD, 111, 063002, doi: 10.1103/PhysRevD.111.063002
Chung, A. K.-W., & Yunes, N. 2025. https://arxiv.org/abs/2506.14695
Colladay, D., & Kostelecký, V. A. 1998, PhRvD, 58, 116002, doi: 10.1103/PhysRevD.58.116002
Colleoni, M., Ramis Vidal, F. A., Johnson-McDaniel, N. K., et al. 2025a, PhRvD, 111, 064025, doi: 10.1103/PhysRevD.111.064025
Colleoni, M., Vidal, F. A. R., García-Quirós, C., Akçay, S., & Bera, S. 2025b, PhRvD, 111, 104019, doi: 10.1103/PhysRevD.111.104019
Cornish, N., Sampson, L., Yunes, N., & Pretorius, F. 2011, PhRvD, 84, 062003, doi: 10.1103/PhysRevD.84.062003
Cornish, N. J., & Littenberg, T. B. 2015, CQGra, 32, 135012, doi: 10.1088/0264-9381/32/13/135012
Cornish, N. J., Littenberg, T. B., Bécsy, B., et al. 2021, PhRvD, 103, 044006, doi: 10.1103/PhysRevD.103.044006
Cotesta, R., Marsat, S., & Pürrer, M. 2020, PhRvD, 101, 124040, doi: 10.1103/PhysRevD.101.124040
Cutler, C., & Flanagan, É. É. 1994, PhRvD, 49, 2658, doi: 10.1103/PhysRevD.49.2658
Datta, S., & Bose, S. 2019, PhRvD, 99, 084001, doi: 10.1103/PhysRevD.99.084001
Datta, S., Brito, R., Bose, S., Pani, P., & Hughes, S. A. 2020, PhRvD, 101, 044004, doi: 10.1103/PhysRevD.101.044004
Datta, S., Gupta, A., Kastha, S., Arun, K. G., & Sathyaprakash, B. S. 2021, PhRvD, 103, 024036, doi: 10.1103/PhysRevD.103.024036
Datta, S., Saleem, M., Arun, K. G., & Sathyaprakash, B. S. 2024, PhRvD, 109, 044036, doi: 10.1103/PhysRevD.109.044036
Davies, G. S., Dent, T., Tápai, M., et al. 2020, PhRvD, 102, 022004, doi: 10.1103/PhysRevD.102.022004
Davis, D., Littenberg, T. B., Romero-Shaw, I. M., et al. 2022, CQGra, 39, 245013, doi: 10.1088/1361-6382/aca238
de Rham, C., & Melville, S. 2018, PhRvL, 121, 221101, doi: 10.1103/PhysRevLett.121.221101
Dietrich, T., Samajdar, A., Khan, S., et al. 2019, PhRvD, 100, 044003, doi: 10.1103/PhysRevD.100.044003
Divyajyoti, Krishnendu, N. V., Saleem, M., et al. 2024, PhRvD, 109, 023016, doi: 10.1103/PhysRevD.109.023016
Einstein, A., Infeld, L., & Hoffmann, B. 1938, AnMat, 39, 65, doi: 10.2307/1968714
Essick, R., Farr, W. M., Fishbach, M., Holz, D. E., & Katsavounidis, E. 2023, PhRvD, 107, 043016, doi: 10.1103/PhysRevD.107.043016
Essick, R., Godwin, P., Hanna, C., Blackburn, L., & Katsavounidis, E. 2020, MLS&T, 2, 015004, doi: 10.1088/2632-2153/abab5f
Ezquiaga, J. M., Hu, W., Lagos, M., Lin, M.-X., & Xu, F. 2022, JCAP, 08, 016, doi: 10.1088/1475-7516/2022/08/016
Fisher, R. P., Hemming, G., Bizouard, M.-A., et al. 2021, SoftX, 14, 100677, doi: 10.1016/j.softx.2021.100677
Gao, B., Tang, S.-P., Wang, H.-T., Yan, J., & Fan, Y.-Z. 2024, PhRvD, 110, 044022, doi: 10.1103/PhysRevD.110.044022
Gross, D. J., & Sloan, J. H. 1987, NuPhB, 291, 41, doi: 10.1016/0550-3213(87)90465-2
Gupta, A., Datta, S., Kastha, S., et al. 2020, PhRvL, 125, 201101, doi: 10.1103/PhysRevLett.125.201101
Gupta, T., & Cornish, N. J. 2024, PhRvD, 109, 064040, doi: 10.1103/PhysRevD.109.064040
Haegel, L., O'Neal-Ault, K., Bailey, Q. G., et al. 2023, PhRvD, 107, 064031, doi: 10.1103/PhysRevD.107.064031
Hanna, C., Caudill, S., Messick, C., et al. 2020, PhRvD, 101, 022003, doi: 10.1103/PhysRevD.101.022003
Hannam, M., Schmidt, P., Bohé, A., et al. 2014, PhRvL, 113, 151101, doi: 10.1103/PhysRevLett.113.151101
Hansen, R. O. 1974, JMP, 15, 46, doi: 10.1063/1.1666501
Harris, C. R., Millman, K. J., van der Walt, S. J., et al. 2020, Nature, 585, 357, doi: 10.1038/s41586-020-2649-2
Harry, I., & Hinderer, T. 2018, CQGra, 35, 145010, doi: 10.1088/1361-6382/aac7e3
Harry, I., & Noller, J. 2022, GReGr, 54, 133, doi: 10.1007/s10714-022-03016-0
Hess, P. O. 2016, MNRAS, 462, 3026, doi: 10.1093/mnras/stw1919
Hess, P. O., & Greiner, W. 2009, IJMPE, 18, 51, doi: 10.1142/S0218301309012045
Hořava, P. 2009, PhRvD, 79, 084008, doi: 10.1103/PhysRevD.79.084008
Horbatsch, M. W., & Burgess, C. P. 2012, JCAP, 05, 010, doi: 10.1088/1475-7516/2012/05/010
Hoy, C., & Raymond, V. 2021, SoftX, 15, 100765, doi: 10.1016/j.softx.2021.100765
Hunter, J. D. 2007, CSE, 9, 90, doi: 10.1109/MCSE.2007.55
Husa, S., Khan, S., Hannam, M., et al. 2016, PhRvD, 93, 044006, doi: 10.1103/PhysRevD.93.044006

Jacobson, T. 1999, PhRvL, 83, 2699, doi: 10.1103/PhysRevLett.83.2699

Johnson-McDaniel, N. K., Ghosh, A., Ghonge, S., et al. 2022, PhRvD, 105, 044020, doi: 10.1103/PhysRevD.105.044020

Johnson-McDaniel, N. K., Mukherjee, A., Kashyap, R., et al. 2020, PhRvD, 102, 123010, doi: 10.1103/PhysRevD.102.123010

Julié, F.-L., Pompili, L., & Buonanno, A. 2025, PhRvD, 111, 024016, doi: 10.1103/PhysRevD.111.024016

Julié, F.-L. 2018, JCAP, 10, 033, doi: 10.1088/1475-7516/2018/10/033

Kanti, P., Mavromatos, N. E., Rizos, J., Tamvakis, K., & Winstanley, E. 1996, PhRvD, 54, 5049, doi: 10.1103/PhysRevD.54.5049

Kastha, S., Gupta, A., Arun, K. G., Sathyaprakash, B. S., & Van Den Broeck, C. 2018, PhRvD, 98, 124033, doi: 10.1103/PhysRevD.98.124033

—. 2019, PhRvD, 100, 044007, doi: 10.1103/PhysRevD.100.044007

Khalil, M., Sennett, N., Steinhoff, J., & Buonanno, A. 2019, PhRvD, 100, 124013, doi: 10.1103/PhysRevD.100.124013

Khalil, M., Sennett, N., Steinhoff, J., Vines, J., & Buonanno, A. 2018, PhRvD, 98, 104010, doi: 10.1103/PhysRevD.98.104010

Khan, S., Chatziioannou, K., Hannam, M., & Ohme, F. 2019, PhRvD, 100, 024059, doi: 10.1103/PhysRevD.100.024059

Khan, S., Husa, S., Hannam, M., et al. 2016, PhRvD, 93, 044007, doi: 10.1103/PhysRevD.93.044007

Khan, S., Ohme, F., Chatziioannou, K., & Hannam, M. 2020, PhRvD, 101, 024056, doi: 10.1103/PhysRevD.101.024056

Klimenko, S., Vedovato, G., Drago, M., et al. 2016, PhRvD, 93, 042004, doi: 10.1103/PhysRevD.93.042004

Klimenko, S., Yakushin, I., Rakhmanov, M., & Mitselmakher, G. 2004, CQGra, 21, S1685, doi: 10.1088/0264-9381/21/20/011

Klimenko, S., Vedovato, G., Drago, M., et al. 2011, PhRvD, 83, 102001, doi: 10.1103/PhysRevD.83.102001

Kostelecký, V. A. 2004, PhRvD, 69, 105009, doi: 10.1103/PhysRevD.69.105009

Kostelecký, V. A., & Mewes, M. 2016, PhLB, 757, 510, doi: 10.1016/j.physletb.2016.04.040

Kostelecký, V. A., & Russell, N. 2026. https://arxiv.org/abs/0801.0287v19

Kramer, M., Stairs, I. H., Manchester, R. N., et al. 2021, PhRvX, 11, 041050, doi: 10.1103/PhysRevX.11.041050

Krishnendu, N. V., Arun, K. G., & Mishra, C. K. 2017, PhRvL, 119, 091101, doi: 10.1103/PhysRevLett.119.091101

Krishnendu, N. V., Mishra, C. K., & Arun, K. G. 2019a, PhRvD, 99, 064008, doi: 10.1103/PhysRevD.99.064008

Krishnendu, N. V., Saleem, M., Samajdar, A., et al. 2019b, PhRvD, 100, 104019, doi: 10.1103/PhysRevD.100.104019

Lang, R. N. 2014, PhRvD, 89, 084014, doi: 10.1103/PhysRevD.89.084014

—. 2015, PhRvD, 91, 084027, doi: 10.1103/PhysRevD.91.084027

Li, T. G. F., Del Pozzo, W., Vitale, S., et al. 2012a, PhRvD, 85, 082003, doi: 10.1103/PhysRevD.85.082003

—. 2012b, JPhCS, 363, 012028, doi: 10.1088/1742-6596/363/1/012028

LIGO Scientific Collaboration and Virgo Collaboration. 2018, Data quality report user documentation, docs.ligo.org/detchar/data-quality-report/

LIGO Scientific, Virgo, and KAGRA Collaboration. 2026a, Data release for GWTC-4.0: Tests of General Relativity. II. Parameterized Tests. https://dcc.ligo.org/P2600128/public

—. 2026b, LVK Algorithm Library - LALSuite, doi: 10.7935/GT1W-FZ16

Lin, J. 1991, IEEE Trans. Info. Theor., 37, 145, doi: 10.1109/18.61115

Littenberg, T. B., Kanner, J. B., Cornish, N. J., & Millhouse, M. 2016, PhRvD, 94, 044050, doi: 10.1103/PhysRevD.94.044050

Liu, H., & Yunes, N. 2025, PhRvD, 111, 084049, doi: 10.1103/PhysRevD.111.084049

Lyu, Z., Jiang, N., & Yagi, K. 2022, PhRvD, 105, 064001, doi: 10.1103/PhysRevD.105.064001

Macleod, D., Goetz, E., Davis, D., et al. 2021a, gwdetchar/gwdetchar, v2.3.1, Zenodo, doi: 10.5281/zenodo.2575786

Macleod, D. M., Areeda, J. S., Coughlin, S. B., Massinger, T. J., & Urban, A. L. 2021b, SoftX, 13, 100657, doi: 10.1016/j.softx.2021.100657

Maenaut, S., Carullo, G., Cano, P. A., et al. 2026, PhRvD, 113, 044039, doi: 10.1103/k3hv-cqfn

Maggiore, M. 2007, Gravitational Waves. Vol. 1: Theory and Experiments (Oxford University Press), doi: 10.1093/acprof:oso/9780198570745.001.0001

Mahapatra, P. 2024, PhRvD, 109, 024050, doi: 10.1103/PhysRevD.109.024050

Mahapatra, P., Datta, S., Gupta, I., et al. 2025, PhRvD, 112, 104007, doi: 10.1103/c1sj-jc4v

Mahapatra, P., & Kastha, S. 2024, PhRvD, 109, 084069, doi: 10.1103/PhysRevD.109.084069

Mahapatra, P., Kastha, S., Gupta, A., Sathyaprakash, B. S., & Arun, K. G. 2024, PhRvD, 109, 064036, doi: 10.1103/PhysRevD.109.064036

Maimon, Y. I., Nielsen, A. B., & Birnholtz, O. 2025, CQGra, 42, 185011, doi: 10.1088/1361-6382/ae008a

Mariani, V., Fienga, A., Minazzoli, O., Gastineau, M., & Laskar, J. 2023, PhRvD, 108, 024047, doi: 10.1103/PhysRevD.108.024047

Marsat, S. 2015, CQGra, 32, 085008, doi: 10.1088/0264-9381/32/8/085008

Maselli, A., Pani, P., Cardoso, V., et al. 2018, PhRvL, 120, 081101, doi: 10.1103/PhysRevLett.120.081101

Matas, A., Dietrich, T., Buonanno, A., et al. 2020, PhRvD, 102, 043023, doi: 10.1103/PhysRevD.102.043023

Mehta, A. K., Buonanno, A., Cotesta, R., et al. 2023, PhRvD, 107, 044020, doi: 10.1103/PhysRevD.107.044020

Meidam, J., Tsang, K. W., Goldstein, J., et al. 2018, PhRvD, 97, 044033, doi: 10.1103/PhysRevD.97.044033

Messick, C., Blackburn, K., Brady, P., et al. 2017, PhRvD, 95, 042001, doi: 10.1103/PhysRevD.95.042001

Mewes, M. 2019, PhRvD, 99, 104062, doi: 10.1103/PhysRevD.99.104062

Mirshekari, S., & Will, C. M. 2013, PhRvD, 87, 084070, doi: 10.1103/PhysRevD.87.084070

Mirshekari, S., Yunes, N., & Will, C. M. 2012, PhRvD, 85, 024041, doi: 10.1103/PhysRevD.85.024041

Mishra, C. K., Arun, K. G., Iyer, B. R., & Sathyaprakash, B. S. 2010, PhRvD, 82, 064010, doi: 10.1103/PhysRevD.82.064010

Mishra, C. K., Kela, A., Arun, K. G., & Faye, G. 2016, PhRvD, 93, 084054, doi: 10.1103/PhysRevD.93.084054

Nair, R., Perkins, S., Silva, H. O., & Yunes, N. 2019, PhRvL, 123, 191101, doi: 10.1103/PhysRevLett.123.191101

Nair, R., & Yunes, N. 2020, PhRvD, 101, 104011, doi: 10.1103/PhysRevD.101.104011

Narikawa, T., Uchikata, N., & Tanaka, T. 2021, PhRvD, 104, 084056, doi: 10.1103/PhysRevD.104.084056

Nielsen, A. B., & Birnholtz, O. 2018, AN, 339, 298, doi: 10.1002/asna.201813473

Nitz, A. H., Dent, T., Dal Canton, T., Fairhurst, S., & Brown, D. A. 2017, ApJ, 849, 118, doi: 10.3847/1538-4357/aa8f50

O'Neal-Ault, K., Bailey, Q. G., Dumerchat, T., Haegel, L., & Tasson, J. 2021, Univ, 7, 380, doi: 10.3390/universe7100380

Pacilio, C., Vaglio, M., Maselli, A., & Pani, P. 2020, PhRvD, 102, 083002, doi: 10.1103/PhysRevD.102.083002

Pai, A., & Arun, K. G. 2013, CQGra, 30, 025011, doi: 10.1088/0264-9381/30/2/025011

Pappas, G., & Apostolatos, T. A. 2012a. https://arxiv.org/abs/1211.6299

—. 2012b, PhRvL, 108, 231104, doi: 10.1103/PhysRevLett.108.231104

Pedregosa, F., Varoquaux, G., Gramfort, A., et al. 2011, JMLR, 12, 2825

Perkins, S., & Yunes, N. 2022, PhRvD, 105, 124047, doi: 10.1103/PhysRevD.105.124047

Perkins, S. E., Nair, R., Silva, H. O., & Yunes, N. 2021, PhRvD, 104, 024060, doi: 10.1103/PhysRevD.104.024060

Poisson, E., & Will, C. M. 2014, Gravity (Cambridge, UK: Cambridge University Press), doi: 10.1017/CBO9781139507486

Pompili, L., Buonanno, A., Estellés, H., et al. 2023, PhRvD, 108, 124035, doi: 10.1103/PhysRevD.108.124035

Pratten, G., García-Quirós, C., Colleoni, M., et al. 2021, PhRvD, 103, 104056, doi: 10.1103/PhysRevD.103.104056

Pratten, G., Husa, S., García-Quirós, C., et al. 2020, PhRvD, 102, 064001, doi: 10.1103/PhysRevD.102.064001

Robinet, F., Arnaud, N., Leroy, N., et al. 2020, SoftX, 12, 100620, doi: 10.1016/j.softx.2020.100620

Romero-Shaw, I. M., Talbot, C., Biscoveanu, S., et al. 2020, MNRAS, 499, 3295, doi: 10.1093/mnras/staa2850

Roy, S., Haney, M., Pratten, G., Pang, P. T. H., & Van Den Broeck, C. 2026, PhRvD, 113, 024016, doi: 10.1103/855k-sys5

Ryan, F. D. 1997, PhRvD, 55, 6081, doi: 10.1103/PhysRevD.55.6081

Sachdev, S., Caudill, S., Fong, H., et al. 2019. https://arxiv.org/abs/1901.08580

Saleem, M., Datta, S., Arun, K. G., & Sathyaprakash, B. S. 2022, PhRvD, 105, 084062, doi: 10.1103/PhysRevD.105.084062

Sampson, L., Cornish, N., & Yunes, N. 2013, PhRvD, 87, 102001, doi: 10.1103/PhysRevD.87.102001

—. 2014, PhRvD, 89, 064037, doi: 10.1103/PhysRevD.89.064037

Sänger, E. M., Roy, S., Agathos, M., et al. 2026, PhRvD, 113, 084070, doi: 10.1103/r43k-51yq

Sathyaprakash, B. S., & Dhurandhar, S. V. 1991, PhRvD, 44, 3819, doi: 10.1103/PhysRevD.44.3819

Sefiedgar, A. S., Nozari, K., & Sepangi, H. R. 2011, PhLB, 696, 119, doi: 10.1016/j.physletb.2010.11.067

Sennett, N., Hinderer, T., Steinhoff, J., Buonanno, A., & Ossokine, S. 2017, PhRvD, 96, 024002, doi: 10.1103/PhysRevD.96.024002

Shiralilou, B., Hinderer, T., Nissanke, S. M., Ortiz, N., & Witek, H. 2022, CQGra, 39, 035002, doi: 10.1088/1361-6382/ac4196

Shoom, A. A., Gupta, P. K., Krishnan, B., Nielsen, A. B., & Capano, C. D. 2023, GReGr, 55, 55, doi: 10.1007/s10714-023-03100-z

Silva, H. O., Ghosh, A., & Buonanno, A. 2023, PhRvD, 107, 044030, doi: 10.1103/PhysRevD.107.044030

Silva, H. O., Holgado, A. M., Cárdenas-Avendaño, A., & Yunes, N. 2021, PhRvL, 126, 181101, doi: 10.1103/PhysRevLett.126.181101

Smith, J. R., Abbott, T., Hirose, E., et al. 2011, CQGra, 28, 235005, doi: 10.1088/0264-9381/28/23/235005

Smith, R., Ashton, G., Vajpeyi, A., & Talbot, C. 2020, MNRAS, 498, 4492, doi: 10.1093/mnras/staa2483

Sotiriou, T. P., & Barausse, E. 2007, PhRvD, 75, 084007, doi: 10.1103/PhysRevD.75.084007

Speagle, J. S. 2020, MNRAS, 493, 3132, doi: 10.1093/mnras/staa278

Taylor, J. H., & Weisberg, J. M. 1982, ApJ, 253, 908, doi: 10.1086/159690

—. 1989, ApJ, 345, 434, doi: 10.1086/167917

Thompson, J. E., Fauchon-Jones, E., Khan, S., et al. 2020, PhRvD, 101, 124059, doi: 10.1103/PhysRevD.101.124059

Thorne, K. S. 1980, RvMP, 52, 299, doi: 10.1103/RevModPhys.52.299

Tiwari, A., Vijaykumar, A., Kapadia, S. J., Ghosh, S., & Nielsen, A. B. 2026, PhRvD, 113, 104072, doi: 10.1103/qtw8-3g56

Uchikata, N., & Yoshida, S. 2016, CQGra, 33, 025005, doi: 10.1088/0264-9381/33/2/025005
Usman, S. A., Nitz, A. H., Harry, I. W., et al. 2016, CQGra, 33, 215004, doi: 10.1088/0264-9381/33/21/215004
Varma, V., Field, S. E., Scheel, M. A., et al. 2019, PhRvR, 1, 033015, doi: 10.1103/PhysRevResearch.1.033015
Viets, A. D., Wade, M., Urban, A. L., et al. 2018, CQGra, 35, 095015, doi: 10.1088/1361-6382/aab658
Vijaykumar, A., Tiwari, A., Kapadia, S. J., Arun, K. G., & Ajith, P. 2023, ApJ, 954, 105, doi: 10.3847/1538-4357/acd77d
Virgo Collaboration. 2021, PythonVirgoTools, v5.1.1, git.ligo.org/virgo/virgoapp/PythonVirgoTools
Virtanen, P., Gommers, R., Oliphant, T. E., et al. 2020, NatMe, 17, 261, doi: 10.1038/s41592-019-0686-2
Waskom, M. L. 2021, JOSS, 6, 3021, doi: 10.21105/joss.03021
Wette, K. 2020, SoftX, 12, 100634, doi: 10.1016/j.softx.2020.100634
Will, C. M. 1998, PhRvD, 57, 2061, doi: 10.1103/PhysRevD.57.2061
—. 2014, LRR, 17, 4, doi: 10.12942/lrr-2014-4
Will, C. M. 2018, Theory and Experiment in Gravitational Physics, 2nd edn. (Cambridge, UK: Cambridge University Press), doi: 10.1017/9781316338612
Williams, D., Veitch, J., Chiofalo, M. L., et al. 2023, JOSS, 8, 4170, doi: 10.21105/joss.04170
Yagi, K., Stein, L. C., & Yunes, N. 2016, PhRvD, 93, 024010, doi: 10.1103/PhysRevD.93.024010
Yagi, K., Stein, L. C., Yunes, N., & Tanaka, T. 2012a, PhRvD, 85, 064022, doi: 10.1103/PhysRevD.85.064022
Yagi, K., Yunes, N., & Tanaka, T. 2012b, PhRvL, 109, 251105, doi: 10.1103/PhysRevLett.116.169902
Yunes, N., & Hughes, S. A. 2010, PhRvD, 82, 082002, doi: 10.1103/PhysRevD.82.082002
Yunes, N., & Pretorius, F. 2009, PhRvD, 80, 122003, doi: 10.1103/PhysRevD.80.122003
Yunes, N., Yagi, K., & Pretorius, F. 2016, PhRvD, 94, 084002, doi: 10.1103/PhysRevD.94.084002
Zweizig, J. 2006, The Data Monitor Tool Project, labcit.ligo.caltech.edu/~jzweizig/DMT-Project.html

The LIGO Scientific Collaboration, the Virgo Collaboration, and the KAGRA Collaboration, A. G. Abac,[1]
I. Abouelfettouh,[2] F. Acernese,[3,4] K. Ackley,[5] C. Adamcewicz,[6] S. Adhicary,[7] D. Adhikari,[8,9] N. Adhikari,[10]
R. X. Adhikari,[11] V. K. Adkins,[12] S. Afroz,[13] A. Agapito,[14] D. Agarwal,[15] M. Agathos,[16] N. Aggarwal,[17] S. Aggarwal,[18]
O. D. Aguiar,[19] I.-L. Ahrend,[20] L. Aiello,[21,22] A. Ain,[23] P. Ajith,[24] T. Akutsu,[25,26] S. Albanesi,[27,28] W. Ali,[29,30]
S. Al-Kershi,[8,9] C. Alléné,[31] A. Allocca,[32,4] S. Al-Shammari,[33] P. A. Altin,[34] S. Alvarez-Lopez,[35] W. Amar,[31]
O. Amarasinghe,[33] A. Amato,[36,37] F. Amicucci,[38,39] C. Amra,[40] A. Ananyeva,[11] S. B. Anderson,[11] W. G. Anderson,[11]
M. Andia,[41] M. Ando,[42] M. Andrés-Carcasona,[43] T. Andrić,[44,45,8,9] J. Anglin,[46] S. Ansoldi,[47,48] J. M. Antelis,[49]
S. Antier,[41] M. Aoumi,[50] E. Z. Appavuravther,[51,52] S. Appert,[11] S. K. Apple,[53] K. Arai,[11] A. Araya,[42] M. C. Araya,[11]
M. Arca Sedda,[44,45] J. S. Areeda,[54] N. Aritomi,[2] F. Armato,[29,30] S. Armstrong,[55] N. Arnaud,[56] M. Arogeti,[57]
S. M. Aronson,[12] K. G. Arun,[58] G. Ashton,[59] Y. Aso,[25,60] L. Asprea,[28] M. Assiduo,[61,62] S. Assis de Souza Melo,[63]
S. M. Aston,[64] P. Astone,[38] F. Attadio,[39,38] F. Aubin,[65] K. AultONeal,[66] G. Avallone,[67] E. A. Avila,[49] S. Babak,[20]
C. Badger,[68] S. Bae,[69] S. Bagnasco,[28] L. Baiotti,[70] R. Bajpai,[71] T. Baka,[72,37] A. M. Baker,[6] K. A. Baker,[73] T. Baker,[74]
G. Baldi,[75,76] N. Baldicchi,[77,51] M. Ball,[78] G. Ballardin,[63] S. W. Ballmer,[79] S. Banagiri,[6] B. Banerjee,[44] D. Bankar,[80]
T. M. Baptiste,[12] P. Baral,[10] M. Baratti,[81,82] J. C. Barayoga,[11] B. C. Barish,[11] D. Barker,[2] N. Barman,[80]
P. Barneo,[83,84,85] F. Barone,[86,4] B. Barr,[87] L. Barsotti,[35] M. Barsuglia,[20] D. Barta,[88] A. M. Bartoletti,[89]
M. A. Barton,[87] I. Bartos,[46] A. Basalaev,[8,9] R. Bassiri,[90] A. Basti,[82,81] M. Bawaj,[77,51] P. Baxi,[91] J. C. Bayley,[87]
A. C. Baylor,[10] P. A. Baynard II,[57] M. Bazzan,[92,93] V. M. Bedakihale,[94] F. Beirnaert,[95] M. Bejger,[96] D. Belardinelli,[22]
A. S. Bell,[87] D. S. Bellie,[97] L. Bellizzi,[81,82] W. Benoit,[18] I. Bentara,[56] J. D. Bentley,[98] M. Ben Yaala,[55] S. Bera,[99,100]
F. Bergamin,[33] B. K. Berger,[90] S. Bernuzzi,[27] M. Beroiz,[11] C. P. L. Berry,[87] D. Bersanetti,[29] T. Bertheas,[101]
A. Bertolini,[37,36] J. Betzwieser,[64] D. Beveridge,[73] G. Bevilacqua,[102] N. Bevins,[103] S. Bhagwat,[104] R. Bhandare,[105]
S. A. Bhat,[80] R. Bhatt,[11] D. Bhattacharjee,[106,107] S. Bhattacharyya,[108] S. Bhaumik,[46] V. Biancalana,[102]
A. Bianchi,[37,109] I. A. Bilenko,[110] G. Billingsley,[11] A. Binetti,[111] S. Bini,[11,75,76] C. Binu,[112] S. Biot,[113] O. Birnholtz,[114]
S. Biscoveanu,[97] A. Bisht,[9] M. Bitossi,[63,81] M.-A. Bizouard,[115] S. Blaber,[116] J. K. Blackburn,[11] L. A. Blagg,[78]
C. D. Blair,[73,64] D. G. Blair,[73] N. Bode,[8,9] N. Boettner,[98] G. Boileau,[115] M. Boldrini,[38] G. N. Bolingbroke,[117]
A. Bolliand,[118,40] L. D. Bonavena,[46] R. Bondarescu,[83] F. Bondu,[119] E. Bonilla,[90] M. S. Bonilla,[54] A. Bonino,[104]
R. Bonnand,[31,118] A. Borchers,[8,9] V. Boschi,[81] S. Bose,[120] V. Bossilkov,[64] Y. Bothra,[37,109] A. Boudon,[56] L. Bourg,[57]
M. Boyle,[121] A. Bozzi,[63] C. Bradaschia,[81] P. R. Brady,[10] A. Branch,[64] M. Branchesi,[44,45] I. Braun,[106] T. Briant,[122]
A. Brillet,[115] M. Brinkmann,[8,9] P. Brockill,[10] E. Brockmueller,[8,9] A. F. Brooks,[11] B. C. Brown,[46] D. D. Brown,[117]
M. L. Brozzetti,[77,51] S. Brunett,[11] G. Bruno,[15] R. Bruntz,[123] J. Bryant,[104] Y. Bu,[124] F. Bucci,[62] J. Buchanan,[123]
O. Bulashenko,[83,84] T. Bulik,[125] H. J. Bulten,[37] A. Buonanno,[126,1] K. Burtnyk,[2] R. Buscicchio,[127,128] D. Buskulic,[31]
C. Buy,[101] R. L. Byer,[90] G. S. Cabourn Davies,[74] R. Cabrita,[15] V. Cáceres-Barbosa,[7] L. Cadonati,[57] G. Cagnoli,[129]
C. Cahillane,[79] A. Calafat,[99] T. A. Callister,[130] E. Calloni,[32,4] S. R. Callos,[78] M. Canepa,[30,29] G. Caneva Santoro,[43]
K. C. Cannon,[42] H. Cao,[35] L. A. Capistran,[131] E. Capocasa,[20] E. Capote,[2,11] G. Capurri,[82,81] G. Carapella,[67,132]
F. Carbognani,[63] M. Carlassara,[8,9] J. B. Carlin,[124] T. K. Carlson,[133] M. F. Carney,[106] M. Carpinelli,[127,63]
G. Carrillo,[78] J. J. Carter,[8,9] G. Carullo,[104,134] A. Casallas-Lagos,[135] J. Casanueva Diaz,[63] C. Casentini,[136,22]
S. Y. Castro-Lucas,[137] S. Caudill,[133] M. Cavaglià,[107] R. Cavalieri,[63] A. Ceja,[54] G. Cella,[81] P. Cerdá-Durán,[138,139]
E. Cesarini,[22] N. Chabbra,[34] W. Chaibi,[115] A. Chakraborty,[13] P. Chakraborty,[8,9] S. Chakraborty,[105]
S. Chalathadka Subrahmanya,[98] J. C. L. Chan,[140] M. Chan,[116] K. Chang,[141] S. Chao,[142,141] P. Charlton,[143]
E. Chassande-Mottin,[20] C. Chatterjee,[144] Debarati Chatterjee,[80] Deep Chatterjee,[35] M. Chaturvedi,[105] S. Chaty,[20]
K. Chatziioannou,[11] A. Chen,[145] A. H.-Y. Chen,[146] D. Chen,[147] H. Chen,[142] H. Y. Chen,[148] S. Chen,[144] Yanbei Chen,[149]
Yitian Chen,[121] H. P. Cheng,[150] P. Chessa,[77,51] H. T. Cheung,[91] S. Y. Cheung,[6] F. Chiadini,[151,132] G. Chiarini,[8,9,93]
A. Chiba,[152] A. Chincarini,[29] M. L. Chiofalo,[82,81] A. Chiummo,[4,63] C. Chou,[146] S. Choudhary,[73] N. Christensen,[115,153]
S. S. Y. Chua,[34] G. Ciani,[75,76] P. Ciecielag,[96] M. Cieślar,[125] M. Cifaldi,[22] B. Cirok,[154] F. Clara,[2] J. A. Clark,[11,57]
T. A. Clarke,[6] P. Clearwater,[155] S. Clesse,[113] F. Cleva,[115,118] E. Coccia,[44,45,43] E. Codazzo,[156,157] P.-F. Cohadon,[122]
S. Colace,[30] E. Colangeli,[74] M. Colleoni,[99] C. G. Collette,[158] J. Collins,[64] S. Colloms,[87] A. Colombo,[159,128]
C. M. Compton,[2] G. Connolly,[78] L. Conti,[93] T. R. Corbitt,[12] I. Cordero-Carrión,[160] S. Corezzi,[77,51] M. Corman,[1]
N. J. Cornish,[161] I. Coronado,[162] A. Corsi,[163] R. Cottingham,[64] M. W. Coughlin,[18] A. Couineaux,[38] P. Couvares,[11,57]
D. M. Coward,[73] R. Coyne,[164] A. Cozzumbo,[44] J. D. E. Creighton,[10] T. D. Creighton,[165] P. Cremonese,[99] S. Crook,[64]
R. Crouch,[2] J. Csizmazia,[2] J. R. Cudell,[166] T. J. Cullen,[11] A. Cumming,[87] E. Cuoco,[167,168] M. Cusinato,[138]
L. V. Da Conceição,[169] T. Dal Canton,[41] S. Dal Pra,[170] G. Dálya,[101] O. Dan,[114] B. D'Angelo,[29] S. Danilishin,[36,37]
S. D'Antonio,[38] K. Danzmann,[9,8,9] K. E. Darroch,[123] L. P. Dartez,[64] R. Das,[108] A. Dasgupta,[94] Sayantani Datta,[58]
V. Dattilo,[63] A. Daumas,[20] N. Davari,[171,172] I. Dave,[105] A. Davenport,[137] M. Davier,[41] T. F. Davies,[73] D. Davis,[11]
L. Davis,[73] M. C. Davis,[18] P. Davis,[173,174] E. J. Daw,[175] M. Dax,[1] J. De Bolle,[95] M. Deenadayalan,[80] J. Degallaix,[176]
M. De Laurentis,[32,4] F. De Lillo,[23] S. Della Torre,[128] W. Del Pozzo,[82,81] A. Demagny,[31] F. De Marco,[39,38]
G. Demasi,[177,62] F. De Matteis,[21,22] N. Demos,[35] T. Dent,[178] A. Depasse,[15] N. DePergola,[103] R. De Pietri,[179,180]
R. De Rosa,[32,4] C. De Rossi,[63] M. Desai,[35] R. DeSalvo,[181] A. DeSimone,[182] R. De Simone,[151,132] A. Dhani,[1] R. Diab,[46]
M. C. Díaz,[165] M. Di Cesare,[32,4] G. Dideron,[183] T. Dietrich,[1] L. Di Fiore,[4] C. Di Fronzo,[73] M. Di Giovanni,[39,38]
T. Di Girolamo,[32,4] D. Diksha,[37,36] J. Ding,[20,184] S. Di Pace,[39,38] I. Di Palma,[39,38] D. Di Piero,[185,48] F. Di Renzo,[56]
Divyajyoti,[33] A. Dmitriev,[104] J. P. Docherty,[87] Z. Doctor,[97] N. Doerksen,[169] E. Dohmen,[2] A. Doke,[133]
A. Domiciano De Souza,[186] L. D'Onofrio,[38] F. Donovan,[35] K. L. Dooley,[33] T. Dooney,[72] S. Doravari,[80] O. Dorosh,[187]
W. J. D. Doyle,[123] M. Drago,[39,38] J. C. Driggers,[2] L. Dunn,[124] U. Dupletsa,[44] P.-A. Duverne,[20] D. D'Urso,[171,156]
P. Dutta Roy,[46] H. Duval,[188] S. E. Dwyer,[2] C. Eassa,[2] W. East,[183] M. Ebersold,[189,31] T. Eckhardt,[98] G. Eddolls,[79]
A. Effler,[64] J. Eichholz,[34] H. Einsle,[115] M. Eisenmann,[25] M. Emma,[59] K. Endo,[152] R. Enficiaud,[1] L. Errico,[32,4]
R. Espinosa,[165] M. Esposito,[4,32] R. C. Essick,[190] H. Estellés,[1] T. Etzel,[11] M. Evans,[35] T. Evstafyeva,[183] B. E. Ewing,[7]

J. M. Ezquiaga,[140] F. Fabrizi,[61,62] V. Fafone,[21,22] S. Fairhurst,[33] A. M. Farah,[130] B. Farr,[78] W. M. Farr,[191,192] G. Favaro,[92] M. Favata,[193] M. Fays,[166] M. Fazio,[55] J. Feicht,[11] M. M. Fejer,[90] R. Felicetti,[185,48] E. Fenyvesi,[88,194] J. Fernandes,[195] T. Fernandes,[196,138] D. Fernando,[112] S. Ferraiuolo,[197,39,38] T. A. Ferreira,[12] F. Fidecaro,[82,81] A. Fienga,[115] P. Figura,[96] A. Fiori,[81,82] I. Fiori,[63] M. Fishbach,[190] R. P. Fisher,[123] R. Fittipaldi,[198,132] V. Fiumara,[199,132] R. Flaminio,[31] S. M. Fleischer,[200] L. S. Fleming,[201] E. Floden,[18] H. Fong,[116] J. A. Font,[138,139] F. Fontinele-Nunes,[18] C. Foo,[1] B. Fornal,[202] K. Franceschetti,[179] F. Frappez,[31] S. Frasca,[39,38] F. Frasconi,[81] J. P. Freed,[66] Z. Frei,[203] A. Freise,[37,109] O. Freitas,[196,138] R. Frey,[78] W. Frischhertz,[64] P. Fritschel,[35] V. V. Frolov,[64] G. G. Fronzé,[28] M. Fuentes-Garcia,[11] S. Fujii,[204] T. Fujimori,[205] P. Fulda,[46] M. Fyffe,[64] B. Gadre,[72] J. R. Gair,[1] S. Galaudage,[186] V. Galdi,[206] R. Gamba,[7] A. Gamboa,[1] S. Gamoji,[181] D. Ganapathy,[207] A. Ganguly,[80] B. Garaventa,[29] J. García-Bellido,[208] C. García-Quirós,[189] J. W. Gardner,[34] K. A. Gardner,[116] S. Garg,[42] J. Gargiulo,[63] X. Garrido,[41] A. Garron,[99] F. Garufi,[32,4] P. A. Garver,[90] C. Gasbarra,[21,22] B. Gateley,[2] F. Gautier,[209] V. Gayathri,[10] T. Gayer,[79] G. Gemme,[29] A. Gennai,[81] V. Gennari,[101] J. George,[105] R. George,[148] O. Gerberding,[98] L. Gergely,[154] Archisman Ghosh,[95] Sayantan Ghosh,[195] Shaon Ghosh,[193] Shrobana Ghosh,[8,9] Suprovo Ghosh,[210] Tathagata Ghosh,[80] J. A. Giaime,[12,64] K. D. Giardina,[64] D. R. Gibson,[201] C. Gier,[55] S. Gkaitatzis,[82,81] J. Glanzer,[11] F. Glotin,[41] J. Godfrey,[78] R. V. Godley,[8,9] P. Godwin,[11] A. S. Goettel,[33] E. Goetz,[116] J. Golomb,[11] S. Gomez Lopez,[39,38] B. Goncharov,[44] G. González,[12] P. Goodarzi,[211] S. Goode,[6] A. W. Goodwin-Jones,[15] M. Gosselin,[63] R. Gouaty,[31] D. W. Gould,[34] K. Govorkova,[35] A. Grado,[77,51] V. Graham,[87] A. E. Granados,[18] M. Granata,[176] V. Granata,[212,132] S. Gras,[35] P. Grassia,[11] J. Graves,[57] C. Gray,[2] R. Gray,[87] G. Greco,[51] A. C. Green,[37,109] L. Green,[213] S. M. Green,[74] S. R. Green,[214] C. Greenberg,[133] A. M. Gretarsson,[66] H. K. Griffin,[18] D. Griffith,[11] H. L. Griggs,[57] G. Grignani,[77,51] C. Grimaud,[31] H. Grote,[33] S. Grunewald,[1] D. Guerra,[138] D. Guetta,[215] G. M. Guidi,[61,62] A. R. Guimaraes,[12] H. K. Gulati,[94] F. Gulminelli,[173,174] H. Guo,[145] W. Guo,[73] Y. Guo,[37,36] Anuradha Gupta,[216] I. Gupta,[7] N. C. Gupta,[94] S. K. Gupta,[46] V. Gupta,[18] N. Gupte,[1] J. Gurs,[98] N. Gutierrez,[176] N. Guttman,[6] F. Guzman,[131] D. Haba,[217] M. Haberland,[1] S. Haino,[218] E. D. Hall,[35] E. Z. Hamilton,[99] G. Hammond,[87] M. Haney,[37] J. Hanks,[2] C. Hanna,[7] M. D. Hannam,[33] O. A. Hannuksela,[219] A. G. Hanselman,[130] H. Hansen,[2] J. Hanson,[64] S. Hanumasagar,[57] R. Harada,[42] A. R. Hardison,[182] S. Harikumar,[187] K. Haris,[37,72] I. Harley-Trochimczyk,[131] T. Harmark,[134] J. Harms,[44,45] G. M. Harry,[220] I. W. Harry,[74] J. Hart,[106] B. Haskell,[96,221,222] C.-J. Haster,[213] K. Haughian,[87] H. Hayakawa,[50] K. Hayama,[223] M. C. Heintze,[64] J. Heinze,[104] J. Heinzel,[35] H. Heitmann,[115] F. Hellman,[207] A. F. Helmling-Cornell,[78] G. Hemming,[63] O. Henderson-Sapir,[117] M. Hendry,[87] I. S. Heng,[87] M. H. Hennig,[87] C. Henshaw,[57] M. Heurs,[8,9] A. L. Hewitt,[224,225] J. Heynen,[15] J. Heyns,[35] S. Higginbotham,[33] S. Hild,[36,37] S. Hill,[87] Y. Himemoto,[226] N. Hirata,[25] C. Hirose,[227] D. Hofman,[176] B. E. Hogan,[66] N. A. Holland,[37,109] K. Holley-Bockelmann,[144] I. J. Hollows,[175] D. E. Holz,[130] L. Honet,[113] D. J. Horton-Bailey,[207] J. Hough,[87] S. Hourihane,[11] N. T. Howard,[144] E. J. Howell,[73] C. G. Hoy,[74] C. A. Hrishikesh,[21] P. Hsi,[35] H.-F. Hsieh,[142] H.-Y. Hsieh,[142] C. Hsiung,[228] S.-H. Hsu,[146] W.-F. Hsu,[111] Q. Hu,[87] H. Y. Huang,[141] Y. Huang,[7] Y. T. Huang,[79] A. D. Huddart,[229] B. Hughey,[66] V. Hui,[31] S. Husa,[99] R. Huxford,[7] L. Iampieri,[39,38] G. A. Iandolo,[36] M. Ianni,[22,21] G. Iannone,[132] J. Iascau,[78] K. Ide,[230] R. Iden,[217] A. Ierardi,[44,45] S. Ikeda,[147] H. Imafuku,[42] Y. Inoue,[141] G. Iorio,[92] P. Iosif,[185,48] M. H. Iqbal,[34] J. Irwin,[87] R. Ishikawa,[230] M. Isi,[191,192] K. S. Isleif,[231] Y. Itoh,[205,232] M. Iwaya,[204] B. R. Iyer,[24] C. Jacquet,[101] P.-E. Jacquet,[122] T. Jacquot,[41] S. J. Jadhav,[233] S. P. Jadhav,[155] M. Jain,[133] T. Jain,[224] A. L. James,[11] K. Jani,[144] J. Janquart,[15] N. N. Janthalur,[233] S. Jaraba,[234] P. Jaranowski,[235] R. Jaume,[99] W. Javed,[33] A. Jennings,[2] M. Jensen,[2] W. Jia,[35] J. Jiang,[150] H.-B. Jin,[236,237] G. R. Johns,[123] N. A. Johnson,[46] N. K. Johnson-McDaniel,[216] M. C. Johnston,[213] R. Johnston,[87] N. Johny,[8,9] D. H. Jones,[34] D. I. Jones,[210] R. Jones,[87] H. E. Jose,[78] P. Joshi,[7] S. K. Joshi,[80] G. Joubert,[56] J. Ju,[238] L. Ju,[73] K. Jung,[239] J. Junker,[34] V. Juste,[113] H. B. Kabagoz,[64,35] T. Kajita,[240] I. Kaku,[205] V. Kalogera,[97] M. Kalomenopoulos,[213] M. Kamiizumi,[50] N. Kanda,[232,205] S. Kandhasamy,[80] G. Kang,[241] N. C. Kannachel,[6] J. B. Kanner,[11] S. A. KantiMahanty,[18] S. J. Kapadia,[80] D. P. Kapasi,[54] M. Karthikeyan,[133] M. Kasprzack,[11] H. Kato,[152] T. Kato,[204] E. Katsavounidis,[35] W. Katzman,[64] R. Kaushik,[105] K. Kawabe,[2] R. Kawamoto,[205] D. Keitel,[99] L. J. Kemperman,[117] J. Kennington,[7] F. A. Kerkow,[18] R. Kesharwani,[80] J. S. Key,[242] R. Khadela,[8,9] S. Khadka,[90] S. S. Khadkikar,[7] F. Y. Khalili,[110] F. Khan,[8,9] T. Khanam,[163] M. Khursheed,[105] N. M. Khusid,[191,192] W. Kiendrebeogo,[115,243] N. Kijbunchoo,[117] C. Kim,[244] J. C. Kim,[245] K. Kim,[246] M. H. Kim,[238] S. Kim,[247] Y.-M. Kim,[246] C. Kimball,[97] K. Kimes,[54] M. Kinnear,[33] J. S. Kissel,[2] S. Klimenko,[46] A. M. Knee,[116] E. J. Knox,[78] N. Knust,[8,9] K. Kobayashi,[204] S. M. Koehlenbeck,[90] G. Koekoek,[37,36] K. Kohri,[248,249] K. Kokeyama,[33,250] S. Koley,[44,166] P. Kolitsidou,[104] A. E. Koloniari,[251] K. Komori,[42] A. K. H. Kong,[142] A. Kontos,[252] L. M. Koponen,[104] M. Korobko,[98] X. Kou,[18] A. Koushik,[23] N. Kouvatsos,[68] M. Kovalam,[73] T. Koyama,[152] D. B. Kozak,[11] S. L. Kranzhoff,[36,37] V. Kringel,[8,9] N. V. Krishnendu,[104] S. Kroker,[253] A. Królak,[254,187] K. Kruska,[8,9] J. Kubisz,[255] G. Kuehn,[8,9] S. Kulkarni,[216] A. Kulur Ramamohan,[34] Achal Kumar,[46] Anil Kumar,[233] Praveen Kumar,[178] Prayush Kumar,[24] Rahul Kumar,[2] Rakesh Kumar,[94] J. Kume,[256,257,42] K. Kuns,[35] N. Kuntimaddi,[33] S. Kuroyanagi,[208,258] S. Kuwahara,[42] K. Kwak,[239] K. Kwan,[34] S. Kwon,[42] G. Lacaille,[87] D. Laghi,[189,101] A. H. Laity,[164] E. Lalande,[259] M. Lalleman,[23] P. C. Lalremruati,[260] M. Landry,[2] B. B. Lane,[35] R. N. Lang,[35] J. Lange,[148] R. Langgin,[213] B. Lantz,[90] I. La Rosa,[99] J. Larsen,[200] A. Lartaux-Vollard,[41] P. D. Lasky,[6] J. Lawrence,[165] M. Laxen,[64] C. Lazarte,[138] A. Lazzarini,[11] C. Lazzaro,[157,156] P. Leaci,[39,38] L. Leali,[18] Y. K. Lecoeuche,[116] H. M. Lee,[261] H. W. Lee,[262] J. Lee,[79] K. Lee,[238] R.-K. Lee,[142] R. Lee,[35] Sungho Lee,[246] Sunjae Lee,[238] Y. Lee,[141] I. N. Legred,[11] J. Lehmann,[8,9] L. Lehner,[183] M. Le Jean,[176,118] A. Lemaître,[263] M. Lenti,[62,177] M. Leonardi,[75,76,264] M. Lequime,[40] N. Leroy,[41] M. Lesovsky,[11] N. Letendre,[31] M. Lethuillier,[56] Y. Levin,[6] K. Leyde,[74] A. K. Y. Li,[11] K. L. Li,[265] T. G. F. Li,[111] X. Li,[149] Y. Li,[97] Z. Li,[87] A. Lihos,[123] E. T. Lin,[142] F. Lin,[141] L. C.-C. Lin,[265] Y.-C. Lin,[142] C. Lindsay,[201] S. D. Linker,[181] A. Liu,[219] G. C. Liu,[228] Jian Liu,[73] F. Llamas Villarreal,[165] J. Llobera-Querol,[99] R. K. L. Lo,[140] J.-P. Locquet,[111] S. C. G. Loggins,[266] M. R. Loizou,[133] L. T. London,[68] A. Longo,[61,62] D. Lopez,[166] M. Lopez Portilla,[72] M. Lorenzini,[21,22] A. Lorenzo-Medina,[178] V. Loriette,[41] M. Lormand,[64] G. Losurdo,[267,81] E. Lotti,[133] T. P. Lott IV,[57] J. D. Lough,[8,9] H. A. Loughlin,[35] C. O. Lousto,[112] N. Low,[124] N. Lu,[34]

L. Lucchesi,[81] H. Lück,[9,8,9] D. Lumaca,[22] A. P. Lundgren,[268,269] A. W. Lussier,[259] R. Macas,[74] M. MacInnis,[35]
D. M. Macleod,[33] I. A. O. MacMillan,[11] A. Macquet,[41] K. Maeda,[152] S. Maenaut,[111] S. S. Magare,[80] R. M. Magee,[11]
E. Maggio,[1] R. Maggiore,[37,109] M. Magnozzi,[29,30] P. Mahapatra,[33] M. Mahesh,[98] Y. Maimon,[114] M. Maini,[164] S. Majhi,[80]
E. Majorana,[39,38] C. N. Makarem,[11] D. Malakar,[107] J. A. Malaquias-Reis,[19] U. Mali,[190] S. Maliakal,[11] A. Malik,[105]
L. Mallick,[169,190] A.-K. Malz,[59] N. Man,[115] M. Mancarella,[100] V. Mandic,[18] V. Mangano,[171,156] B. Mannix,[78]
G. L. Mansell,[79] M. Manske,[10] M. Mantovani,[63] M. Mapelli,[92,93,270] C. Marinelli,[102] F. Marion,[31] A. S. Markosyan,[90]
A. Markowitz,[11] E. Maros,[11] S. Marsat,[101] F. Martelli,[61,62] I. W. Martin,[87] R. M. Martin,[193] B. B. Martinez,[131]
D. A. Martinez,[54] M. Martinez,[43,271] V. Martinez,[129] A. Martini,[75,76] J. C. Martins,[19] D. V. Martynov,[104] E. J. Marx,[35]
L. Massaro,[36,37] A. Masserot,[31] M. Masso-Reid,[87] S. Mastrogiovanni,[38] T. Matcovich,[51] M. Matiushechkina,[8,9]
L. Maurin,[209] N. Mavalvala,[35] N. Maxwell,[2] G. McCarrol,[64] R. McCarthy,[2] D. E. McClelland,[34] S. McCormick,[64]
L. McCuller,[11] S. McEachin,[123] C. McElhenny,[123] G. I. McGhee,[87] K. B. M. McGowan,[144] J. McIver,[116] A. McLeod,[73]
I. McMahon,[189] T. McRae,[34] R. McTeague,[87] D. Meacher,[10] B. N. Meagher,[79] R. Mechum,[112] Q. Meijer,[72] A. Melatos,[124]
C. S. Menoni,[137] F. Mera,[2] R. A. Mercer,[10] L. Mereni,[176] K. Merfeld,[163] E. L. Merilh,[64] J. R. Mérou,[99] J. D. Merritt,[78]
M. Merzougui,[115] C. Messick,[10] B. Mestichelli,[44] M. Meyer-Conde,[272] F. Meylahn,[8,9] A. Mhaske,[80] A. Miani,[75,76]
H. Miao,[273] C. Michel,[176] Y. Michimura,[42] H. Middleton,[104] D. P. Mihaylov,[106] S. J. Miller,[11] M. Millhouse,[57]
E. Milotti,[185,48] V. Milotti,[92] Y. Minenkov,[22] E. M. Minihan,[66] Ll. M. Mir,[43] L. Mirasola,[156,157] M. Miravet-Tenés,[138]
C.-A. Miritescu,[43] A. Mishra,[24] C. Mishra,[108] T. Mishra,[46] A. L. Mitchell,[37,109] J. G. Mitchell,[66] S. Mitra,[80]
V. P. Mitrofanov,[110] K. Mitsuhashi,[25] R. Mittleman,[35] O. Miyakawa,[50] S. Miyoki,[50] A. Miyoko,[66] G. Mo,[35]
L. Mobilia,[61,62] S. Mohan S.,[274] S. R. P. Mohapatra,[11] S. R. Mohite,[7] M. Molina-Ruiz,[207] M. Mondin,[181] M. Montani,[61,62]
C. J. Moore,[224] D. Moraru,[2] A. More,[80] S. More,[80] C. Moreno,[135] E. A. Moreno,[35] G. Moreno,[2] A. Moreso Serra,[83]
S. Morisaki,[42,204] Y. Moriwaki,[152] G. Morras,[208] A. Moscatello,[92] M. Mould,[35] B. Mours,[65] C. M. Mow-Lowry,[37,109]
L. Muccillo,[177,62] F. Muciaccia,[39,38] D. Mukherjee,[104] Samanwaya Mukherjee,[24] Soma Mukherjee,[165]
Subroto Mukherjee,[94] Suvodip Mukherjee,[13] N. Mukund,[35] A. Mullavey,[64] H. Mullock,[116] J. Mundi,[220]
C. L. Mungioli,[73] M. Murakoshi,[230] P. G. Murray,[87] D. Nabari,[75,76] S. L. Nadji,[8,9] A. Nagar,[28,275] N. Nagarajan,[87]
K. Nakagaki,[50] K. Nakamura,[25] H. Nakano,[276] M. Nakano,[11] D. Nanadoumgar-Lacroze,[43] D. Nandi,[12] V. Napolano,[63]
P. Narayan,[216] I. Nardecchia,[22] T. Narikawa,[204] H. Narola,[72] L. Naticchioni,[38] R. K. Nayak,[260] L. Negri,[72] A. Nela,[87]
C. Nelle,[78] A. Nelson,[131] T. J. N. Nelson,[64] M. Nery,[8,9] A. Neunzert,[2] S. Ng,[54] L. Nguyen Quynh,[277] S. A. Nichols,[12]
A. B. Nielsen,[278] Y. Nishino,[25,42] A. Nishizawa,[279] S. Nissanke,[280,37] W. Niu,[7] F. Nocera,[63] J. Noller,[281] M. Norman,[33]
C. North,[33] J. Novak,[118,234,282] R. Nowicki,[144] J. F. Nuño Siles,[208] L. K. Nuttall,[74] K. Obayashi,[230] J. Oberling,[2]
J. O'Dell,[229] E. Oelker,[35] M. Oertel,[234,118,283,282] G. Oganesyan,[44,45] T. O'Hanlon,[64] M. Ohashi,[50] F. Ohme,[8,9]
R. Oliveri,[118,283,282] R. Omer,[18] B. O'Neal,[123] M. Onishi,[152] K. Oohara,[284] B. O'Reilly,[64] M. Orselli,[51,77]
R. O'Shaughnessy,[112] S. O'Shea,[87] S. Oshino,[50] C. Osthelder,[11] I. Ota,[12] D. J. Ottaway,[117] A. Ouzriat,[56] H. Overmier,[64]
B. J. Owen,[285] R. Ozaki,[230] A. E. Pace,[7] R. Pagano,[12] M. A. Page,[25] A. Pai,[195] L. Paiella,[44] A. Pal,[286] S. Pal,[260]
M. A. Palaia,[81,82] M. Pálfi,[203] P. P. Palma,[39,21,22] C. Palomba,[38] P. Palud,[20] H. Pan,[142] J. Pan,[73] K. C. Pan,[142] P. K. Panda,[233]
Shiksha Pandey,[7] Swadha Pandey,[35] P. T. H. Pang,[37,72] F. Pannarale,[39,38] K. A. Pannone,[54] B. C. Pant,[105] F. H. Panther,[73]
M. Panzeri,[61,62] F. Paoletti,[81] A. Paolone,[38,287] A. Papadopoulos,[87] E. E. Papalexakis,[211] L. Papalini,[81,82]
G. Papigkiotis,[251] A. Paquis,[41] A. Parisi,[77,51] B.-J. Park,[246] J. Park,[288] W. Parker,[64] G. Pascale,[8,9] D. Pascucci,[95]
A. Pasqualetti,[63] R. Passaquieti,[82,81] L. Passenger,[6] D. Passuello,[81] O. Patane,[2] A. V. Patel,[141] D. Pathak,[80] A. Patra,[33]
B. Patricelli,[82,81] B. G. Patterson,[33] K. Paul,[108] S. Paul,[78] E. Payne,[11] T. Pearce,[33] M. Pedraza,[11] A. Pele,[11]
F. E. Peña Arellano,[289] X. Peng,[104] Y. Peng,[57] S. Penn,[290] M. D. Penuliar,[54] A. Perego,[75,76] Z. Pereira,[133]
C. Périgois,[291,93,92] G. Perna,[92] A. Perreca,[75,76,44] J. Perret,[20] S. Perriès,[56] J. W. Perry,[37,109] D. Pesios,[251] S. Peters,[166]
S. Petracca,[206] C. Petrillo,[77] H. P. Pfeiffer,[1] H. Pham,[64] K. A. Pham,[18] K. S. Phukon,[104] H. Phurailatpam,[219]
M. Piarulli,[101] L. Piccari,[39,38] O. J. Piccinni,[34] M. Pichot,[115] M. Piendibene,[82,81] F. Piergiovanni,[61,62] L. Pierini,[38]
G. Pierra,[38] V. Pierro,[292,132] M. Pietrzak,[96] M. Pillas,[166] F. Pilo,[81] L. Pinard,[176] I. M. Pinto,[292,132,293,32] M. Pinto,[63]
B. J. Piotrzkowski,[10] M. Pirello,[2] M. D. Pitkin,[224,87] A. Placidi,[51] E. Placidi,[39,38] M. L. Planas,[99] W. Plastino,[212,22]
C. Plunkett,[35] R. Poggiani,[82,81] E. Polini,[35] J. Pomper,[81,82] L. Pompili,[1] J. Poon,[219] E. Porcelli,[37] E. K. Porter,[20]
C. Posnansky,[7] R. Poulton,[63] J. Powell,[155] G. S. Prabhu,[80] M. Pracchia,[166] B. K. Pradhan,[80] T. Pradier,[65]
A. K. Prajapati,[94] K. Prasai,[294] R. Prasanna,[233] P. Prasia,[80] G. Pratten,[104] G. Principe,[185,48] G. A. Prodi,[75,76]
P. Prosperi,[81] P. Prosposito,[21,22] A. C. Providence,[66] A. Puecher,[1] J. Pullin,[12] P. Puppo,[38] M. Pürrer,[164] H. Qi,[16] J. Qin,[34]
G. Quéméner,[174,118] V. Quetschke,[165] P. J. Quinonez,[66] N. Qutob,[57] R. Rading,[231] I. Rainho,[138] S. Raja,[105] C. Rajan,[105]
B. Rajbhandari,[112] K. E. Ramirez,[64] F. A. Ramis Vidal,[99] M. Ramos Arevalo,[165] A. Ramos-Buades,[99,37] S. Ranjan,[57]
K. Ransom,[64] P. Rapagnani,[39,38] B. Ratto,[66] A. Ravichandran,[133] A. Ray,[97] V. Raymond,[33] M. Razzano,[82,81] J. Read,[54]
T. Regimbau,[31] S. Reid,[55] C. Reissel,[35] D. H. Reitze,[11] A. I. Renzini,[127,11] B. Revenu,[295,41] A. Revilla Peña,[83] R. Reyes,[181]
L. Ricca,[15] F. Ricci,[39,38] M. Ricci,[38,39] A. Ricciardone,[82,81] J. Rice,[79] J. W. Richardson,[211] M. L. Richardson,[117]
A. Rijal,[66] K. Riles,[91] H. K. Riley,[33] S. Rinaldi,[270] J. Rittmeyer,[98] C. Robertson,[229] F. Robinet,[41] M. Robinson,[2]
A. Rocchi,[22] L. Rolland,[31] J. G. Rollins,[11] A. E. Romano,[296] R. Romano,[3,4] A. Romero,[31] I. M. Romero-Shaw,[224]
J. H. Romie,[64] S. Ronchini,[7] T. J. Roocke,[117] L. Rosa,[4,32] T. J. Rosauer,[211] C. A. Rose,[57] D. Rosińska,[125] M. P. Ross,[53]
M. Rossello-Sastre,[99] S. Rowan,[87] S. K. Roy,[191,192] S. Roy,[15] D. Rozza,[127,128] P. Ruggi,[63] N. Ruhama,[239]
E. Ruiz Morales,[297,208] K. Ruiz-Rocha,[144] S. Sachdev,[57] T. Sadecki,[2] P. Saffarieh,[37,109] S. Safi-Harb,[169] M. R. Sah,[13]
S. Saha,[142] P. Saini,[58] T. Sainrat,[65] S. Sajith Menon,[215,39,38] K. Sakai,[298] Y. Sakai,[272] M. Sakellariadou,[68] S. Sakon,[7]
O. S. Salafia,[159,128,127] F. Salces-Carcoba,[11] L. Salconi,[63] M. Saleem,[148] F. Salemi,[39,38] M. Sallé,[37] S. U. Salunkhe,[80]
S. Salvador,[174,173] A. Salvarese,[148] A. Samajdar,[72,37] A. Sanchez,[2] E. J. Sanchez,[11] L. E. Sanchez,[11] N. Sanchis-Gual,[138]
J. R. Sanders,[182] E. M. Sänger,[1] F. Santoliquido,[44,45] F. Sarandrea,[28] T. R. Saravanan,[80] N. Sarin,[6] P. Sarkar,[8,9]
A. Sasli,[251] P. Sassi,[51,77] B. Sassolas,[176] B. S. Sathyaprakash,[7,33] R. Sato,[227] S. Sato,[152] Yukino Sato,[152] Yu Sato,[152]

O. Sauter,[46] R. L. Savage,[2] T. Sawada,[50] H. L. Sawant,[80] S. Sayah,[176] V. Scacco,[21,22] D. Schaetzl,[11] M. Scheel,[149] A. Schiebelbein,[190] M. G. Schiworski,[79] P. Schmidt,[104] S. Schmidt,[72] R. Schnabel,[98] M. Schneewind,[8,9] R. M. S. Schofield,[78] K. Schouteden,[111] B. W. Schulte,[8,9] B. F. Schutz,[33,8,9] E. Schwartz,[299] M. Scialpi,[300] J. Scott,[87] S. M. Scott,[34] R. M. Sedas,[64] T. C. Seetharamu,[87] M. Seglar-Arroyo,[43] Y. Sekiguchi,[301] D. Sellers,[64] N. Sembo,[205] A. S. Sengupta,[302] E. G. Seo,[87] J. W. Seo,[111] V. Sequino,[32,4] M. Serra,[38] A. Sevrin,[188] T. Shaffer,[2] U. S. Shah,[57] M. A. Shaikh,[261] L. Shao,[303] A. K. Sharma,[99] Preeti Sharma,[12] Prianka Sharma,[105] Ritwik Sharma,[18] S. Sharma Chaudhary,[107] P. Shawhan,[126] N. S. Shcheblanov,[304,263] E. Sheridan,[144] Z.-H. Shi,[142] M. Shikauchi,[42] R. Shimomura,[305] H. Shinkai,[305] S. Shirke,[80] D. H. Shoemaker,[35] D. M. Shoemaker,[148] R. W. Short,[2] S. ShyamSundar,[105] A. Sider,[158] H. Siegel,[191,192] D. Sigg,[2] L. Silenzi,[36,37] L. Silvestri,[39,170] M. Simmonds,[117] L. P. Singer,[306] Amitesh Singh,[216] Anika Singh,[11] D. Singh,[207] N. Singh,[99] S. Singh,[217,60] A. M. Sintes,[99] V. Sipala,[171,156] V. Skliris,[33] B. J. J. Slagmolen,[34] D. A. Slater,[200] T. J. Slaven-Blair,[73] J. Smetana,[104] J. R. Smith,[54] L. Smith,[87,185,48] R. J. E. Smith,[6] W. J. Smith,[144] S. Soares de Albuquerque Filho,[61] M. Soares-Santos,[189] K. Somiya,[217] I. Song,[142] S. Soni,[35] V. Sordini,[56] F. Sorrentino,[29] H. Sotani,[307] F. Spada,[81] V. Spagnuolo,[37] A. P. Spencer,[87] P. Spinicelli,[63] A. K. Srivastava,[94] F. Stachurski,[87] C. J. Stark,[123] D. A. Steer,[308] J. Steinhoff,[1] N. Steinle,[169] J. Steinlechner,[36,37] S. Steinlechner,[36,37] N. Stergioulas,[251] P. Stevens,[41] M. StPierre,[164] M. D. Strong,[12] A. Strunk,[2] A. L. Stuver,[103,*] M. Suchenek,[96] S. Sudhagar,[96] Y. Sudo,[230] N. Sueltmann,[98] L. Suleiman,[54] K. D. Sullivan,[12] J. Sun,[241] L. Sun,[34] S. Sunil,[94] J. Suresh,[115] B. J. Sutton,[68] P. J. Sutton,[33] K. Suzuki,[217] M. Suzuki,[204] S. Swain,[104] B. L. Swinkels,[37] A. Syx,[118] M. J. Szczepańczyk,[309] P. Szewczyk,[125] M. Tacca,[37] H. Tagoshi,[204] S. C. Tait,[11] K. Takada,[204] H. Takahashi,[272] R. Takahashi,[25] A. Takamori,[42] S. Takano,[310] H. Takeda,[311,312] K. Takeshita,[217] I. Takimoto Schmiegelow,[44,45] M. Takou-Ayaoh,[79] C. Talbot,[130] M. Tamaki,[204] N. Tamanini,[101] D. Tanabe,[141] K. Tanaka,[50] S. J. Tanaka,[230] S. Tanioka,[33] D. B. Tanner,[46] W. Tanner,[8,9] L. Tao,[211] R. D. Tapia,[7] E. N. Tapia San Martín,[37] C. Taranto,[21,22] A. Taruya,[313] J. D. Tasson,[153] J. G. Tau,[112] D. Tellez,[54] R. Tenorio,[99] H. Themann,[181] A. Theodoropoulos,[138] M. P. Thirugnanasambandam,[80] L. M. Thomas,[11] M. Thomas,[64] P. Thomas,[2] J. E. Thompson,[210] S. R. Thondapu,[105] K. A. Thorne,[64] E. Thrane,[6] J. Tissino,[44,45] A. Tiwari,[80] Pawan Tiwari,[44] Praveer Tiwari,[195] S. Tiwari,[189] V. Tiwari,[104] M. R. Todd,[79] M. Toffano,[92] A. M. Toivonen,[18] K. Toland,[87] A. E. Tolley,[74] T. Tomaru,[25] V. Tommasini,[11] T. Tomura,[50] H. Tong,[6] C. Tong-Yu,[141] A. Torres-Forné,[138,139] C. I. Torrie,[11] I. Tosta e Melo,[314] E. Tournefier,[31] M. Trad Nery,[115] K. Tran,[123] A. Trapananti,[52,51] R. Travaglini,[168] F. Travasso,[52,51] G. Traylor,[64] M. Trevor,[126] M. C. Tringali,[63] A. Tripathee,[91] G. Troian,[185,48] A. Trovato,[185,48] L. Trozzo,[4] R. J. Trudeau,[11] T. Tsang,[33] S. Tsuchida,[315] L. Tsukada,[213] K. Turbang,[188,23] M. Turconi,[115] C. Turski,[95] H. Ubach,[83,84] N. Uchikata,[204] T. Uchiyama,[50] R. P. Udall,[11] T. Uehara,[316] K. Ueno,[42] V. Undheim,[278] L. E. Uronen,[219] T. Ushiba,[50] M. Vacatello,[81,82] H. Vahlbruch,[8,9] N. Vaidya,[11] G. Vajente,[11] A. Vajpeyi,[6] J. Valencia,[99] M. Valentini,[109,37] S. A. Vallejo-Peña,[296] S. Vallero,[28] V. Valsan,[10] M. van Dael,[37,317] E. Van den Bossche,[188] J. F. J. van den Brand,[36,109,37] C. Van Den Broeck,[72,37] M. van der Sluys,[37,72] A. Van de Walle,[41] J. van Dongen,[37,109] K. Vandra,[103] M. VanDyke,[120] H. van Haevermaet,[23] J. V. van Heijningen,[37,109] P. Van Hove,[65] J. Vanier,[259] M. VanKeuren,[106] J. Vanosky,[2] N. van Remortel,[23] M. Vardaro,[36,37] A. F. Vargas,[124] V. Varma,[133] A. N. Vazquez,[90] A. Vecchio,[104] G. Vedovato,[93] J. Veitch,[87] P. J. Veitch,[117] S. Venikoudis,[15] R. C. Venterea,[18] P. Verdier,[56] M. Vereecken,[15] D. Verkindt,[31] B. Verma,[133] Y. Verma,[105] S. M. Vermeulen,[11] F. Vetrano,[61] A. Veutro,[38,39] A. Viceré,[61,62] S. Vidyant,[79] A. D. Viets,[89] A. Vijaykumar,[190] A. Vilkha,[112] N. Villanueva Espinosa,[138] V. Villa-Ortega,[178] E. T. Vincent,[57] J.-Y. Vinet,[115] S. Viret,[56] S. Vitale,[35] H. Vocca,[77,51] D. Voigt,[98] E. R. G. von Reis,[2] J. S. A. von Wrangel,[8,9] W. E. Vossius,[231] L. Vujeva,[140] S. P. Vyatchanin,[110] J. Wack,[11] L. E. Wade,[106] M. Wade,[106] K. J. Wagner,[112] R. M. Wald,[130] L. Wallace,[11] E. J. Wang,[90] H. Wang,[217] J. Z. Wang,[91] W. H. Wang,[165] Y. F. Wang,[1] G. Waratkar,[195] J. Warner,[2] M. Was,[31] T. Washimi,[25] N. Y. Washington,[11] D. Watarai,[42] B. Weaver,[2] S. A. Webster,[87] N. L. Weickhardt,[98] M. Weinert,[8,9] A. J. Weinstein,[11] R. Weiss,[35,†] L. Wen,[73] K. Wette,[34] J. T. Whelan,[112] B. F. Whiting,[46] C. Whittle,[11] E. G. Wickens,[74] D. Wilken,[8,9,9] A. T. Wilkin,[211] B. M. Williams,[120] D. Williams,[87] M. J. Williams,[74] N. S. Williams,[1] J. L. Willis,[11] B. Willke,[9,8,9] M. Wils,[111] L. Wilson,[106] C. W. Winborn,[107] J. Winterflood,[73] C. C. Wipf,[11] G. Woan,[87] J. Woehler,[36,37] N. E. Wolfe,[35] H. T. Wong,[141] I. C. F. Wong,[219,111] K. Wong,[190] T. Wouters,[72,37] J. L. Wright,[2] M. Wright,[87,72] B. Wu,[79] C. Wu,[142] D. S. Wu,[8,9] H. Wu,[142] K. Wu,[120] Q. Wu,[53] Y. Wu,[97] Z. Wu,[101] E. Wuchner,[54] D. M. Wysocki,[10] V. A. Xu,[207] Y. Xu,[99] N. Yadav,[28] H. Yamamoto,[11] K. Yamamoto,[152] T. S. Yamamoto,[42] T. Yamamoto,[50] R. Yamazaki,[230] T. Yan,[104] K. Z. Yang,[18] Y. Yang,[146] Z. Yarbrough,[12] J. Yebana,[99] S.-W. Yeh,[142] A. B. Yelikar,[144] X. Yin,[35] J. Yokoyama,[318,42] T. Yokozawa,[50] S. Yuan,[73] H. Yuzurihara,[50] M. Zanolin,[66] M. Zeeshan,[112] T. Zelenova,[63] J.-P. Zendri,[93] M. Zeoli,[15] M. Zerrad,[40] M. Zevin,[97] L. Zhang,[11] N. Zhang,[57] R. Zhang,[150] T. Zhang,[104] C. Zhao,[73] J. Zhao,[319] Yue Zhao,[162] Yuhang Zhao,[20] Z.-C. Zhao,[319] Y. Zheng,[107] H. Zhong,[18] H. Zhou,[79] H. O. Zhu,[73] Z.-H. Zhu,[319,320] A. B. Zimmerman,[148] L. Zimmermann,[56] M. E. Zucker,[35,11] and J. Zweizig[11]

[1]*Max Planck Institute for Gravitational Physics (Albert Einstein Institute), D-14476 Potsdam, Germany*
[2]*LIGO Hanford Observatory, Richland, WA 99352, USA*
[3]*Dipartimento di Farmacia, Università di Salerno, I-84084 Fisciano, Salerno, Italy*
[4]*INFN, Sezione di Napoli, I-80126 Napoli, Italy*
[5]*University of Warwick, Coventry CV4 7AL, United Kingdom*
[6]*OzGrav, School of Physics & Astronomy, Monash University, Clayton 3800, Victoria, Australia*
[7]*The Pennsylvania State University, University Park, PA 16802, USA*
[8]*Max Planck Institute for Gravitational Physics (Albert Einstein Institute), D-30167 Hannover, Germany*
[9]*Leibniz Universität Hannover, D-30167 Hannover, Germany*
[10]*University of Wisconsin-Milwaukee, Milwaukee, WI 53201, USA*

[11]LIGO Laboratory, California Institute of Technology, Pasadena, CA 91125, USA
[12]Louisiana State University, Baton Rouge, LA 70803, USA
[13]Tata Institute of Fundamental Research, Mumbai 400005, India
[14]Centre de Physique Théorique, Aix-Marseille Université, Campus de Luminy, 163 Av. de Luminy, 13009 Marseille, France
[15]Université catholique de Louvain, B-1348 Louvain-la-Neuve, Belgium
[16]Queen Mary University of London, London E1 4NS, United Kingdom
[17]University of California, Davis, Davis, CA 95616, USA
[18]University of Minnesota, Minneapolis, MN 55455, USA
[19]Instituto Nacional de Pesquisas Espaciais, 12227-010 São José dos Campos, São Paulo, Brazil
[20]Université Paris Cité, CNRS, Astroparticule et Cosmologie, F-75013 Paris, France
[21]Università di Roma Tor Vergata, I-00133 Roma, Italy
[22]INFN, Sezione di Roma Tor Vergata, I-00133 Roma, Italy
[23]Universiteit Antwerpen, 2000 Antwerpen, Belgium
[24]International Centre for Theoretical Sciences, Tata Institute of Fundamental Research, Bengaluru 560089, India
[25]Gravitational Wave Science Project, National Astronomical Observatory of Japan, 2-21-1 Osawa, Mitaka City, Tokyo 181-8588, Japan
[26]Advanced Technology Center, National Astronomical Observatory of Japan, 2-21-1 Osawa, Mitaka City, Tokyo 181-8588, Japan
[27]Theoretisch-Physikalisches Institut, Friedrich-Schiller-Universität Jena, D-07743 Jena, Germany
[28]INFN Sezione di Torino, I-10125 Torino, Italy
[29]INFN, Sezione di Genova, I-16146 Genova, Italy
[30]Dipartimento di Fisica, Università degli Studi di Genova, I-16146 Genova, Italy
[31]Univ. Savoie Mont Blanc, CNRS, Laboratoire d'Annecy de Physique des Particules - IN2P3, F-74000 Annecy, France
[32]Università di Napoli "Federico II", I-80126 Napoli, Italy
[33]Cardiff University, Cardiff CF24 3AA, United Kingdom
[34]OzGrav, Australian National University, Canberra, Australian Capital Territory 0200, Australia
[35]LIGO Laboratory, Massachusetts Institute of Technology, Cambridge, MA 02139, USA
[36]Maastricht University, 6200 MD Maastricht, Netherlands
[37]Nikhef, 1098 XG Amsterdam, Netherlands
[38]INFN, Sezione di Roma, I-00185 Roma, Italy
[39]Università di Roma "La Sapienza", I-00185 Roma, Italy
[40]Aix Marseille Univ, CNRS, Centrale Med, Institut Fresnel, F-13013 Marseille, France
[41]Université Paris-Saclay, CNRS/IN2P3, IJCLab, 91405 Orsay, France
[42]University of Tokyo, Tokyo, 113-0033, Japan
[43]Institut de Física d'Altes Energies (IFAE), The Barcelona Institute of Science and Technology, Campus UAB, E-08193 Bellaterra (Barcelona), Spain
[44]Gran Sasso Science Institute (GSSI), I-67100 L'Aquila, Italy
[45]INFN, Laboratori Nazionali del Gran Sasso, I-67100 Assergi, Italy
[46]University of Florida, Gainesville, FL 32611, USA
[47]Dipartimento di Scienze Matematiche, Informatiche e Fisiche, Università di Udine, I-33100 Udine, Italy
[48]INFN, Sezione di Trieste, I-34127 Trieste, Italy
[49]Tecnologico de Monterrey, Escuela de Ingeniería y Ciencias, 64849 Monterrey, Nuevo León, Mexico
[50]Institute for Cosmic Ray Research, KAGRA Observatory, The University of Tokyo, 238 Higashi-Mozumi, Kamioka-cho, Hida City, Gifu 506-1205, Japan
[51]INFN, Sezione di Perugia, I-06123 Perugia, Italy
[52]Università di Camerino, I-62032 Camerino, Italy
[53]University of Washington, Seattle, WA 98195, USA
[54]California State University Fullerton, Fullerton, CA 92831, USA
[55]SUPA, University of Strathclyde, Glasgow G1 1XQ, United Kingdom
[56]Université Claude Bernard Lyon 1, CNRS, IP2I Lyon / IN2P3, UMR 5822, F-69622 Villeurbanne, France
[57]Georgia Institute of Technology, Atlanta, GA 30332, USA
[58]Chennai Mathematical Institute, Chennai 603103, India
[59]Royal Holloway, University of London, London TW20 0EX, United Kingdom
[60]Astronomical course, The Graduate University for Advanced Studies (SOKENDAI), 2-21-1 Osawa, Mitaka City, Tokyo 181-8588, Japan
[61]Università degli Studi di Urbino "Carlo Bo", I-61029 Urbino, Italy
[62]INFN, Sezione di Firenze, I-50019 Sesto Fiorentino, Firenze, Italy
[63]European Gravitational Observatory (EGO), I-56021 Cascina, Pisa, Italy
[64]LIGO Livingston Observatory, Livingston, LA 70754, USA
[65]Université de Strasbourg, CNRS, IPHC UMR 7178, F-67000 Strasbourg, France
[66]Embry-Riddle Aeronautical University, Prescott, AZ 86301, USA
[67]Dipartimento di Fisica "E.R. Caianiello", Università di Salerno, I-84084 Fisciano, Salerno, Italy

[68]King's College London, University of London, London WC2R 2LS, United Kingdom
[69]Korea Institute of Science and Technology Information, Daejeon 34141, Republic of Korea
[70]International College, Osaka University, 1-1 Machikaneyama-cho, Toyonaka City, Osaka 560-0043, Japan
[71]Accelerator Laboratory, High Energy Accelerator Research Organization (KEK), 1-1 Oho, Tsukuba City, Ibaraki 305-0801, Japan
[72]Institute for Gravitational and Subatomic Physics (GRASP), Utrecht University, 3584 CC Utrecht, Netherlands
[73]OzGrav, University of Western Australia, Crawley, Western Australia 6009, Australia
[74]University of Portsmouth, Portsmouth, PO1 3FX, United Kingdom
[75]Università di Trento, Dipartimento di Fisica, I-38123 Povo, Trento, Italy
[76]INFN, Trento Institute for Fundamental Physics and Applications, I-38123 Povo, Trento, Italy
[77]Università di Perugia, I-06123 Perugia, Italy
[78]University of Oregon, Eugene, OR 97403, USA
[79]Syracuse University, Syracuse, NY 13244, USA
[80]Inter-University Centre for Astronomy and Astrophysics, Pune 411007, India
[81]INFN, Sezione di Pisa, I-56127 Pisa, Italy
[82]Università di Pisa, I-56127 Pisa, Italy
[83]Institut de Ciències del Cosmos (ICCUB), Universitat de Barcelona (UB), c. Martí i Franquès, 1, 08028 Barcelona, Spain
[84]Departament de Física Quàntica i Astrofísica (FQA), Universitat de Barcelona (UB), c. Martí i Franqués, 1, 08028 Barcelona, Spain
[85]Institut d'Estudis Espacials de Catalunya, c. Gran Capità, 2-4, 08034 Barcelona, Spain
[86]Dipartimento di Medicina, Chirurgia e Odontoiatria "Scuola Medica Salernitana", Università di Salerno, I-84081 Baronissi, Salerno, Italy
[87]IGR, University of Glasgow, Glasgow G12 8QQ, United Kingdom
[88]HUN-REN Wigner Research Centre for Physics, H-1121 Budapest, Hungary
[89]Concordia University Wisconsin, Mequon, WI 53097, USA
[90]Stanford University, Stanford, CA 94305, USA
[91]University of Michigan, Ann Arbor, MI 48109, USA
[92]Università di Padova, Dipartimento di Fisica e Astronomia, I-35131 Padova, Italy
[93]INFN, Sezione di Padova, I-35131 Padova, Italy
[94]Institute for Plasma Research, Bhat, Gandhinagar 382428, India
[95]Universiteit Gent, B-9000 Gent, Belgium
[96]Nicolaus Copernicus Astronomical Center, Polish Academy of Sciences, 00-716, Warsaw, Poland
[97]Northwestern University, Evanston, IL 60208, USA
[98]Universität Hamburg, D-22761 Hamburg, Germany
[99]IAC3–IEEC, Universitat de les Illes Balears, E-07122 Palma de Mallorca, Spain
[100]Aix-Marseille Université, Université de Toulon, CNRS, CPT, Marseille, France
[101]Laboratoire des 2 Infinis - Toulouse (L2IT-IN2P3), F-31062 Toulouse Cedex 9, France
[102]Università di Siena, Dipartimento di Scienze Fisiche, della Terra e dell'Ambiente, I-53100 Siena, Italy
[103]Villanova University, Villanova, PA 19085, USA
[104]University of Birmingham, Birmingham B15 2TT, United Kingdom
[105]RRCAT, Indore, Madhya Pradesh 452013, India
[106]Kenyon College, Gambier, OH 43022, USA
[107]Missouri University of Science and Technology, Rolla, MO 65409, USA
[108]Indian Institute of Technology Madras, Chennai 600036, India
[109]Department of Physics and Astronomy, Vrije Universiteit Amsterdam, 1081 HV Amsterdam, Netherlands
[110]Lomonosov Moscow State University, Moscow 119991, Russia
[111]Katholieke Universiteit Leuven, Oude Markt 13, 3000 Leuven, Belgium
[112]Rochester Institute of Technology, Rochester, NY 14623, USA
[113]Université libre de Bruxelles, 1050 Bruxelles, Belgium
[114]Bar-Ilan University, Ramat Gan, 5290002, Israel
[115]Université Côte d'Azur, Observatoire de la Côte d'Azur, CNRS, Artemis, F-06304 Nice, France
[116]University of British Columbia, Vancouver, BC V6T 1Z4, Canada
[117]OzGrav, University of Adelaide, Adelaide, South Australia 5005, Australia
[118]Centre national de la recherche scientifique, 75016 Paris, France
[119]Univ Rennes, CNRS, Institut FOTON - UMR 6082, F-35000 Rennes, France
[120]Washington State University, Pullman, WA 99164, USA
[121]Cornell University, Ithaca, NY 14850, USA
[122]Laboratoire Kastler Brossel, Sorbonne Université, CNRS, ENS-Université PSL, Collège de France, F-75005 Paris, France
[123]Christopher Newport University, Newport News, VA 23606, USA
[124]OzGrav, University of Melbourne, Parkville, Victoria 3010, Australia

[125]Astronomical Observatory Warsaw University, 00-478 Warsaw, Poland
[126]University of Maryland, College Park, MD 20742, USA
[127]Università degli Studi di Milano-Bicocca, I-20126 Milano, Italy
[128]INFN, Sezione di Milano-Bicocca, I-20126 Milano, Italy
[129]Université de Lyon, Université Claude Bernard Lyon 1, CNRS, Institut Lumière Matière, F-69622 Villeurbanne, France
[130]University of Chicago, Chicago, IL 60637, USA
[131]University of Arizona, Tucson, AZ 85721, USA
[132]INFN, Sezione di Napoli, Gruppo Collegato di Salerno, I-80126 Napoli, Italy
[133]University of Massachusetts Dartmouth, North Dartmouth, MA 02747, USA
[134]Niels Bohr Institute, Copenhagen University, 2100 København, Denmark
[135]Universidad de Guadalajara, 44430 Guadalajara, Jalisco, Mexico
[136]Istituto di Astrofisica e Planetologia Spaziali di Roma, 00133 Roma, Italy
[137]Colorado State University, Fort Collins, CO 80523, USA
[138]Departamento de Astronomía y Astrofísica, Universitat de València, E-46100 Burjassot, València, Spain
[139]Observatori Astronòmic, Universitat de València, E-46980 Paterna, València, Spain
[140]Niels Bohr Institute, University of Copenhagen, 2100 Kóbenhavn, Denmark
[141]National Central University, Taoyuan City 320317, Taiwan
[142]National Tsing Hua University, Hsinchu City 30013, Taiwan
[143]OzGrav, Charles Sturt University, Wagga Wagga, New South Wales 2678, Australia
[144]Vanderbilt University, Nashville, TN 37235, USA
[145]University of the Chinese Academy of Sciences / International Centre for Theoretical Physics Asia-Pacific, Bejing 100049, China
[146]Department of Electrophysics, National Yang Ming Chiao Tung University, 101 Univ. Street, Hsinchu, Taiwan
[147]Kamioka Branch, National Astronomical Observatory of Japan, 238 Higashi-Mozumi, Kamioka-cho, Hida City, Gifu 506-1205, Japan
[148]University of Texas, Austin, TX 78712, USA
[149]CaRT, California Institute of Technology, Pasadena, CA 91125, USA
[150]Northeastern University, Boston, MA 02115, USA
[151]Dipartimento di Ingegneria Industriale (DIIN), Università di Salerno, I-84084 Fisciano, Salerno, Italy
[152]Faculty of Science, University of Toyama, 3190 Gofuku, Toyama City, Toyama 930-8555, Japan
[153]Carleton College, Northfield, MN 55057, USA
[154]University of Szeged, Dóm tér 9, Szeged 6720, Hungary
[155]OzGrav, Swinburne University of Technology, Hawthorn VIC 3122, Australia
[156]INFN Cagliari, Physics Department, Università degli Studi di Cagliari, Cagliari 09042, Italy
[157]Università degli Studi di Cagliari, Via Università 40, 09124 Cagliari, Italy
[158]Université Libre de Bruxelles, Brussels 1050, Belgium
[159]INAF, Osservatorio Astronomico di Brera sede di Merate, I-23807 Merate, Lecco, Italy
[160]Departamento de Matemáticas, Universitat de València, E-46100 Burjassot, València, Spain
[161]Montana State University, Bozeman, MT 59717, USA
[162]The University of Utah, Salt Lake City, UT 84112, USA
[163]Johns Hopkins University, Baltimore, MD 21218, USA
[164]University of Rhode Island, Kingston, RI 02881, USA
[165]The University of Texas Rio Grande Valley, Brownsville, TX 78520, USA
[166]Université de Liège, B-4000 Liège, Belgium
[167]DIFA- Alma Mater Studiorum Università di Bologna, Via Zamboni, 33 - 40126 Bologna, Italy
[168]Istituto Nazionale Di Fisica Nucleare - Sezione di Bologna, viale Carlo Berti Pichat 6/2 - 40127 Bologna, Italy
[169]University of Manitoba, Winnipeg, MB R3T 2N2, Canada
[170]INFN-CNAF - Bologna, Viale Carlo Berti Pichat, 6/2, 40127 Bologna BO, Italy
[171]Università degli Studi di Sassari, I-07100 Sassari, Italy
[172]INFN, Laboratori Nazionali del Sud, I-95125 Catania, Italy
[173]Université de Normandie, ENSICAEN, UNICAEN, CNRS/IN2P3, LPC Caen, F-14000 Caen, France
[174]Laboratoire de Physique Corpusculaire Caen, 6 boulevard du maréchal Juin, F-14050 Caen, France
[175]The University of Sheffield, Sheffield S10 2TN, United Kingdom
[176]Université Claude Bernard Lyon 1, CNRS, Laboratoire des Matériaux Avancés (LMA), IP2I Lyon / IN2P3, UMR 5822, F-69622 Villeurbanne, France
[177]Università di Firenze, Sesto Fiorentino I-50019, Italy
[178]IGFAE, Universidade de Santiago de Compostela, E-15782 Santiago de Compostela, Spain
[179]Dipartimento di Scienze Matematiche, Fisiche e Informatiche, Università di Parma, I-43124 Parma, Italy
[180]INFN, Sezione di Milano Bicocca, Gruppo Collegato di Parma, I-43124 Parma, Italy
[181]California State University, Los Angeles, Los Angeles, CA 90032, USA

[182]Marquette University, Milwaukee, WI 53233, USA
[183]Perimeter Institute, Waterloo, ON N2L 2Y5, Canada
[184]Corps des Mines, Mines Paris, Université PSL, 60 Bd Saint-Michel, 75272 Paris, France
[185]Dipartimento di Fisica, Università di Trieste, I-34127 Trieste, Italy
[186]Université Côte d'Azur, Observatoire de la Côte d'Azur, CNRS, Lagrange, F-06304 Nice, France
[187]National Center for Nuclear Research, 05-400 Świerk-Otwock, Poland
[188]Vrije Universiteit Brussel, 1050 Brussel, Belgium
[189]University of Zurich, Winterthurerstrasse 190, 8057 Zurich, Switzerland
[190]Canadian Institute for Theoretical Astrophysics, University of Toronto, Toronto, ON M5S 3H8, Canada
[191]Stony Brook University, Stony Brook, NY 11794, USA
[192]Center for Computational Astrophysics, Flatiron Institute, New York, NY 10010, USA
[193]Montclair State University, Montclair, NJ 07043, USA
[194]HUN-REN Institute for Nuclear Research, H-4026 Debrecen, Hungary
[195]Indian Institute of Technology Bombay, Powai, Mumbai 400 076, India
[196]Centro de Física das Universidades do Minho e do Porto, Universidade do Minho, PT-4710-057 Braga, Portugal
[197]Aix Marseille Univ, CNRS/IN2P3, CPPM, Marseille, France
[198]CNR-SPIN, I-84084 Fisciano, Salerno, Italy
[199]Scuola di Ingegneria, Università della Basilicata, I-85100 Potenza, Italy
[200]Western Washington University, Bellingham, WA 98225, USA
[201]SUPA, University of the West of Scotland, Paisley PA1 2BE, United Kingdom
[202]Barry University, Miami Shores, FL 33168, USA
[203]Eötvös University, Budapest 1117, Hungary
[204]Institute for Cosmic Ray Research, KAGRA Observatory, The University of Tokyo, 5-1-5 Kashiwa-no-Ha, Kashiwa City, Chiba 277-8582, Japan
[205]Department of Physics, Graduate School of Science, Osaka Metropolitan University, 3-3-138 Sugimoto-cho, Sumiyoshi-ku, Osaka City, Osaka 558-8585, Japan
[206]University of Sannio at Benevento, I-82100 Benevento, Italy and INFN, Sezione di Napoli, I-80100 Napoli, Italy
[207]University of California, Berkeley, CA 94720, USA
[208]Instituto de Fisica Teorica UAM-CSIC, Universidad Autonoma de Madrid, 28049 Madrid, Spain
[209]Laboratoire d'Acoustique de l'Université du Mans, UMR CNRS 6613, F-72085 Le Mans, France
[210]University of Southampton, Southampton SO17 1BJ, United Kingdom
[211]University of California, Riverside, Riverside, CA 92521, USA
[212]Dipartimento di Ingegneria Industriale, Elettronica e Meccanica, Università degli Studi Roma Tre, I-00146 Roma, Italy
[213]University of Nevada, Las Vegas, Las Vegas, NV 89154, USA
[214]University of Nottingham NG7 2RD, UK
[215]Ariel University, Ramat HaGolan St 65, Ari'el, Israel
[216]The University of Mississippi, University, MS 38677, USA
[217]Graduate School of Science, Institute of Science Tokyo, 2-12-1 Ookayama, Meguro-ku, Tokyo 152-8551, Japan
[218]Institute of Physics, Academia Sinica, 128 Sec. 2, Academia Rd., Nankang, Taipei 11529, Taiwan
[219]The Chinese University of Hong Kong, Shatin, NT, Hong Kong
[220]American University, Washington, DC 20016, USA
[221]Dipartimento di Fisica, Università degli studi di Milano, Via Celoria 16, I-20133, Milano, Italy
[222]INFN, sezione di Milano, Via Celoria 16, I-20133, Milano, Italy
[223]Department of Applied Physics, Fukuoka University, 8-19-1 Nanakuma, Jonan, Fukuoka City, Fukuoka 814-0180, Japan
[224]University of Cambridge, Cambridge CB2 1TN, United Kingdom
[225]University of Lancaster, Lancaster LA1 4YW, United Kingdom
[226]College of Industrial Technology, Nihon University, 1-2-1 Izumi, Narashino City, Chiba 275-8575, Japan
[227]Faculty of Engineering, Niigata University, 8050 Ikarashi-2-no-cho, Nishi-ku, Niigata City, Niigata 950-2181, Japan
[228]Department of Physics, Tamkang University, No. 151, Yingzhuan Rd., Danshui Dist., New Taipei City 25137, Taiwan
[229]Rutherford Appleton Laboratory, Didcot OX11 0DE, United Kingdom
[230]Department of Physical Sciences, Aoyama Gakuin University, 5-10-1 Fuchinobe, Sagamihara City, Kanagawa 252-5258, Japan
[231]Helmut Schmidt University, D-22043 Hamburg, Germany
[232]Nambu Yoichiro Institute of Theoretical and Experimental Physics (NITEP), Osaka Metropolitan University, 3-3-138 Sugimoto-cho, Sumiyoshi-ku, Osaka City, Osaka 558-8585, Japan
[233]Directorate of Construction, Services & Estate Management, Mumbai 400094, India
[234]Observatoire Astronomique de Strasbourg, 11 Rue de l'Université, 67000 Strasbourg, France
[235]Faculty of Physics, University of Białystok, 15-245 Białystok, Poland
[236]National Astronomical Observatories, Chinese Academic of Sciences, 20A Datun Road, Chaoyang District, Beijing, China
[237]School of Astronomy and Space Science, University of Chinese Academy of Sciences, 20A Datun Road, Chaoyang District, Beijing, China

[238] *Sungkyunkwan University, Seoul 03063, Republic of Korea*
[239] *Department of Physics, Ulsan National Institute of Science and Technology (UNIST), 50 UNIST-gil, Ulju-gun, Ulsan 44919, Republic of Korea*
[240] *Institute for Cosmic Ray Research, The University of Tokyo, 5-1-5 Kashiwa-no-Ha, Kashiwa City, Chiba 277-8582, Japan*
[241] *Chung-Ang University, Seoul 06974, Republic of Korea*
[242] *University of Washington Bothell, Bothell, WA 98011, USA*
[243] *Laboratoire de Physique et de Chimie de l'Environnement, Université Joseph KI-ZERBO, 9GH2+3V5, Ouagadougou, Burkina Faso*
[244] *Ewha Womans University, Seoul 03760, Republic of Korea*
[245] *National Institute for Mathematical Sciences, Daejeon 34047, Republic of Korea*
[246] *Korea Astronomy and Space Science Institute, Daejeon 34055, Republic of Korea*
[247] *Department of Astronomy and Space Science, Chungnam National University, 9 Daehak-ro, Yuseong-gu, Daejeon 34134, Republic of Korea*
[248] *Institute of Particle and Nuclear Studies (IPNS), High Energy Accelerator Research Organization (KEK), 1-1 Oho, Tsukuba City, Ibaraki 305-0801, Japan*
[249] *Division of Science, National Astronomical Observatory of Japan, 2-21-1 Osawa, Mitaka City, Tokyo 181-8588, Japan*
[250] *Nagoya University, Nagoya, 464-8601, Japan*
[251] *Department of Physics, Aristotle University of Thessaloniki, 54124 Thessaloniki, Greece*
[252] *Bard College, Annandale-On-Hudson, NY 12504, USA*
[253] *Technical University of Braunschweig, D-38106 Braunschweig, Germany*
[254] *Institute of Mathematics, Polish Academy of Sciences, 00656 Warsaw, Poland*
[255] *Astronomical Observatory, Jagiellonian University, 31-007 Cracow, Poland*
[256] *Department of Physics and Astronomy, University of Padova, Via Marzolo, 8-35151 Padova, Italy*
[257] *Sezione di Padova, Istituto Nazionale di Fisica Nucleare (INFN), Via Marzolo, 8-35131 Padova, Italy*
[258] *Department of Physics, Nagoya University, ES building, Furocho, Chikusa-ku, Nagoya, Aichi 464-8602, Japan*
[259] *Université de Montréal/Polytechnique, Montreal, Quebec H3T 1J4, Canada*
[260] *Indian Institute of Science Education and Research, Kolkata, Mohanpur, West Bengal 741252, India*
[261] *Seoul National University, Seoul 08826, Republic of Korea*
[262] *Department of Computer Simulation, Inje University, 197 Inje-ro, Gimhae, Gyeongsangnam-do 50834, Republic of Korea*
[263] *NAVIER, École des Ponts, Univ Gustave Eiffel, CNRS, Marne-la-Vallée, France*
[264] *Gravitational Wave Science Project, National Astronomical Observatory of Japan (NAOJ), Mitaka City, Tokyo 181-8588, Japan*
[265] *Department of Physics, National Cheng Kung University, No.1, University Road, Tainan City 701, Taiwan*
[266] *St. Thomas University, Miami Gardens, FL 33054, USA*
[267] *Scuola Normale Superiore, I-56126 Pisa, Italy*
[268] *Institució Catalana de Recerca i Estudis Avançats, E-08010 Barcelona, Spain*
[269] *Institut de Física d'Altes Energies, E-08193 Barcelona, Spain*
[270] *Institut fuer Theoretische Astrophysik, Zentrum fuer Astronomie Heidelberg, Universitaet Heidelberg, Albert Ueberle Str. 2, 69120 Heidelberg, Germany*
[271] *Institucio Catalana de Recerca i Estudis Avançats (ICREA), Passeig de Lluís Companys, 23, 08010 Barcelona, Spain*
[272] *Research Center for Space Science, Advanced Research Laboratories, Tokyo City University, 3-3-1 Ushikubo-Nishi, Tsuzuki-Ku, Yokohama, Kanagawa 224-8551, Japan*
[273] *Tsinghua University, Beijing 100084, China*
[274] *Department of Physics, National Institute of Technology, Calicut, 673601, Kerala, India*
[275] *Institut des Hautes Etudes Scientifiques, F-91440 Bures-sur-Yvette, France*
[276] *Faculty of Law, Ryukoku University, 67 Fukakusa Tsukamoto-cho, Fushimi-ku, Kyoto City, Kyoto 612-8577, Japan*
[277] *Phenikaa Institute for Advanced Study (PIAS), Phenikaa University, Yen Nghia, Ha Dong, Hanoi, Vietnam*
[278] *University of Stavanger, 4021 Stavanger, Norway*
[279] *Physics Program, Graduate School of Advanced Science and Engineering, Hiroshima University, 1-3-1 Kagamiyama, Higashihiroshima City, Hiroshima 739-8526, Japan*
[280] *GRAPPA, Anton Pannekoek Institute for Astronomy and Institute for High-Energy Physics, University of Amsterdam, 1098 XH Amsterdam, Netherlands*
[281] *University College London, London WC1E 6BT, United Kingdom*
[282] *Observatoire de Paris, 75014 Paris, France*
[283] *Laboratoire Univers et Théories, Observatoire de Paris, 92190 Meudon, France*
[284] *Graduate School of Science and Technology, Niigata University, 8050 Ikarashi-2-no-cho, Nishi-ku, Niigata City, Niigata 950-2181, Japan*
[285] *University of Maryland, Baltimore County, Baltimore, MD 21250, USA*
[286] *CSIR-Central Glass and Ceramic Research Institute, Kolkata, West Bengal 700032, India*
[287] *Consiglio Nazionale delle Ricerche - Istituto dei Sistemi Complessi, I-00185 Roma, Italy*
[288] *Department of Astronomy, Yonsei University, 50 Yonsei-Ro, Seodaemun-Gu, Seoul 03722, Republic of Korea*
[289] *Department of Physics, University of Guadalajara, Av. Revolucion 1500, Colonia Olimpica C.P. 44430, Guadalajara, Jalisco, Mexico*
[290] *Hobart and William Smith Colleges, Geneva, NY 14456, USA*
[291] *INAF, Osservatorio Astronomico di Padova, I-35122 Padova, Italy*
[292] *Dipartimento di Ingegneria, Università del Sannio, I-82100 Benevento, Italy*

[293]Museo Storico della Fisica e Centro Studi e Ricerche "Enrico Fermi", I-00184 Roma, Italy
[294]Kennesaw State University, Kennesaw, GA 30144, USA
[295]Subatech, CNRS/IN2P3 - IMT Atlantique - Nantes Université, 4 rue Alfred Kastler BP 20722 44307 Nantes CÉDEX 03, France
[296]Universidad de Antioquia, Medellín, Colombia
[297]Departamento de Física - ETSIDI, Universidad Politécnica de Madrid, 28012 Madrid, Spain
[298]Department of Electronic Control Engineering, National Institute of Technology, Nagaoka College, 888 Nishikatakai, Nagaoka City, Niigata 940-8532, Japan
[299]Trinity College, Hartford, CT 06106, USA
[300]Dipartimento di Fisica e Scienze della Terra, Università Degli Studi di Ferrara, Via Saragat, 1, 44121 Ferrara FE, Italy
[301]Faculty of Science, Toho University, 2-2-1 Miyama, Funabashi City, Chiba 274-8510, Japan
[302]Indian Institute of Technology, Palaj, Gandhinagar, Gujarat 382355, India
[303]Kavli Institute for Astronomy and Astrophysics, Peking University, Yiheyuan Road 5, Haidian District, Beijing 100871, China
[304]Laboratoire MSME, Cité Descartes, 5 Boulevard Descartes, Champs-sur-Marne, 77454 Marne-la-Vallée Cedex 2, France
[305]Faculty of Information Science and Technology, Osaka Institute of Technology, 1-79-1 Kitayama, Hirakata City, Osaka 573-0196, Japan
[306]NASA Goddard Space Flight Center, Greenbelt, MD 20771, USA
[307]Faculty of Science and Technology, Kochi University, 2-5-1 Akebono-cho, Kochi-shi, Kochi 780-8520, Japan
[308]Laboratoire de Physique de l'École Normale Supérieure, ENS, (CNRS, Université PSL, Sorbonne Université, Université Paris Cité), F-75005 Paris, France
[309]Faculty of Physics, University of Warsaw, Ludwika Pasteura 5, 02-093 Warszawa, Poland
[310]Laser Interferometry and Gravitational Wave Astronomy, Max Planck Institute for Gravitational Physics, Callinstrasse 38, 30167 Hannover, Germany
[311]The Hakubi Center for Advanced Research, Kyoto University, Yoshida-honmachi, Sakyou-ku, Kyoto City, Kyoto 606-8501, Japan
[312]Department of Physics, Kyoto University, Kita-Shirakawa Oiwake-cho, Sakyou-ku, Kyoto City, Kyoto 606-8502, Japan
[313]Yukawa Institute for Theoretical Physics (YITP), Kyoto University, Kita-Shirakawa Oiwake-cho, Sakyou-ku, Kyoto City, Kyoto 606-8502, Japan
[314]University of Catania, Department of Physics and Astronomy, Via S. Sofia, 64, 95123 Catania CT, Italy
[315]National Institute of Technology, Fukui College, Geshi-cho, Sabae-shi, Fukui 916-8507, Japan
[316]Department of Communications Engineering, National Defense Academy of Japan, 1-10-20 Hashirimizu, Yokosuka City, Kanagawa 239-8686, Japan
[317]Eindhoven University of Technology, 5600 MB Eindhoven, Netherlands
[318]Kavli Institute for the Physics and Mathematics of the Universe (Kavli IPMU), WPI, The University of Tokyo, 5-1-5 Kashiwa-no-Ha, Kashiwa City, Chiba 277-8583, Japan
[319]Department of Astronomy, Beijing Normal University, Xinjiekouwai Street 19, Haidian District, Beijing 100875, China
[320]School of Physics and Technology, Wuhan University, Bayi Road 299, Wuchang District, Wuhan, Hubei, 430072, China